U.PORTO

FEUP FACULDADE DE ENGENHARIA
UNIVERSIDADE DO PORTO

Multi-material adhesive joints for automotive industry

Submitted by:
Mircea Roșioară

Supervisors:

Lucas F.M. da Silva (FEUP-DEMec-SMPT)

Mariana Banea (INEGI-FEUP)

Ricardo Carbas (INEGI-FEUP)

Departamento de Engenharia Mecânica
FACULDADE DE ENGENHARIA DA UNIVERSIDADE DO PORTO

Oporto, Portugal, July of 2015

`

Abstract

The application of adhesively bonded joints in automotive industry has increased significantly in recent years mainly because of the potential for lighter weight vehicles, fuel savings, and reduced emissions. The principal benefits are design flexibility and joining of dissimilar and/or new materials, among others. On the other hand, the use of lightweight materials such as high strength steel, aluminum alloys as well as composites in making automotive body components to achieve a reduced vehicle mass has also continuously increased. In addition, smart combination of materials might be the key to develop lighter vehicles. Carbon fiber reinforced plastic (CFRP) parts are increasingly being selected in combination with metals- for instance aluminum and hard steel - to reduce weight without compromising passenger safety. Room temperature curing adhesives (i.e. polyurethanes) are preferred for multi-material joints to avoid thermal stress concentration. However, different materials and joint geometries will give rise to distinct stress states in the adhesive layer, and the performance of a specific adhesive will invariably depend on these parameters.

In this work, balanced and unbalanced multi-material joins were investigated experimentally and numerically. Several important factors, such as overlap length and adherend axial stiffness, influencing the strengths of multi-material adhesive joint (high strength steel, aluminum and composite adherends) were investigated. For relatively short overlaps in SLJs bonded with structural modern tough adhesives, failure is dominated by adhesive global yielding and the influence of geometry and/or material combination on joint strength is not significant. However, for larger overlaps, the failure is not anymore due to global yielding and the effect of material becomes more important. Overall numerical values of the maximum load were very close to experimental results, validating the numerical methodology to predict the lap shear strength and providing the necessary data to explain

Rezumat

Utilizarea adevizilor structurali în industria producătoare de mașini a cunoscut o visibilă creștere în ultimii ani datorită potențialului acestora de reducere a masei vehiculelor și implicit facilitarea economiei de combustibil și a reducerii emisiilor.

Principalele atuuri oferite de îmbinările realizate utilizând adevizi structurali, se numără facilitarea procesului de proiectare a autovehiculelor, posibilitatea de îmbinarea a diferitelor material și altele. Din alt punct de vedere, cerința de utilizarea a materialelor care conduc la scăderea masei autovehiculelor, este intr-o continuă creștere. În acest scop, realizarea combinațiilor de materiale disimilare poate reprezenta soluția actualei problem.

Tot mai multe componente realizate din fibra de carbon sunt utilizate în combinații cu materiale metalice, cum ar fi aluminul și oțeluri înalt aliate, cu scopul de a reduce masa autovehiculelor, dar fără a atenta la siguranța pasagerilor. În vederea realizărilor îmbinărilor cu adezivi folosind materialele menționante anterior, sunt preferați adezivii care se întăresc la temperature camerei în scopul evitării apariției tensiunilor datorate contracției termice.

În scopul realizării acestei lucrări îmbinaări echilibrate și neechilibrate îmbinate prin intermediul adezivilor structurali au fost realizate, analizate experimental și numeric. Astfel parametrii cum ar fi lungimea de suprapunere, elasticitatea axiala a aderenților au fost studiați, fiind factori de influnță a capacității portante a îmbinării materialelor disimilare (oțeluri înalt aliate, aluminiu și materiale composite) cu adezivi structurali.

Acknowledgements

I would like to thank:

- Professor Lucas da Silva for giving me the opportunity to work under his supervision, for putting his trust on me for the work I have done, for the guidance and advice given;
- Dr. Mariana Banea, for her invaluable help, patience and trust during the theoretical and experimental parts of this study and also for being there whenever I needed help;
- Dr. Ricardo Carbas for his essential contribution during the experimental part of the study;
- All of the AdFEUP group for all the help and the advices they offered me whenever I needed;
- My home university IMST (UPB) for giving me the opportunity to enjoy this international learning experience and FEUP for their warm welcome and hospitality;
- My friends for their endless support, especially Catalina, Mihai and Radu, who were always by my side during this period;
- My family for making this possible and for allowing me to make them feel proud.

Contents

List of figures

`

`

`

List of tables

List of acronyms and symbols

Acronyms

CFRP	Carbon fiber reinforced plastic
CTE	Coefficient of thermal expansion
FEA	Finite element analysis
RT	Room temperature
SLJ	Single lap joint

Symbol

b	Joint Width
E	Young`s Modulus
G	Transverse elastic modulus
Gn^c	Mode I fracture toughness
Gs^c	Mode II fracture toughness
L	Overlap length
L	Overlap length
P	Applied load
s	Adherend transverse area
t	Adhesive thickness
ts^0	Tensile stess
ts^0	Tensile shear stress
σ	Tensile stress
σ_y	Shear stress
τ_{xy}	Peel stress

`

1 Introduction

1.1 Background and motivation

The increasing demand for energy-efficient vehicles lead the manufacturers to increasing use of lightweight materials such as high strength steel, magnesium alloys, aluminum alloys as well as composites in making automotive body components to achieve a reduced vehicle mass. In addition, combinations of different materials give more design flexibility. Adhesive bonding can be used to virtually join all types of materials and combinations of materials and is more and more used in automotive industry. However, combining dissimilar materials brings great challenges to the body assembly process. Thus, adequate understanding of the behavior of multi-material adhesively bonded joints is necessary to ensure efficiency, safety and reliability of such joints.

1.2 Problem definition

The application of the adhesive bonded joints in automotive industry has significantly increased. The principal benefits provided are design flexibility and joining of dissimilar and/or new materials. On the other hand, the use of lightweight materials such as high strength steel, aluminum, magnesium and composite materials in manufacturing automotive body components in order to achieve a reduced mass has also continually increased. Material combinations are also becoming common nowadays and smart combination of materials might be the key to develop light vehicles.

1.3 Objectives

The main objective of this thesis is to investigate multi-material joints for automotive applications by using various combination of materials. Single lap joints with different materials (CFRP, aluminum and hard steel) were studied experimentally and numerically. Several important factors, such as the overlap length, adherend thickness and stiffness, influencing the strengths of multi-material adhesive joints were investigated. The adhesive studied, used in the automotive industry, combines properties of an epoxy adhesive and typical polyurethane adhesive, giving high strength, elongation and toughness.

`

Single lap joint were experimentally tested in order to investigate the efficiency and reliability of multi-material adhesive joints. Also, numerical analysis were performed in order to replicate the results obtained experimentally and to validate the numerical methodology to predict the lap shear strength providing the necessary data to explain the obtained behavior.

1.4 Research methodology

In order to achieve the goals established for the thesis, the following work was done:

1. A literature review of the adhesive bonding, giving a special attention to dissimilar adherend joints, was done;

2. Single lap joints using dissimilar adherends with different overlaps length were manufactured;

3. Joint strength determination of the multi-material adhesive joints.

4. A numerical analysis was performed for stress analysis and strength prediction and the results were compared to the experimental results.

1.5 Outline of the thesis

The structure of the thesis was divided in the following sections:

Chapter 1: A short introduction of the thesis was done.

Chapter 2: A summarized review of adhesive bonding was made, starting by describing the general usage of adhesive bonding, characteristics of the adhesives, and the most typical methods to predict the joints strength.

Chapter 3: This section describes the process of manufacturing and testing of the specimens. It contains information about the adhesive and the adherends used, the surface treatment applied, geometry of the joints, testing procedure, experimental results obtained and discussions;

`

Chapter 4: In this section, a finite element model was used in order to replicate the results obtained experimentally and to determine the stress distribution for a better understanding of the joints strength.

Chapter 5: The conclusions from the experimental and numerical analysis were drawn.

`

2 Literature review

2.1 Adhesive bonding

A proper definition of adhesion cannot be given, but the following definition can be accepted:

Adhesion refers to the state in which two dissimilar bodies are held together by intimate interfacial contact such that mechanical force or work can be transferred across the interface. The interfacial forces holding the two phases together may arise from van der Waals forces, chemical bonding, or electrostatic attraction. Mechanical strength of the system is determined not only by the interfacial forces, but also by the mechanical properties of the interfacial zone and the two bulk phases (Wu, 1982).

A structural adhesive is an adhesive that can resist substantial loads and that is responsible for the strength and stiffness of the structure (Adams, 2005).

2.1.1 Application of bonded joints

The advantages provided by adhesive joints, such as improving the strength, a better load transfer, corrosion resistance and durability improvement, and taking in consideration the evolution of new advance adhesives has allowed to replace some of the traditional fastened joints with bonded joints. Adhesive bonding has become an important joining tool for modern structures with applications in automotive, aerospace, rolling stock, marine and civil engineering.

Automobile manufacturers are always looking for ways to make their cars lighter without sacrificing the safety of the passengers. In the past decade, many companies including Jaguar, Lexus, Mercedes, BMW, Audi, and Volvo, have been researching the replacement of steel with aluminum, magnesium, composites and foams. In Figure 2.1, the most common materials used in the automotive industry are showed. Therefore the next challenge was developing proper solutions for bonding the dissimilar materials.

Adhesive bonding has become increasingly important for the automotive industry, which is one of the most active industries in using adhesives. A large variety of applications can be found in automotive production. It is a universal technology and allows the joining of different materials, thus enabling lightweight design with the mix of multi-materials (da Silva, et al., 2011).

`

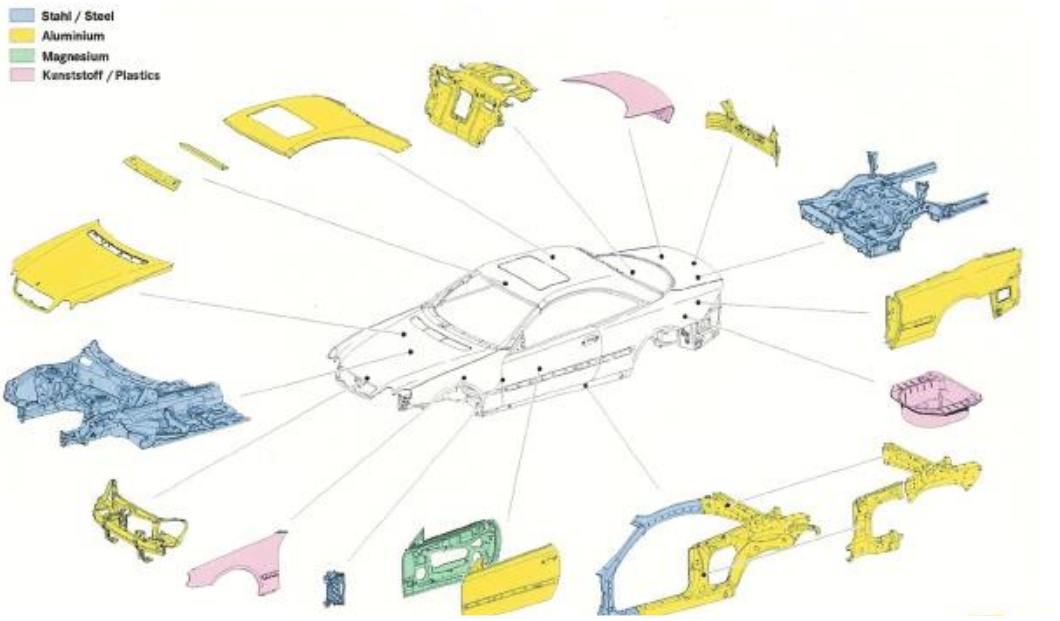

Materials in a Vehicle

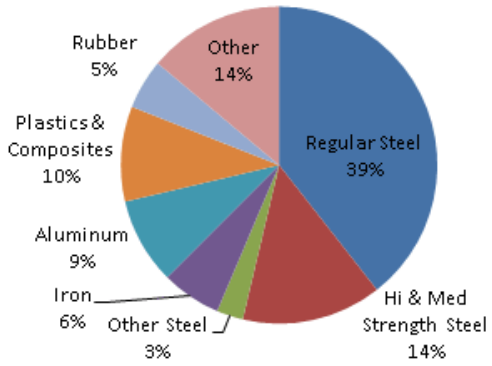

Figure 2.1 Materials used in automotive industry (NIST, n.d.)

New structural adhesives used in the automotive industry have an increasing role in joining dissimilar adherends such as aluminum, carbon fiber, steel, magnesium and other metals, acting both as a galvanic barrier and a stress spreader to both adherends.

For a better understanding of the usage of structural adhesive in the automotive industry some examples are given. The new 2014 Cadillac CTS uses 118 meters of structural adhesive as a bonding agent that holds together and stiffens load-bearing parts and components. The extensive use of adhesive provides a damping effect, which reduces the transmission of vibration through the body structure. That pays off in fewer squeaks and rattles reaching a driver (Car-Engineer, n.d.).

`

In 2012, for manufacturing the body of the new Lexus IS, 100 meters of structural adhesive were used (Figure 2.2), while in 2011 Mercedes CL had used approximately 100 meters of adhesive for bonding the body structure (Omar, 2011).

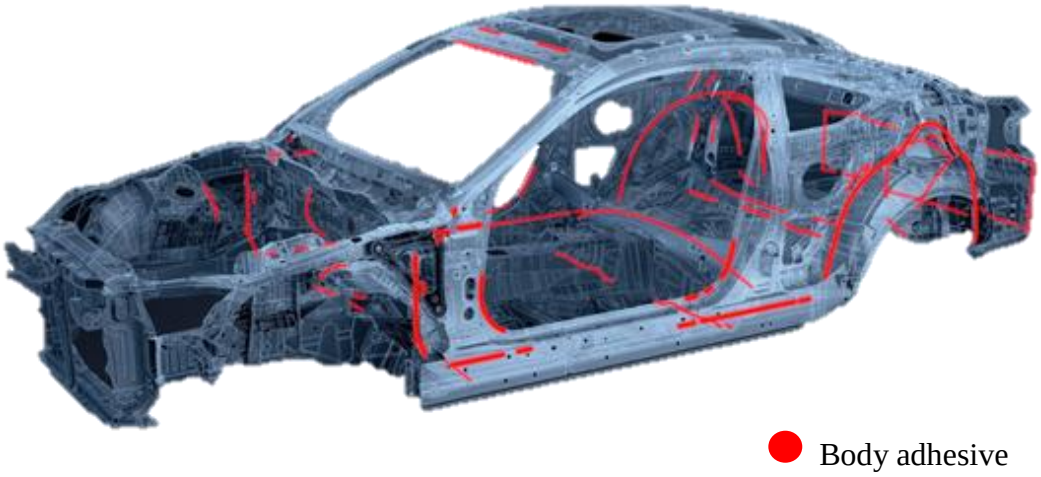

Figure 2.2 Structural adhesive used for Lexus IS body (lexus.co.uk, n.d.)

The most recent auto vehicles launched by BMW car manufacturer, the i3 and i8 models, revolutionized the industry by using only composite materials to manufacture the body, achievement accomplished by using more than 160 m of adhesive bond in each model (CompositesWorld, n.d.).

2.1.2 Joint design

Joint design is critical to the successful use of adhesives. Because of the low cohesive (as opposed to interfacial strengths) of adhesives, purely tensile joints must be avoided. When designing an adhesively bonded joint, it is not advisable to assume that the joint design should be the same as for traditional fixing methods like welding and brazing, it is better the operating load is transferred as a shear stress as opposed to a tensile stress. The design of the adhesive joint will play a significant factor in determining how it will survive service loads.

External loads produce local stresses that may exceed many times the average stress. These stress concentrations are often unexpected, and they may determine the actual force that the joint can sustain. Typical forces, which may be applied to adhesive joints, are presented in Figure 2.3.

`

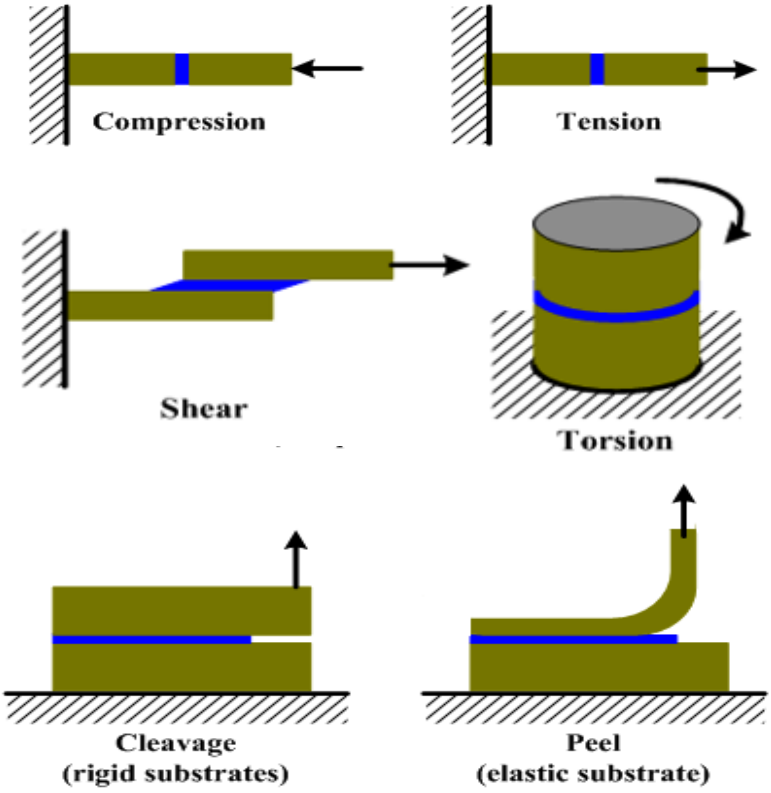

Figure 2.3 Typical forces in adhesive joints (Williams, 2008)

When designing the joint it is necessary to:

- maximise shear and compression forces;
- minimise peel and cleavage forces;
- optimise the area over which the load is distributed.

The most typical design of adhesive joints are presented in Figure 2.4.

`

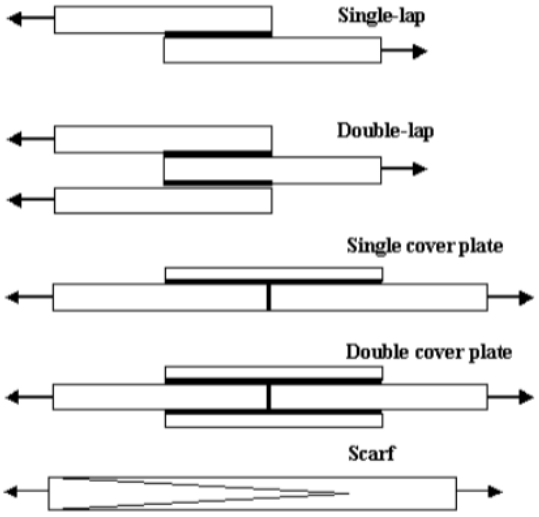

Figure 2.4 Typical design of adhesive joints (Williams, 2008)

In a simple lap joint made from thin metal sheet there are two sorts of stress: shear and peel as shown in Figure 2.5.

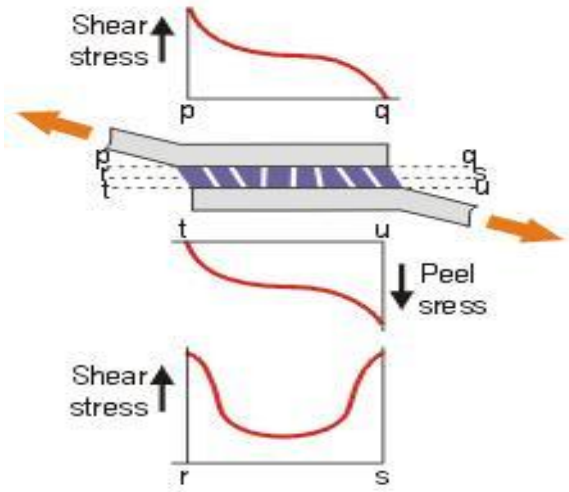

Figure 2.5 Shear stress distribution in a simple lap joint (McGrath, 2001)

Shear stress results when forces acting in the plane of the adhesive try to separate the adherends. Peel stress is defined as the force that pulls an adhesive apart by separating the substrates.

Non-uniform stresses within the adhesive joint can significantly reduce the maximum strength of the joint. Non-uniform stress distributions generally cannot be

`

eliminated, but they can be reduced through proper joint design and selection of certain design variables. There are a large number of variables affecting stress distribution, even in the most common joint designs. The following are most important:

1. Adhesive material properties
2. Adhesive thickness
3. Adherend properties
4. Geometry of the bond area (i.e. overlap length)

2.1.3 Failure modes

To study the failure of an adhesive joint, it is required to understand the difference between *adhesion* and *cohesion*. When two substances are attracted due to the intermolecular forces existing between them it is called adhesion. Cohesion will be if the intermolecular forces are established only inside one substance (da Silva, et al., 2011). There are different modes of bonded joints failure:

- Adhesive failure between the adhesive and the adherend;
- Cohesive failure;
- Thin-layer cohesive failure;
- Fiber-tear failure;
- Light-fiber-tear failure;
- Stock-break failure of the adherend

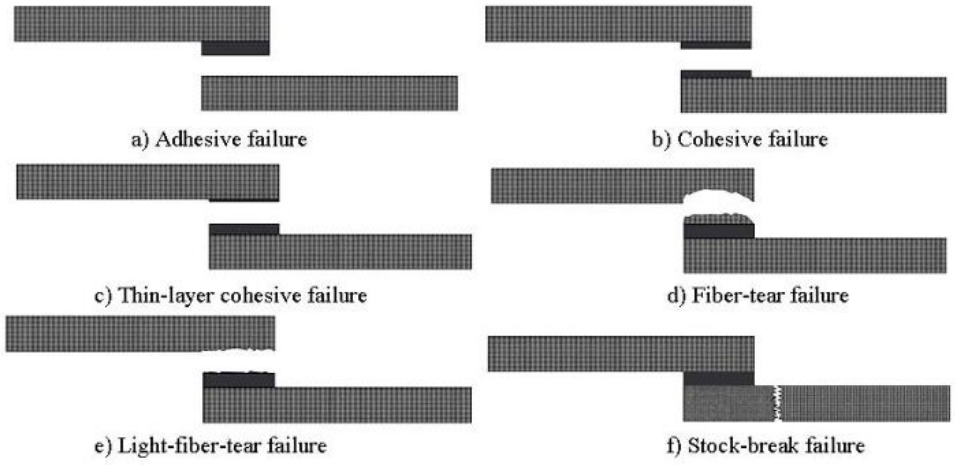

Figure 2.6 Failure modes of an adhesive joint (Banea & da Silva, 2009)

`

Adhesive failure (Figure 2.6 a) can be easily recognized by the detachment of the adhesive layer from one of the adherends, in the separation plane between the substrate and the adhesive. This failure is caused by bad manufacturing of the adhesive bonding or improper substrate treatment.

Cohesive failure (Figure 2.6 b, c) occurs when the fracture propagates into the adhesive layer and can be distinguished by the presence of adhesive on both substrates. Usually the shear loads and proper surface treatment are responsible for this kind of failure, but it can occur due to a combination between peel and shear. The fracture surface of this failure case, can have a lighter color tint than the bulk adhesive material (Davis & Bond, n.d.). If the cohesive failure occur during a product service life, the main cause of the fail it`s a poor joint design.

Fiber-tear failure (Figure 2.6 d) occurs exclusively within the FRP matrix and is characterized by the appearance of reinforcing fibers on both ruptured surfaces, while light fiber-tear failure (Figure 2.6 e) is failure occurring within the FRP substrate, near the surface, characterized by a thin layer of the FRP resin matrix visible on the adhesive, with few or no glass fibers transferred from the substrate to the adhesive.

Stock-break failure (Figure 2.6 f) of the adherend is a result of a properly designed adhesive bond, and appears outside the joint. In this case the strength of the adherent is used at their full capacity, because in this case the adhesive has a bigger lode capacity than the substrates. A particular case of adherend failure is the failure of FRPs, in which case the FRP delaminate due to high transversal stress.

2.2 Multi-material metal to composite joints

There is a growing trend to optimize the strength, weight and durability of automotive structures by combining traditional metals with polymeric composites. Composites are more structurally efficient than metals and do not experience galvanic corrosion. Metals, however, have better damage tolerance and failure predictability than composites and are unaffected by the solvents and temperatures which tend to degrade polymers (James & Pearl, 2000).

In order to optimize the benefits provided by both types of materials, multi-material joints between metals and composite materials are increasingly being developed. Although these structures provide an excellent blend of material properties, their success depends upon the integrity of the joints. When analyzing/designing a bonded multi-material joint, there are

`

a number of considerations that must be addressed, which will be summarised in the following subsections.

2.2.1 Residual thermal stresses due to adhesives high temperature curing process

Dissimilar adherents may have very different coefficients of thermal expansion (CTE) (Table 1). Thus, temperature changes may introduce thermal stresses in addition to the externally applied loads. The adhesive curing and the resulting thermal shrinkage may also introduce internal stresses. Deformations or even cracks can appear. It is important to consider thermal effects because these generally lead to a joint strength reduction, even though in some cases the opposite happens (da Silva, et al., 2011).

Several authors have found that the stresses caused by adhesive shrinkage have much less effect on the lap-joint strength than those generated by the adherend thermal mismatch. Thermal loads are especially important when bonding adherends with different CTEs (Hart-Smith, 1973).

Table 1 Coefficients of linear thermal expansion (Ahmed, et al., 2012)

Material	Coefficients of linear thermal expansion [$m^{-6}K^{-1}$] at 20°C
High strength steel	13
Aluminum	23
Magnesium	26
CFRP	0
Polyurethane flexible adhesive	100-150

In the case of metal/CFRP joints, the metal adherend tends to shrink as the temperature decrease from the curing temperature (usually a high temperature), while the CFRP remains unmodified through all the curing process, thereby residual bond stresses will occur especially at the end of the joint. In this case one edge of the overlap will have a positive residual shear stress and the other will have a negative residual shear stress (Figure 2.7 b).

The thermal stresses are beneficial to one end but disadvantageous to the other edge of the overlap, and it can be calculated using the formula:

$$\Delta T = T_O - T_{SF} \qquad \text{Equation 1}$$

`

Where T_O is the adhesive curing temperature and T_{SF} is the stress-free temperature, also known as room temperature.

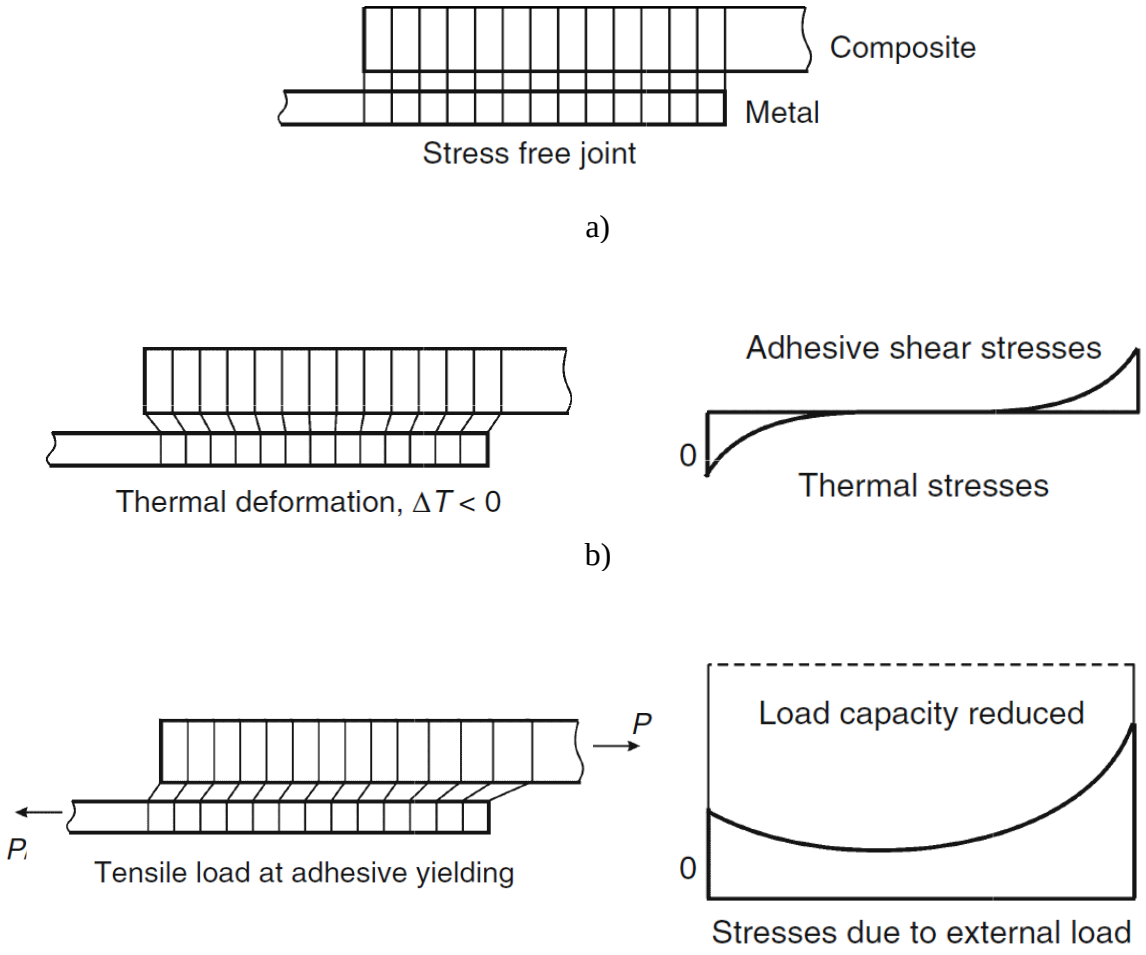

Figure 2.7 Residual thermal stresses due to adhesives high temperature curing process: a) Stress free joint, b) Thermal stress joint, c) Tensile load at adhesive yielding

By the presence of the thermal stresses, the strength of the joint will be affected by a non-nuniform stress distribution along the bonding surface (Figure 2.7c).

2.2.2 Effects of bond defects

Defects in adhesive joints include surface preparation deficiencies, voids and porosity, and thickness variations in the bonded layer. Of the various defects which are of interest, surface preparation deficiencies are probably the greatest concern. These are particularly troublesome because there are no current non-destructive evaluation techniques,

`

which can detect low interfacial strength between the bond and the adherends. Bond thickness variations usually take place in the form of thinning due to excess resin bleed at the joint edges. This leads to overstressing of the adhesive in the vicinity of the edges (Hollaway, 2005).

2.2.3 Stress distribution

Using dissimilar adherends will decrease the strength of the joint due to a non-uniform stress distribution. In order to reduce this problem, the joint needs to be designed so that the longitudinal stiffness of the adherends are equal, stiffness balanced joints (Figure 2.8 a) where $E_1 t_1 = E_2 t_2$, or the thickness of the two adherends is equal, despite the longitudinal stiffness of the adherends, where $t_1 = t_2$ (Figure 2.8 b).

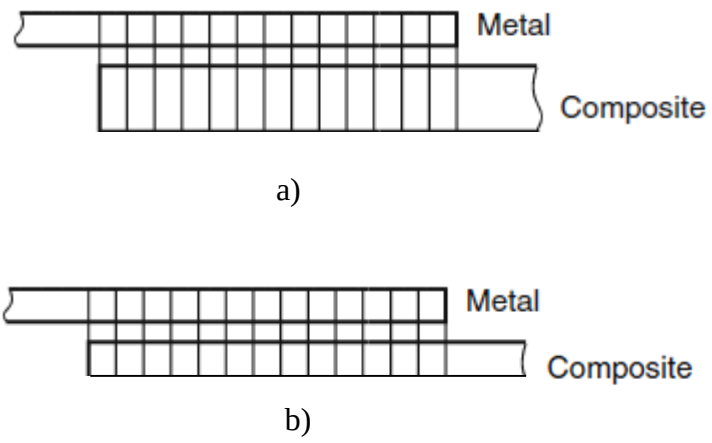

Figure 2.8 Dissimilar bonded joints: a) stiffness balanced joints, b) geometrical balanced joints

2.3 Strength prediction of bonded joints

In the adhesive bonding literature, the single lap joint (SLJ) specimens are the most studied joints due to the simple and efficient geometry to characterize an adhesive joint. However, one of the problems associated with this type of joint is the fact that the stress distribution (shear and peel) is concentrated at the ends of the overlap. This effect is further aggravated when bonding dissimilar materials as the stress is concentrated on the side where the adherend with the lowest rigidity is located. This might lead to joint premature failures at the ends of the overlap. The most common techniques to attenuate this problem are to balance the joint by increasing the thickness of the flexible adherend or the use of adherends

`

with tapers and spew fillets at the ends of the overlap. However, increasing the thickness of the adherend will increase the weight of the structure, while in the case of using tapers and spew fillets the excessive steps in the manufacturing process will led to expensive joints.

For the analysis, some simplifying assumptions are made: substrates deformation due to tension and bending only and adhesive stresses restricted to peel and shear are assumed to be constant across the adhesive layer. However, the stresses in the adhesive are not uniform because of differential straining and the eccentricity of the loading path (Kinloch, 1987).

2.3.1 Continuum mechanics

For this strength prediction approach, the maximum values of the stress, strain and strain energy that were predicted by the finite element method analyses are used forward in the failure criterion and the results are compared with the material allowed values.

Initially, the maximum principal stresses were proposed for very brittle materials whose failure mode is at right angles to the direction of maximum principal stress. This criterion ignores all the other principal stresses, even though they are not nil. Establishing the failure modes in lap joints bonded with brittle adhesives, (Adams & Mallick, 1992) predicted joint strength with this criterion. In this case, due to the stress singularities resulted on the corners of the joints, the value of the stress in the analysis depend on the mesh size. In this case, the values of stresses were calculated using Gauss point near the singularity, or extrapolation of Gauss point values to the singularity. Therefore, care must be taken when using this criterion. Although the criterion is sensitive to the mesh size used, the physical insight into the failure process is very clear, as the maximum principal stress is the most responsible for the failure of joints bonded with brittle adhesives (da Silva & Campilho, 2012).

In general, due to the production process most of the adhesive joint adherends are not sharp at the edges, instead they have a small amount of rounding. This rounding will affect the stress distribution in the area of the corner, and the joint strength in general. The adherend rounding will eliminate the stress concentration factor and facilitates the application of a stress or strain limit criterion.

The early research of Adams and Harris (Adams & Harris, 1987), demonstrated the fact that the strength of the adhesive bonding using rounding edge adherends, have increased in comparison with the sharp edge adherends. More recently the study of Zhao (Zhao, et al.,

`

2011) investigated the effect of the adherent rounding (Figure 2.9), demonstrating that the edge singularity disappears with a small rounding.

To predict the lap joint strength, shear stress haven been usually used, taking in consideration the bulk adhesive shear strength that we consider it to be the limit of the shear stress for the adhesive in the joint.

But the criteria based on stresses cannot be applied for the ductile adhesives, because they can take large loads as the adhesive starts to yield. For the case of ductile adhesives, Adams and Harris (Adams & Harris, 1987) took use of the maximum principal strain as failure criterion. This criterion of predicting the adhesive strength has also issues regarding the mesh size as previously discussion of the stress approach.

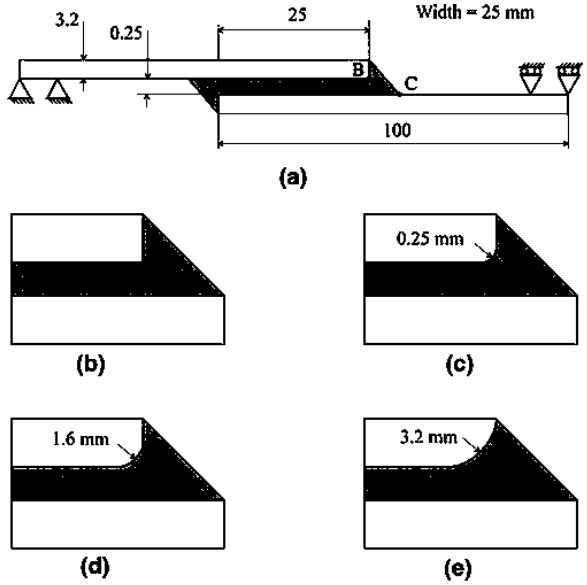

Figure 2.9 Single lap joint with rounded adherends (Zhao, et al., 2011)

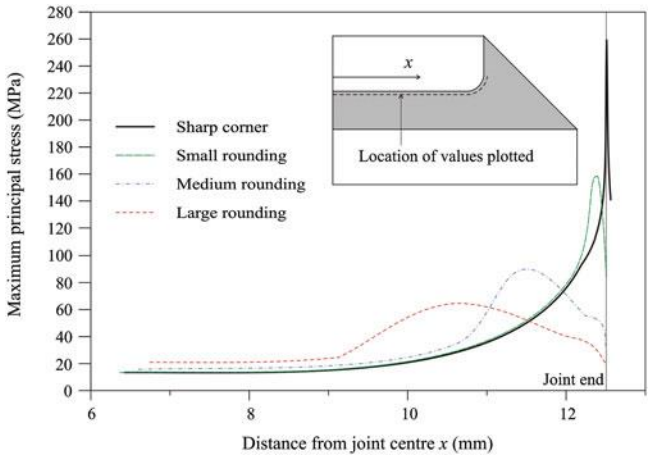

Figure 2.10 Maximum principal stresses in the adhesive with a 20 kN load (Zhao, et al., 2011)

`

The strain energy represent the area beneath the stress-strain curve, so both stress and strain are related to the strain energy. In this case we can observe that the strain energy criterion is taking in consideration both strain and stress components, so it`s more suitable as a failure criterion then using the stress or strain criterions alone.

For largely ductile adhesives, Crocombe (Crocombe & Adams, 1981), in his research of lap joints, found out that all the length of the adhesive layer yielded before it failed. So a new failure criterion was established based on the yielding of all the adhesive overlap. This criteria is very useful for very ductile adhesives, in which case the adhesive cannot stand to a higher load once it all yield. In order to achieve a global yielding before failure, the adhesive need to be very ductile.

All the criteria mentioned above can be used just for continuous structures only, they apply with difficulties once defects occur, or in case of using multi-materials in which case the analytical approach is difficult to apply and numerical solutions are employed.

2.3.2 Fracture mechanics

Criteria based on continuum mechanics assumes that the material does not have defects, and therefore the structure and material behave as a continuous body. The presence of defects or two materials with protuberances infringes the continuum mechanics principles. In the other hand, fracture mechanics assumes the structure not to be continuous, allowing manufacture defects or any other damage caused during its life at work (da Silva & Magalhaes, 2007).

Delamination, debonding, cracks and others imperfections present within materials, often are points of stress concentration and therefore initiation points for fracture to occur and propagate and cause the failure of the component. This method evaluates if the size of each defect does not overcome the critical fracture size leading to structural failure. Fracture mechanics relies on two basic criteria, both implemented for the study of materials with cracks. (Adams, 2005). These criterions are stress intensity factor and another one is based on energetic concepts.

The stress intensity factor K is a scalar parameter that defines the changes that occur in the neighborhood of the crack tip of the stress. For a better understanding of the stress intensity factor K, we have to know the loading mode that lead to fracture.

`

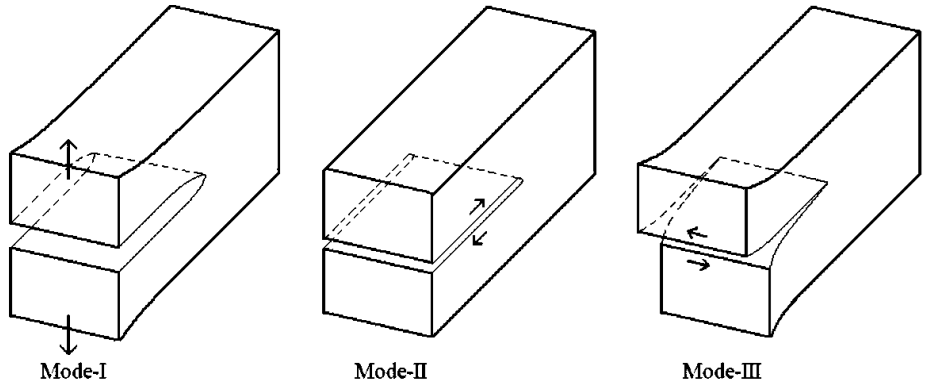

Figure 2.11 Fracture modes

In Figure 2.11 the three different loading modes that lead to the fracture are illustrated. Mode I represents the opening mode, mode II mode III are both shearing modes. For mode I and mode III the crack surfaces slide perpendicularly to the crack tip, and for mode II the crack surfaces slide parallel to the crack tip.

The stress intensity factor characterizes the stress at the crack tip and measures the propagation capability. (Chaves, 2013) For mode I the stress intensity factor can be calculated with the following equation:

$$K_I = Y\sigma_r\sqrt{\pi a} \qquad \text{Equation 2}$$

where Y, is a function depending on geometry and load distribution;

σ_r, is the loading stress;

a, is the crack length.

In this case the crack will occur when:

$$K_I = K_{Ic} \qquad \text{Equation 3}$$

Where K_{Ic} is called mode I fracture toughness and it's characterized by the ability of the material to prevent the crack growth. When the value of K_I is under the value of mode I fracture toughness, the crack will not propagate.

`

2.3.3 Cohesive zone models

For a cohesive damage analysis no initial crack is needed and its propagation is the result of a simulated degradation of the material. The introduction of the FEA in conjunction with the cohesive mixed-mode damage model is a combination of both continuum and fracture mechanics by including both the strength and the energy parameters to characterize the debonding process (da Silva & Öchsner, 2008).

The cohesive zone approach (CZM) can be better analyzed in a detailed view of the crack tip (Figure 2.12).

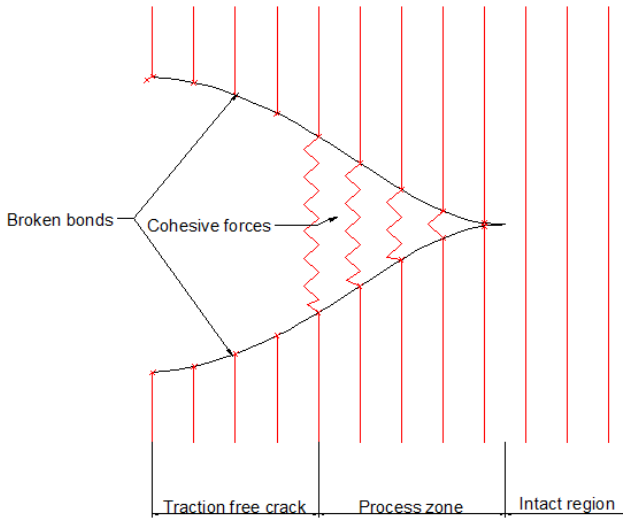

Figure 2.12 Process zone of crack

The process zone illustrated in the Figure 2.12 is a transition zone in crack propagation between the free traction crack and the linear elastic zone. The cohesive forces between the crack edges are represented with the springs. The edge of the crack is drawn like sharp tip of a water drop to show that the cohesive effect is dominant in the cohesive zone only.

For the distribution of the stresses in the process zone, the bilinear model developed by Barenblatt (Barenblatt, 1959) is frequently used, as illustrated in Figure 2.13.

`

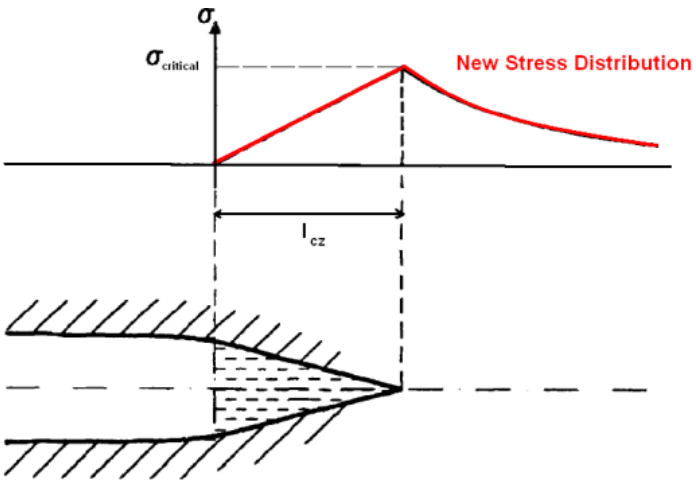

Figure 2.13 Process zone stress distribution (Mi, et al., 1998)

Researches have been made in order to predict the strength of the adhesive bonded joint focused on the numerical simulation of damage and growth. The results were very accurate in predicting a numerical crack growth. Different laws of the cohesive zone were established (Figure 2.14).

CZM are based on a relationship between stresses and relative displacements (in tension or shear) connecting paired nodes of cohesive elements (Figure 2.14), to simulate the elastic behavior up to the cohesive strength and subsequent softening, to model the degradation of material properties up to failure. The shape of the softening region can also be adjusted to conform to the behavior of different materials or interfaces (Campilho, 2009).

The areas under the traction-separation laws in tension or shear (G_n or G_s, respectively) are equaled to the fracture toughness in tension (G_{cn}) or in shear (G_{cs}), by the respective order. Under pure loading, damage grows at a specific integration point when stresses are released in the respective damage law. Under a combined loading, stress and energetic criteria are often used to combine tension and shear (Dugdale, 1960). The triangular law assumes an initial linear elastic behavior followed by linear degradation.

The triangular and exponential cohesive laws are used especially for brittle adhesives, while for ductile adhesives the trapezoidal cohesive damage model is used.

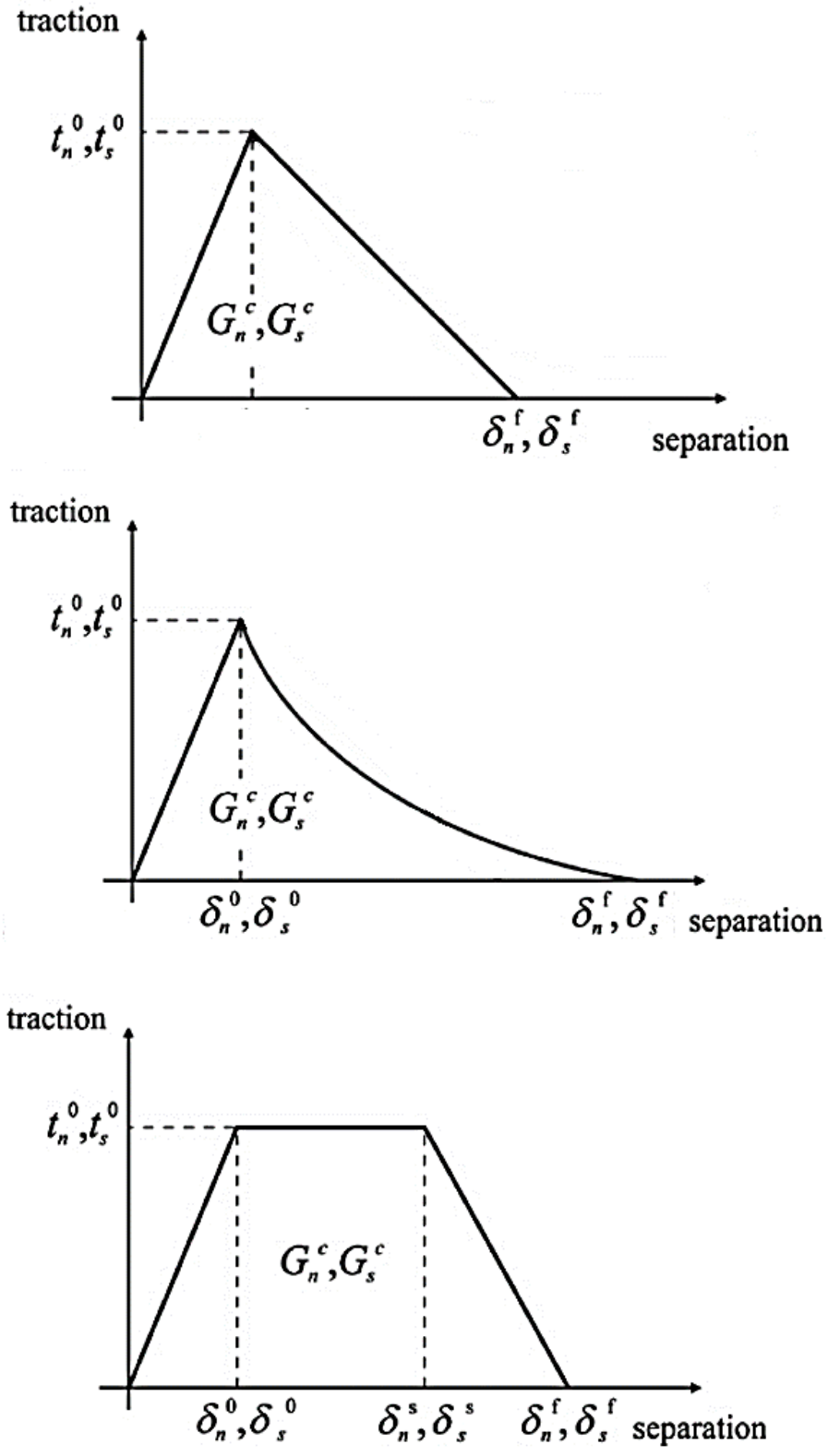

Figure 2.14 Cohesive laws

`

3 Experimental analysis

CFRP parts are increasingly being selected in combination with metals for instance aluminum and hard steel in order to reduce weight without compromising passenger safety. In this thesis, CFRP with hard steel and aluminum single lap joints were tested (unbalanced joints). The joint parameters evaluated were the overlap length, the adherend thickness and the adherend axial stiffness.

While balanced joints are widely used, unbalanced joints are increasingly needed in automotive applications. Thus, it is important to understand how the joint efficiency of such joints is affected.

The most effective method to obtain the strength of an adhesive joint is to test the specific joint at the operational conditions. The manufacture process of the adhesive joints is also a very important issue because it presents many important aspects such as the surface treatment, control of adhesive layer thickness and the cure schedules.

3.1 Materials

3.1.1 Adherends

In order to achieve lightweight construction, without compensating on rigidity, automakers have been investigating the replacement of steel with aluminum, magnesium, composites, and foams (Chiaberge, 2011).

The materials used in this study will be described in the following subsections.

3.1.1.1 High strength steel

Advanced iron and steel technologies have seen considerable development over the past decade and are frequently included into new designs and redesigns by all automakers. The steel industry and component suppliers are investing heavily in innovation. The result of the investment have numerous examples of successful, cost-effective use of stainless steel, new formulations of iron, high-strength steels, and an associated variety of new design, fabrication, and assembly techniques. Applications include not only vehicle bodies, but also engine, chassis, wheels and many other parts. The usages commonly demonstrate weight reduction plus simultaneous improvements in strength, stiffness, and other structural

`

performance characteristics. Thus, a clear potential exists to affordably make vehicles lighter and safer at the same time (DeCicco, 2005).

High-strength steel (HSS) is an alloy that can be categorized by its yield strength. Standard HSS has a yield strength between 450 MPa and 600 MPa, while ultrahigh strength-steel has values of the yield strength over 600 MPa, in some cases higher than 1000 MPa.

HSS can cost more than the traditionally used mild-steel in the automotive industry, but the higher strength of HSS allows them to use a lower thickness of the same material in order to achieve the needed performance required.

For this study, the mechanical properties used for the HSS are showed in Table 2. The thicknesses selected for the HSS in order to perform SLJs are 1 mm and 2 mm thick substrates, thicknesses mostly used automotive industry for body structure manufacture.

Table 2 Mechanical properties of HSS (Banea et al, 2015a)

Young´s modulus [GPa]	210
Tensile strength [MPa]	1300
Yielding stress [MPa]	1050
Tensile strain [%]	14-17

3.1.1.2 Aluminium

There are a broad range of opportunities for employing aluminum in automotive powertrain, chassis, and body structures. The use of aluminum offers considerable potential to reduce the weight of an automobile body (Cole & Sherman, 1995).

The aluminum of choice was the 6082-T651 alloy. It is a high strength alloy and also has very good fatigue resistance. The 6082 alloy's main applications are automotive industry and other parts of the transportation industry.

The mechanical properties of the aluminum used for the adhesive bonding are mentioned in Table 3, while the thickness of the aluminum adherends used are 2 mm and 3 mm.

`

Table 3 Mechanical properties Aluminum 6082-T651 (Campilho, et al., 2011)

Young´s Modulus [GPa]	70
Tensile strength [MPa]	324
Yielding stress [MPa]	264
Tensile strain [%]	21

3.1.1.3 Carbon fiber reinforced plastic

CFRP were manufactured using unidirectional (0°) carbon-epoxy pre-preg with 0.15 mm lay-up, produced by the hand lay-up of the pre-preg layers and cured in a hot press at high temperature.

Manufacturing the CFRP specimens involved the following steps:

1. Unfreezing the pre-preg roll stored in freezer to prevent resin activation;

2. Cutting 300 mm x 300 mm pre-preg squares;

3. Manual lay-up of the pre-preg layers, maintaining the unidirectional fiber alignment until obtaining the desired thickness of the CFRP plate. In this study 14 carbon-epoxy lay-ups were superposed one at the time in order to obtain unidirectional 2.1 mm thick CFRP. During this step, after removing the paper and the teflon coating, the the lay-ups were heated using a heat gun, in order to obtain a good adhesion between the layers, followed by the pressure application on the entire stack;

4. After manually superposing all the layers, the CFRP plate is placed in a mold containing two plates of aluminum and a spacer (Figure 3.11). To prevent the CFRP from sticking to the aluminum plates, three coats of releasing agent, Loctite® Frekote 770-NC™, were applied on the aluminum plates and spacers;

`

Figure 3.1 Mold for hot press curing

5. The mold containing the CFRP plate is introduced in the hot press and cured at a curing cycle recommended by the supplier. This cycle consisted in a gradual heating with 4°C/min, reaching the 140 °C temperature, maintaining this temperature for one hour at 5 bar of pressure and gradually cooling the CFRP using the same slop as in the process of heating;

6. After the curing process, the CFRP plates were cut into specimen size needed using a disc cutting machine.

`

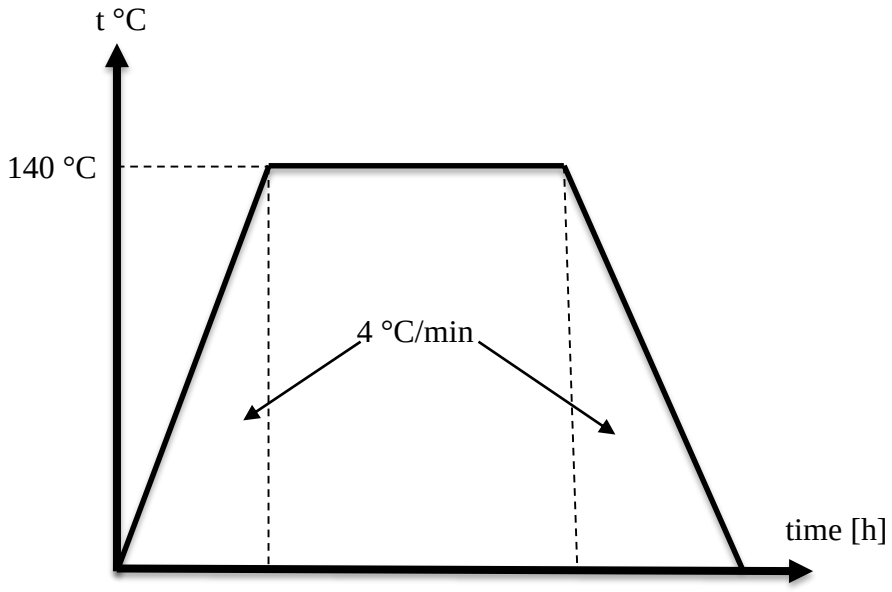

Figure 3.2 CFRP curing cycle

3.1.2 Adhesive

The adhesive used in this study, SikaForce®7888 L10 is a two-component polyurethane and fast curing structural adhesive, which cures by the chemical reaction between its two components. SikaForce®7888 L10 adhesive is supplied by Sika (Portugal), and it combines the high strength of epoxy adhesives and high deformation of elastomers.

SikaForce®7888 L10 is a structural adhesive mostly used in the automotive industry because of the characteristics that make it attractive like the rapid strength development and fast cure. Beside these advantages, this adhesive also can cure at room temperature, providing the same strength and elongation to a wide variety of substrates.

According to the supplier specification, the adhesive fully cures at room temperature in 48 hours, but in order to obtain the fully strength of the joint, it will need 1 week of curing at RT. The properties of SikaForce®7888 L10 were obtained by performing test with the bulk specimens of adhesive. From the test the bulk specimen test and form the stress-strain curve the mechanical property of the adhesive were determined (Figure 3.3).

`

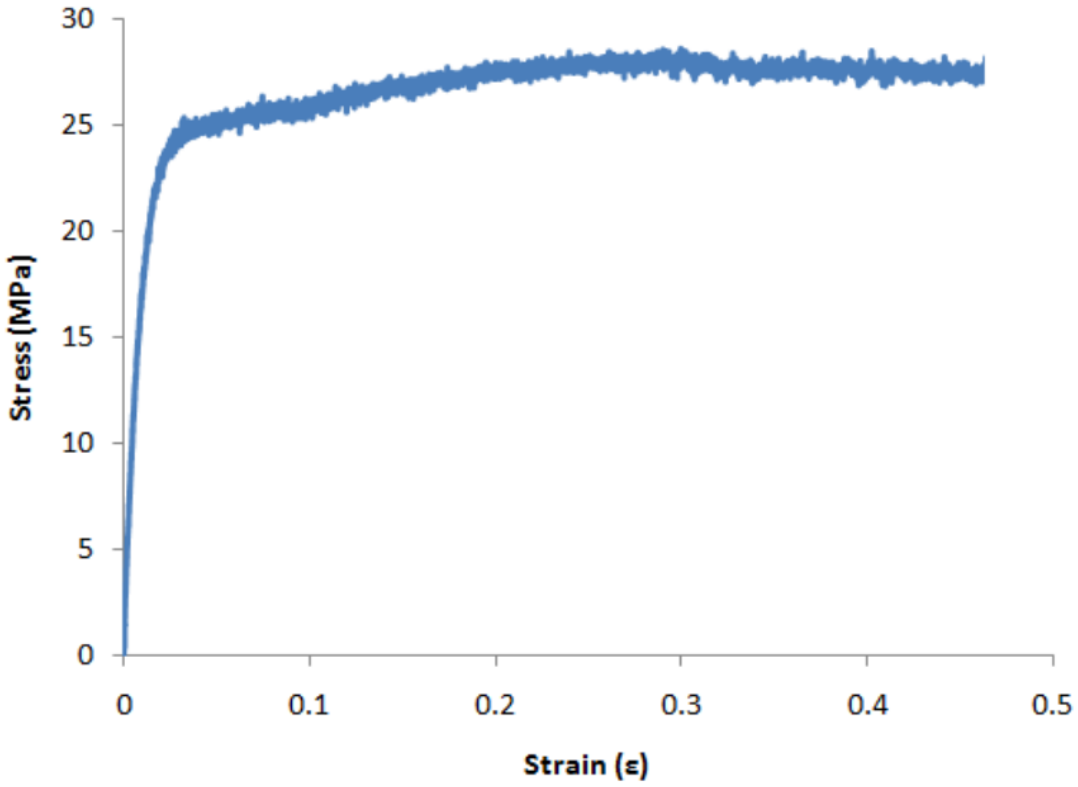

Figure 3.3 Stess-strain curve of the SikaForce®7888 adhesive (Neto, 2011)

Table 4 Mechanical properties of SikaForce®7888 L10 (Banea et al, 2015a)

Property	Value
Young`s modulus E [MPa]	2530
Transverse elastic modulus G [MPa]	720
Tensile stress tn^0 [MPa]	31
Tensile shear stress ts^0 [MPa]	20
Mode I fracture toughness Gn^c [N/mm]	1.2
Mode II fracture toughness Gs^c [N/mm]	8.72

3.2 Joint geometry

The main objective of the present thesis is to investigate the behavior of multi-material joints for automotive applications by using various combination of adherends. Several important factors, such as the overlap length, adherend thickness and stiffness, influencing the strengths of multi-material adhesive joints were investigated. To accomplish this

`

objective single lap joints were manufactured and tested, using CFRP, aluminum and high strength steel adherends.

Regarding the possibilities of combining dissimilar material joint, the following possibilities were studied: CFRP/HS and CFRP/Al.

3.2.1 CFRP/HSS SLJs

HSS substrates characterized by a high tensile strength with a thickness of 1 mm and 2 mm and 25 mm width and CFRP with a thickness of 1.2 mm and 2.1 mm were used to manufacture unbalanced SLJs. The specimen geometries are illustrated in Figure 3.4, in which 12.5 mm, 25 mm and 50 mm overlaps were used. All the specimens configurations manufactured are illustrated in Table 5.

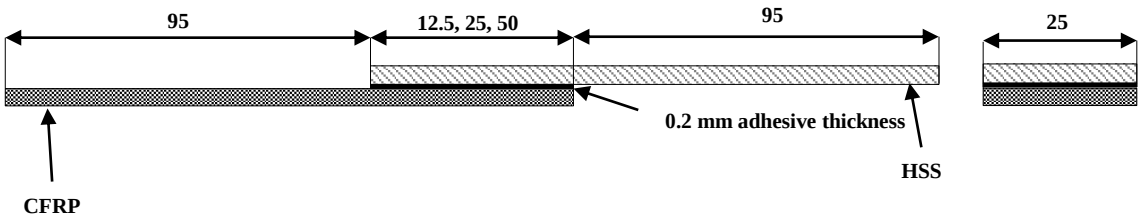

Figure 3.4 CFRP/HSS SLJs configuration

Table 5 CFRP/HSS SLJs combinations

HSS adherend thickness [mm]	CFRP adherend thickness [mm]	Overlap [mm]
2	2.1	12.5
		25
		50
1		12.5
		25
		50
1	1.2	12.5
		25
		50

A number of four SLJs were manufactured for all configuration listed above, but only the best three results were taken into the consideration for average failure load calculation.

`

3.2.2 CFRP/Al SLJs

Aluminum substrates are characterized by a lower tensile strength than the HSS used, with thicknesses of 2 and 3 mm and 25 mm width were used to manufacture SLJs with CFRP substrates of 2.1 mm thick (Figure 3.5).

The only overlap configuration used for the CFRP/Al joint is the 25 mm, due to the large plastic deformation that can occur for the 50 mm overlap, fact analytically proved in the following calculation:

$$\tau_a = \frac{P}{Lb},\ 20 = \frac{P}{50 \cdot 25} \qquad \text{Equation 4}$$

$$P = 25000 \text{ N}$$

Where

τ_a is the shear stress of the adhesive;

P is the load;

L is the overlap length;

b is the width of the adhesive.

For the value of the load calculated, the stress in the aluminum adherent will be:

- For 2 mm thick aluminum:

$$\sigma = \frac{P}{tb} = \frac{25000}{2 \cdot 25} = 500 \text{ MPa} \qquad \text{Equation 5}$$

- For 3 mm thick aluminum:

$$\sigma = \frac{P}{tb} = \frac{25000}{3 \cdot 25} = 333 \text{ MPa} \qquad \text{Equation 6}$$

The stress predicted for the aluminum adherends, in the analytically calculation above, for the 50 mm overlap joint, exceeded the yielding stress of the aluminum mentioned in Table 3.

Thus, the only overlap studied for the CFRP/Al joint was the 25 mm overlap, with the configurations mentioned in Table 6.

`

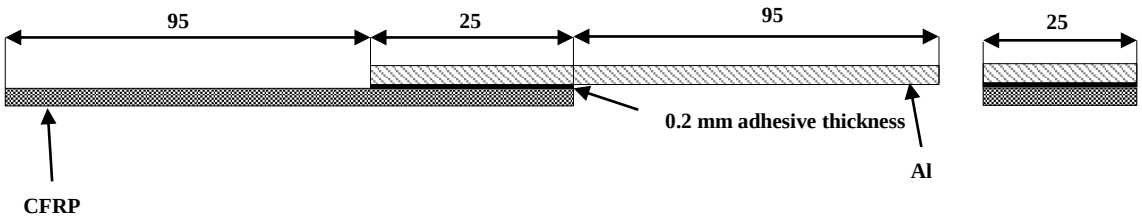

Figure 3.5 CFRP/AL SLJs configuration

Table 6 CFRP/Al SLJs configurations

Aluminum adherend thickness [mm]	CFRP adherend thickness [mm]	Overlap [mm]
2	2.1	25
3		25

A number of four SLJs were manufactured for each configuration listed above.

3.3 Joint fabrication

A good specimen is fundamental to achieve cohesive failure and obtain the best test data. Therefore, manufacture of specimens must be very well attended. The specimens manufacture should be done according to the following steps:

1. **Mould preparation**

The mould should be cleaned before introducing the specimens and all adhesive residues that may exist should be removed using an aluminum spatula. Further the mould needs to be clean using a napkin soaked in acetone, removing the dirt and dust that may exist on the surfaces of the mould. After cleaning the mold was placed in the hot press and a temperature of approximately 45° C was applied. After 10 minutes it was took out from the hot press using thermal gloves. Releasing agent was three times applied against all surfaces of the mould using a brush. The temperature will ensure a rapid evaporation of the releasing agent. Loctite® Frekote 770-NC™ insures that the excessive adhesive does not adhere to the mould;

`

2. Substrate preparation

After the CFRP plates (see section 3.1.1.3) were cut into substrates with specify dimensions given by specimens overlap (107.5 mm, 120 mm and 145 mm), the overlap length on the CFRP substrate is abrased using sandpaper at 45°, creating a X pattern (

Figure 3.6), until the surface of the CFRP becomes mate, in order to obtain a good adhesion. Care was taken to not affect the integrity of the fibers. The specimen were cleaned with a napkin soaked in acetone. The specimen was cleaned repeatedly with clean napkin until there is no trace of carbon fiber left on the surface of the napkin.

Figure 3.6 CFRP substrate abrased

For the metal substrates, after being cut with the same dimensions as the CFRP substrates, the surface of the overlap must be sandblasted in order to achieve a good adhesion on the metal surface.

Figure 3.7 Metal substrates preparation

After that the specimens were placed into a mould that guaranties the correct position of both the substrates, as is illustrated in Figure 3.8. The spacers were used in order to ensure the correct thickness of the adhesive layer, the correct overlap and to prevent edge fillets to

appear. Also the screws and the pressure blocks ensure the correct overlap and prevent the two substrates from sliding on each other.

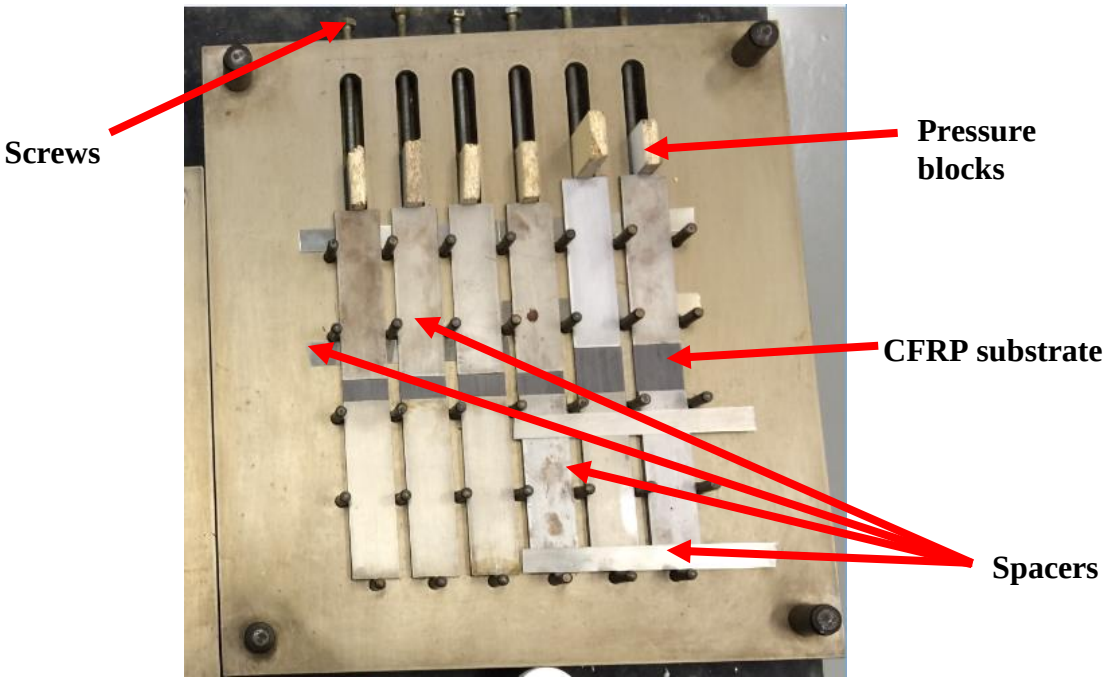

Figure 3.8 Mould for manufacturing of SLJs

Then the SikaForce®7888 L10 adhesive was applied using a compressed air pistol, taking care that the two components of the adhesive are equally distributed. After mixing the two part adhesive, it was applied on both adherends that were superpose in order to create the joint as showed in Figure 3.9.

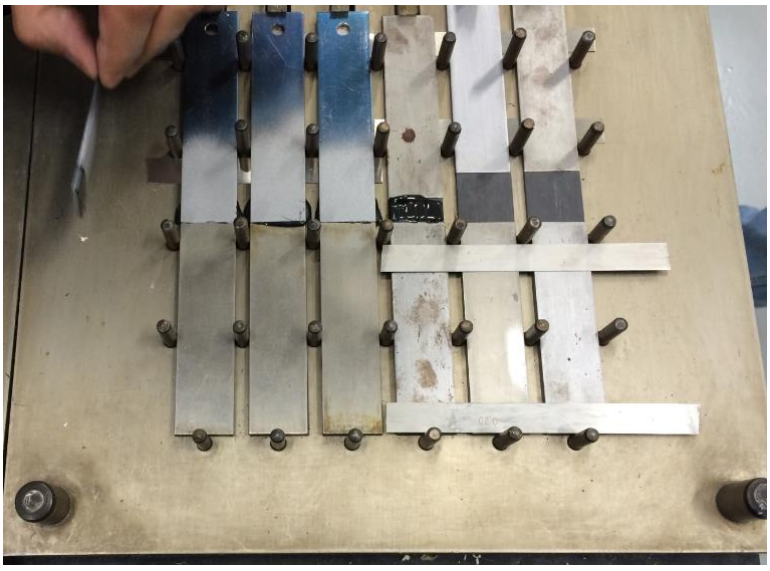

Figure 3.9 Adhesive layer application

`

After applying the adhesive on the surface of the adherends, the upper part of the mould is applied to avoid displacement of the adherends and to assure the correct thickness. At the end, pressure was applied to ensure homogenization and the excess adhesive overflow.

3. Curing of the adhesive

The specimens were hold inside the mould for 24 hours in order for the adhesive to cure at RT. The adhesive fully cures in 24 hours, but in order to obtain the fully strength of the joint, the joints were allowed to cure for 1 week.

4. Removal and cleaning

After 24 hours of curing inside the mould, the specimens were removed and the excessive adhesive was removed using a file and sandpaper.

5. Preparation for testing

Finally 25 mm x 25 mm alignment tabs with the same thickness of the substrate were bonded at the end of each joint to ensure that the loading of the machine is collinear with the specimen.

3.4 Testing procedure

The specimens were tested according to standard [ASTM D1002-01], in an INSTRON® model 3367 universal testing machine (Norwood, Massachusetts, USA) with a capacity of 30 kN, at room temperature and constant displacement rate of 1 mm/min. The different griping system used for holding the specimens are presented below.

3.4.1 Grips for CFRP/HSS joints

For the HSS substrate, due to the high strength of the material, bonding aligning tabs are not necessary, so a pin grip was used to hold the HSS substrate in order to prevent the damage of the wedge-grips. The grip used for the HSS adherend is showed in Figure 3.10 a, b. As it can be seen, two fixing blocks are placed on each side of the adherend while the four screws insures the holding and they prevent the slipping of the substrate while testing. The

`

unbounded tab is applied and hold together by the fixing bolt, in order to insure that the loading of the machine is collinear with the specimen. Finally, the fixing shaft will go on the testing machine.

For the CFRP adherend, 25 mm x 25 mm alignment tabs with the same thickness as the HSS were bonded in order to fix the specimens with mechanical wedge-action grip as showed in Figure 3.10 b.

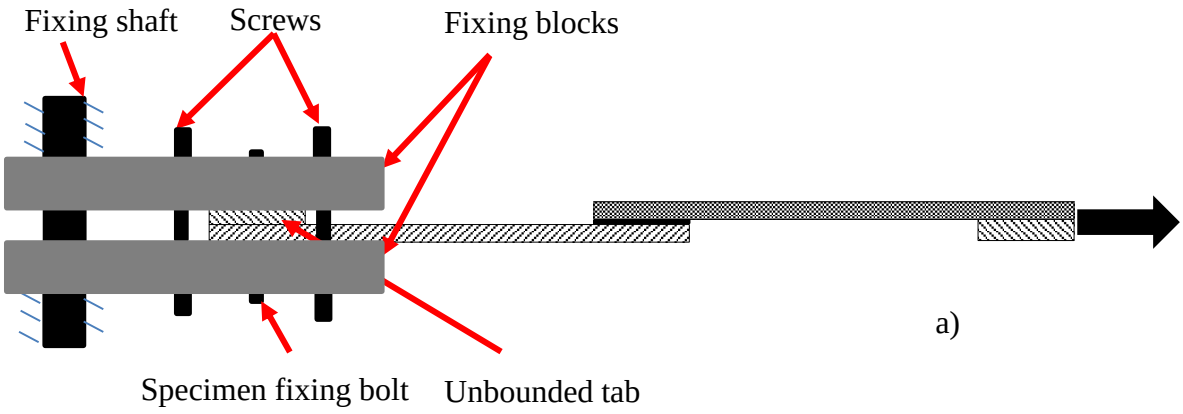

b)

Figure 3.10 CFRP/HSS specimen grips: a) Schematic representation, b) Grips for CFRP/HSS joints

3.4.2 Grips for CFRP/Al joints

In order to test the CFRP/Al specimens, alignment tabs were bonded on the both end of the substrates, and two mechanical wedge-action grips were used to fix the specimens (Figure 3.11).

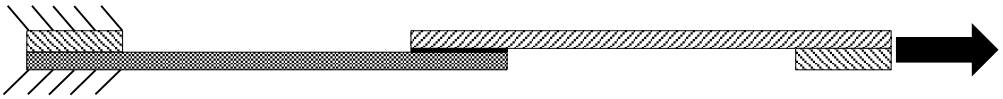

Figure 3.11 CFRP/Al specimen grips

3.5 Experimental results

In this section, the experimental results of multi-material single lap joints for which the two adherends could have different geometries and/or mechanical properties (joints referred to as "unbalanced") compared to "balanced" joints (similar adherend geometry and mechanical properties) are presented.

3.5.1 CFRP/HSS SLJs

3.5.1.1 CFRP (2.1 mm)/HSS (1 mm)

Load-displacement curves for 12.5 mm overlap can be seen in Figure 3.12. A good repeatability of the tests results can be observed.

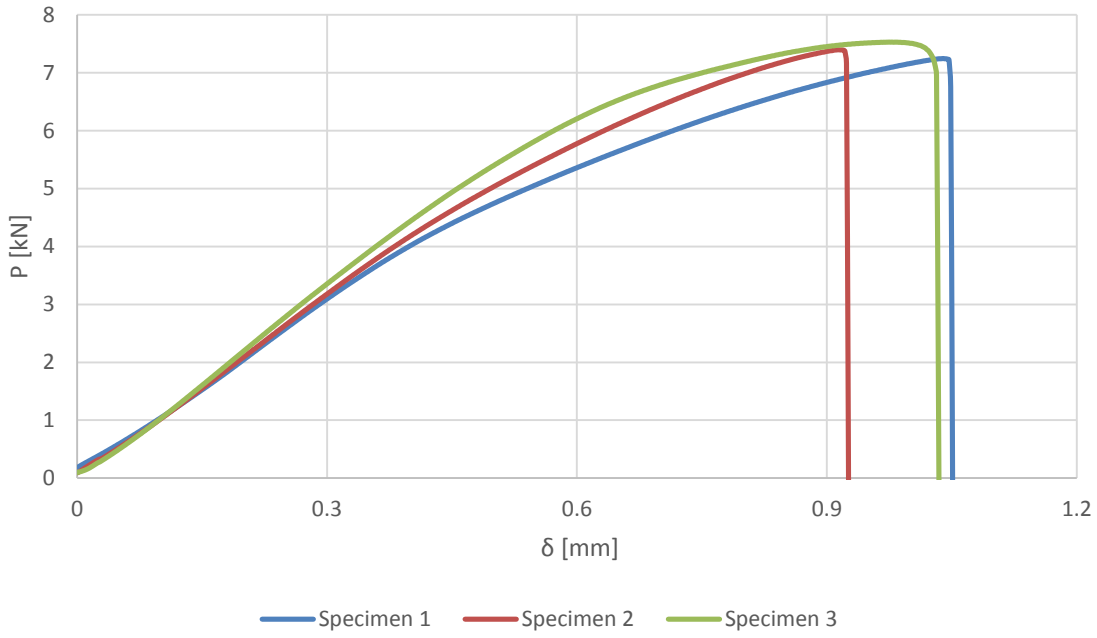

Figure 3.12 CFRP (2.1 mm)/HSS (1 mm) $P - \delta$ curves for 12.5 mm overlap

`

The failure mode for the 12.5 mm overlap joints is shown in Figure 3.13. A cohesive failure mode close to the HSS interface was observed.

Figure 3.13 Failure modes of CFRP (2.1 mm)/HSS (1 mm) 12.5 mm overlap SLJs tested specimens

The results obtained after testing the CFRP (2.1 mm)/HSS (1 mm) specimens are summarized in Table 7.

Table 7 Experimental results of CFRP (2.1 mm)/HSS (1 mm) 12.5 mm overlap SLJs

Sample no.	Failure load (kN)	Average shear stress (MPa)	Displacement (mm)
1	7.24	23.18	1.04
2	7.39	23.66	1.03
3	7.53	24.09	0.98
Average	**7.39**	**23.64**	**1.01**
Standard deviation	**0.14**	**0.45**	**0.03**

Load-displacement curves for 25 mm overlap can be seen in Figure 3.14.

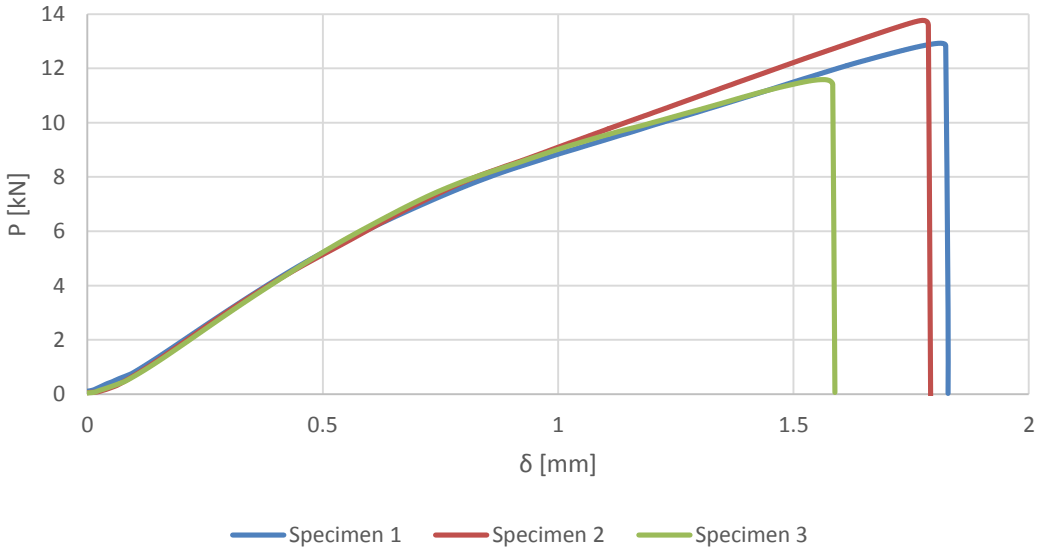

`

Figure 3.14 CFRP (2.1 mm)/HSS (1 mm) $P - \delta$ curves for 25 mm overlap

Failure mode of the 25 mm overlap length joints is illustrated in Figure 3.15. Similar to 12.5 mm overlap, a cohesive failure close to the HSS interface was observed. Even though the failure looks like a mixed mode failure, a fine layer of adhesive can be observed on the HSS adherend surface.

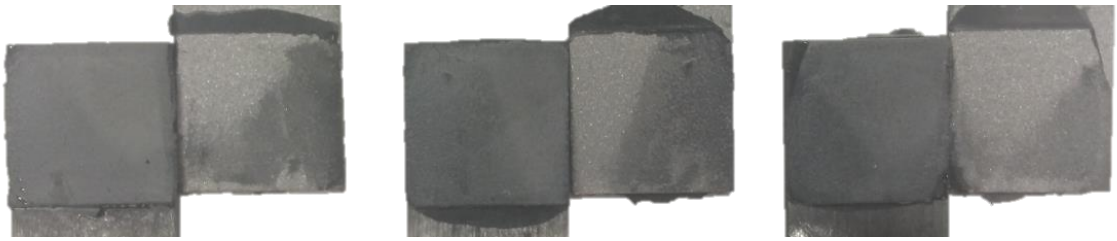

Figure 3.15 Failure modes of CFRP (2.1 mm)/HSS (1 mm) 25 mm overlap SLJs tested specimens

The results obtained after testing the specimens are summarized in Table 8.

Table 8 Experimental results of CFRP (2.1 mm)/HSS (1 mm) 25 mm overlap SLJs

Sample no.	Failure load (kN)	Average shear stress (MPa)	Displacement (mm)
1	12.93	20.68	1.81
2	13.77	22.03	1.77
3	11.59	18.54	1.56
Average	**12.76**	**20.42**	**1.72**
Standard deviation	**1.10**	**1.76**	**0.14**

For the 50 mm overlap, the load-displacement curves can be seen in Figure 3.16.

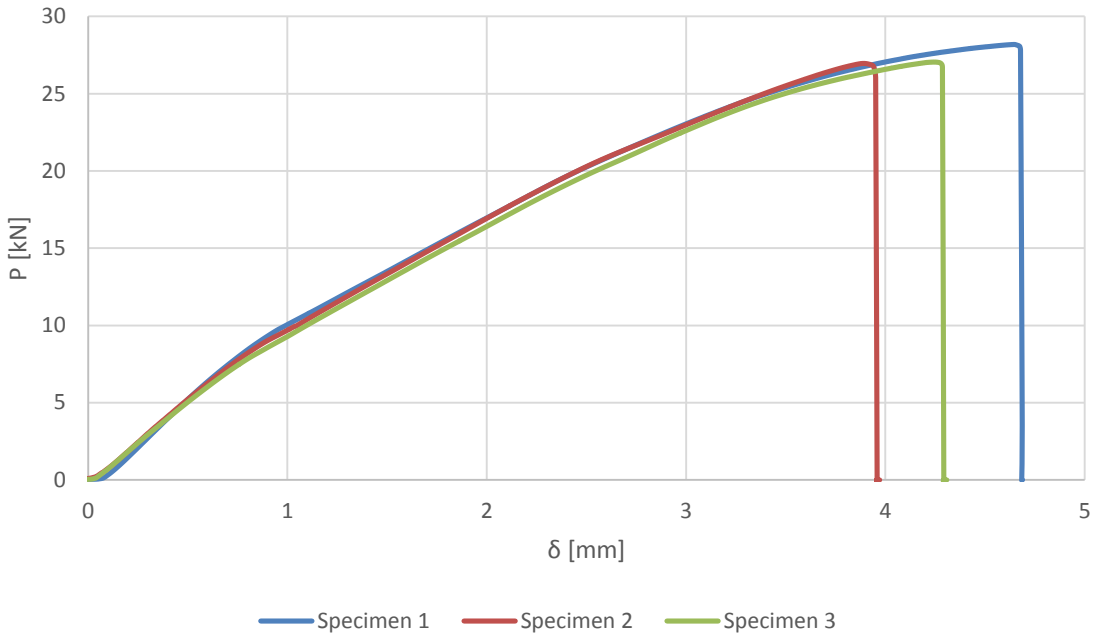

Figure 3.16 CFRP (2.1 mm)/HSS (1 mm) $P - \delta$ curves for 50 mm overlap

After the tests, the failure modes were evaluated visually. Similar to 12.5 and 25 mm overlap, a cohesive failure mode, close to the interface, was observed.

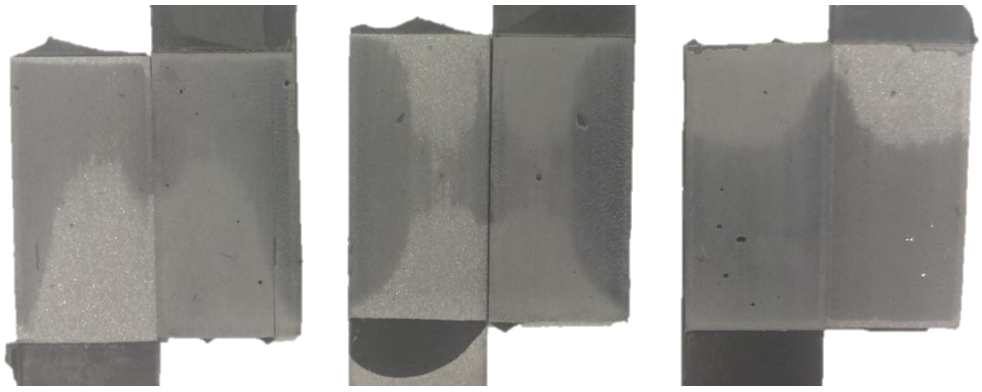

Figure 3.17 Failure modes of CFRP (2.1 mm)/HSS (1 mm) 50 mm overlap SLJs tested specimens

Furthermore, analyzing in more detail the overlap surface of the 50 mm overlap tested specimens, it can be seen that the failure occurred very close to the interface in the HSS substrate (see the light grey area Figure 3.18).

`

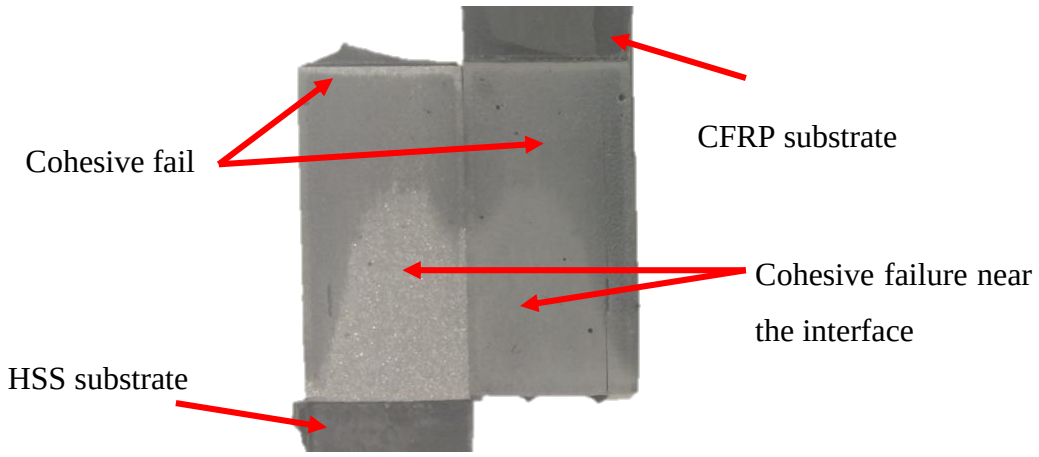

Figure 3.18 Failure mode of CFRP (2.1 mm)/HSS (1 mm) SLJs

The results obtained after testing the specimens are summarized in Table 9.

Table 9 Experimental results of CFRP (2.1 mm)/HSS (1 mm) 50 mm overlap SLJs

Sample no.	Failure load (kN)	Average shear stress (MPa)	Displacement (mm)
1	28.19	22.55	4.64
2	26.96	21.57	3.90
3	27.05	21.64	4.24
Average	**27.40**	**21.92**	**4.26**
Standard deviation	**0.68**	**0.55**	**0.37**

It should be noted that, for this case, the yielding stress of the HSS wasn`t reached so for all the overlap lengths, thus the deformation of the adherends was in the elastic zone. Also, neither the delamination of the CFRP adherend appeared.

Representative curves for all the overlap lengths were plotted in Figure 3.19. It can be seen that the failure load increased almost proportional with the overlap length.

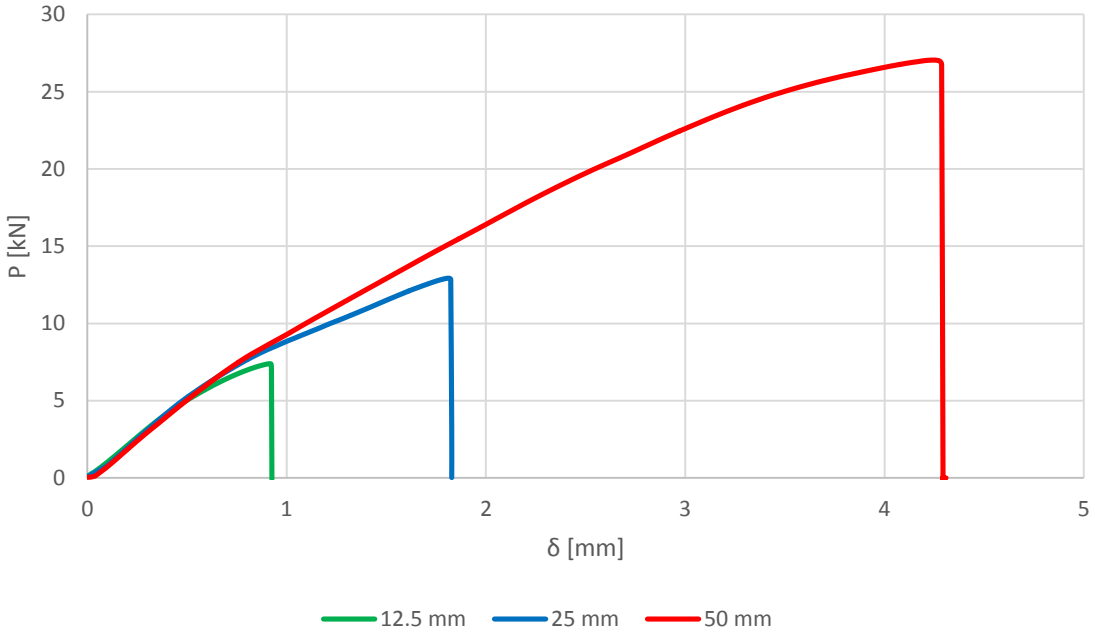

Figure 3.19 CFRP (2.1 mm)/HSS (1 mm) representative load-displacement curves

3.5.1.2 CFRP (2.1 mm)/HSS (2 mm) SLJs

For the 12.5 mm overlap of the joint between the geometric balanced CFRP (2.1 mm) and HSS (2 mm) steel joints, the results obtained are comparable with the case studied before (CFRP (2.1 mm)/HSS (1 mm)). The obtained load-displacement curves are illustrated in Figure 3.20, while the experimental data obtained is summarized in Table 10.

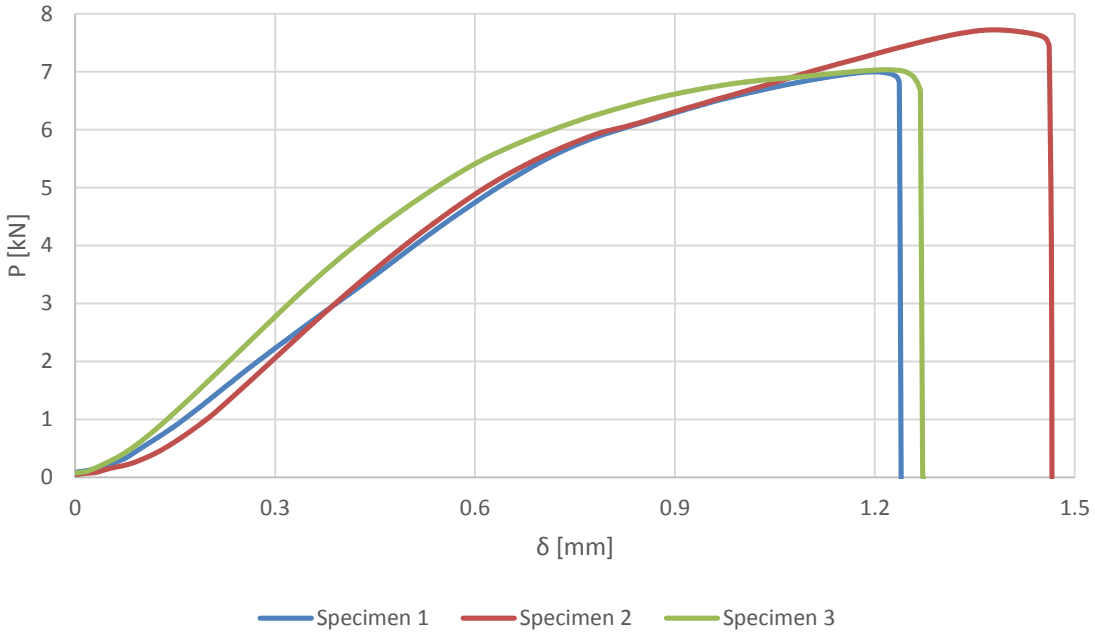

Figure 3.20 CFRP (2.1 mm)/HSS (2 mm) $P - \delta$ curves for 12.5 mm overlap

`

Failure mode of the 12.5 mm overlap length joints is illustrated in Figure 3.21. By visually inspection of the failure surfaces, a cohesive failure mode was observed for all the joints.

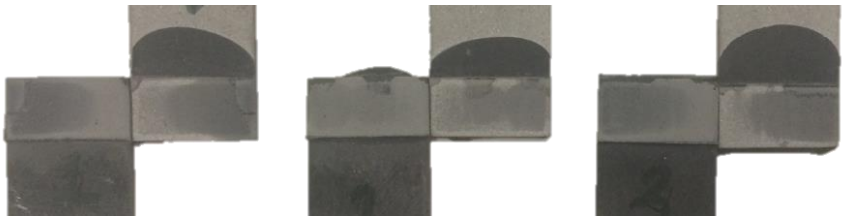

Figure 3.21 Failure modes of CFRP (2.1 mm)/HSS (2 mm) 12.5 mm overlap SLJs tested specimens

The results obtained after testing the specimens are summarized in the Table 10.

Table 10 Experimental results of CFRP (2.1 mm)/HSS (2 mm) 12.5 mm overlap SLJs

Sample no.	Failure load (kN)	Average shear stress (MPa)	Displacement (mm)
1	7.00	22.40	1.22
3	7.72	24.72	1.43
4	7.04	22.51	1.27
Average	**7.25**	**23.21**	**1.31**
Standard deviation	**0.41**	**1.31**	**0.11**

In the case of 25 mm overlap, the load-displacement curves are plotted in Figure 3.22. The experimental results gave an average failure load of the joint of 14.50 kN with a 0.6 kN standard deviation.

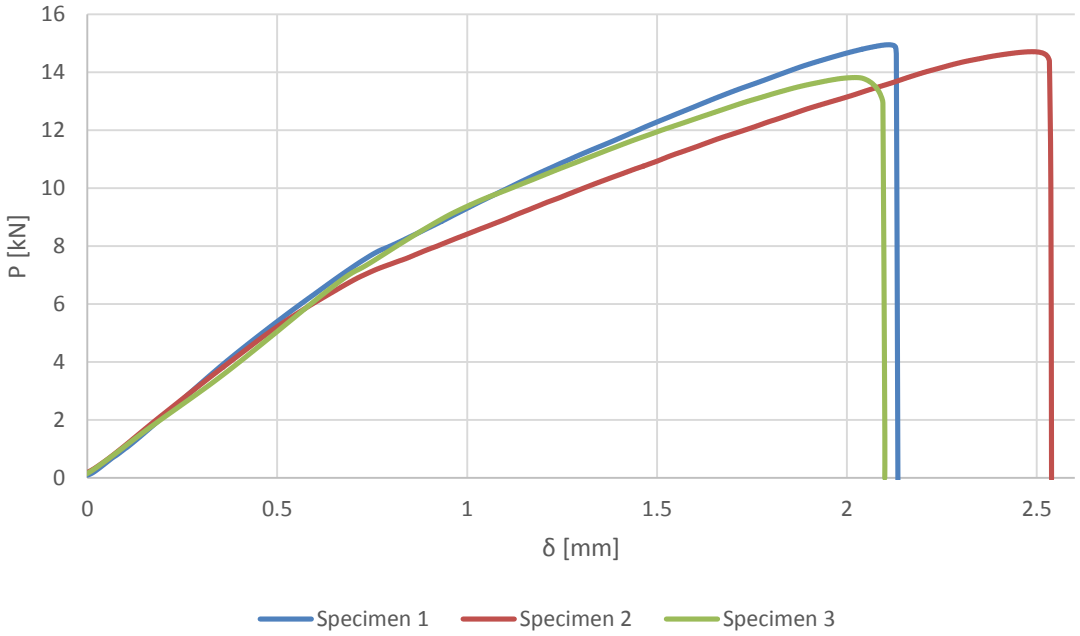

Figure 3.22 CFRP (2.1 mm)/HSS (2 mm) $P - \delta$ curves for 25 mm overlap

Failure mode obtained after testing the 25 mm overlap length joints is illustrated in Figure 3.23. Similar to 12.5 mm overlap length a cohesive failure mode was observed.

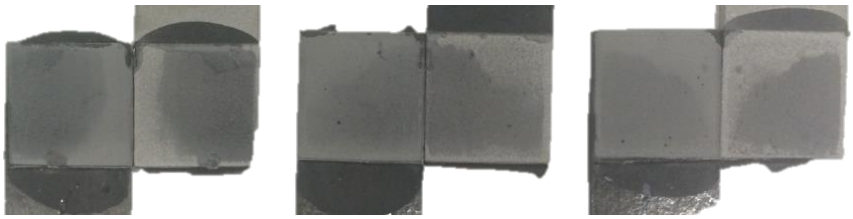

Figure 3.23 Failure modes of CFRP (2.1 mm)/HSS (2 mm) 25 mm overlap SLJs tested specimens

The results obtained after testing the specimens are summarized in Table 11.

Table 11 Experimental results of CFRP (2.1 mm)/HSS (2 mm) 25 mm overlap SLJs

Sample no.	Failure load (kN)	Average shear stress (MPa)	Displacement (mm)
1	14.96	23.95	2.13
2	14.72	23.54	2.54
3	13.82	22.12	2.10
Average	**14.50**	**23.20**	**2.26**
Standard deviation	**0.60**	**0.96**	**0.24**

`

For the 50 mm overlap (Figure 3.24), the average load obtained was 28.44 kN, a standard deviation value of 0.68 kN, and the values obtained are represented in Table 12.

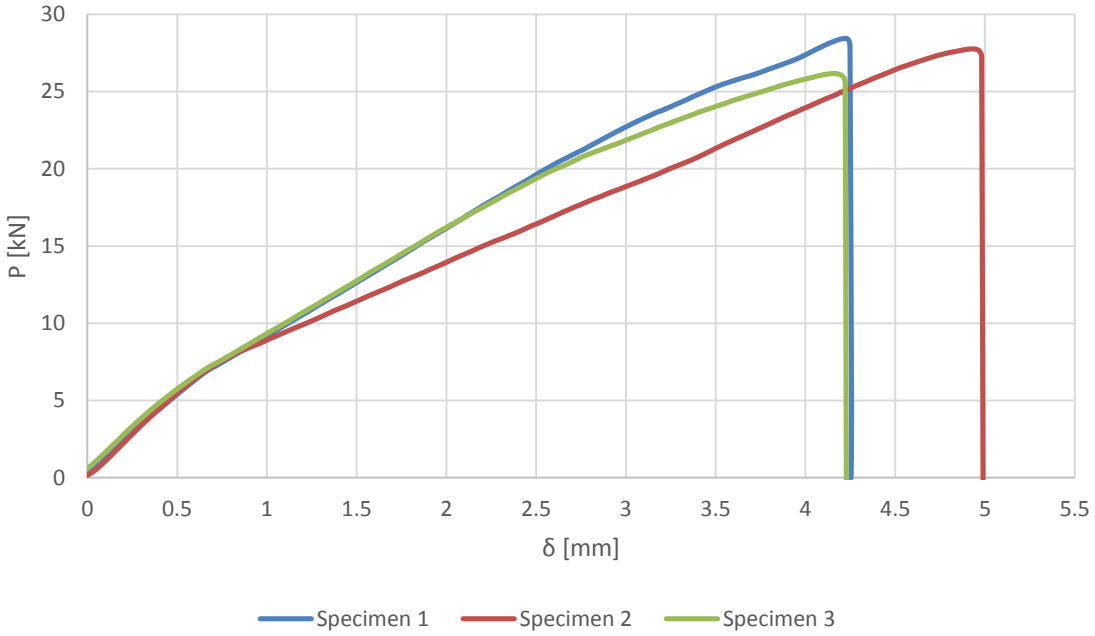

Figure 3.24 CFRP (2.1 mm)/HSS (2 mm) $P - \delta$ curves for 50 mm overlap

Failure mode obtained after testing the 50 mm overlap length joints can be seen in Figure 3.25. Cohesive failure mode close to the interface was observed.

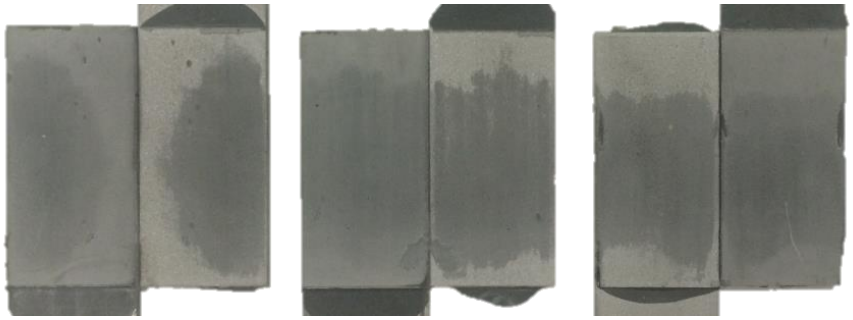

Figure 3.25 Failure modes of CFRP (2.1 mm)/HSS (2 mm) 50 mm overlap SLJs tested specimens

The results obtained after testing the specimens are summarized in Table 12.

`

Table 12 Experimental results of CFRP (2.1 mm)/HSS (2 mm) 50 mm overlap SLJs

Sample no.	Failure load (kN)	Average shear stress (MPa)	Displacement (mm)
1	28.44	22.75	4.25
2	29.12	23.30	4.11
3	27.76	22.21	4.99
Average	**28.44**	**22.75**	**4.45**
Standard deviation	**0.68**	**0.54**	**0.47**

Representative load displacement curves as a function of the overlap length were plotted in Figure 3.19. Similar to CFRP (2.1 mm)/HSS (1 mm) case, it can be seen that the failure load increased with the overlap length.

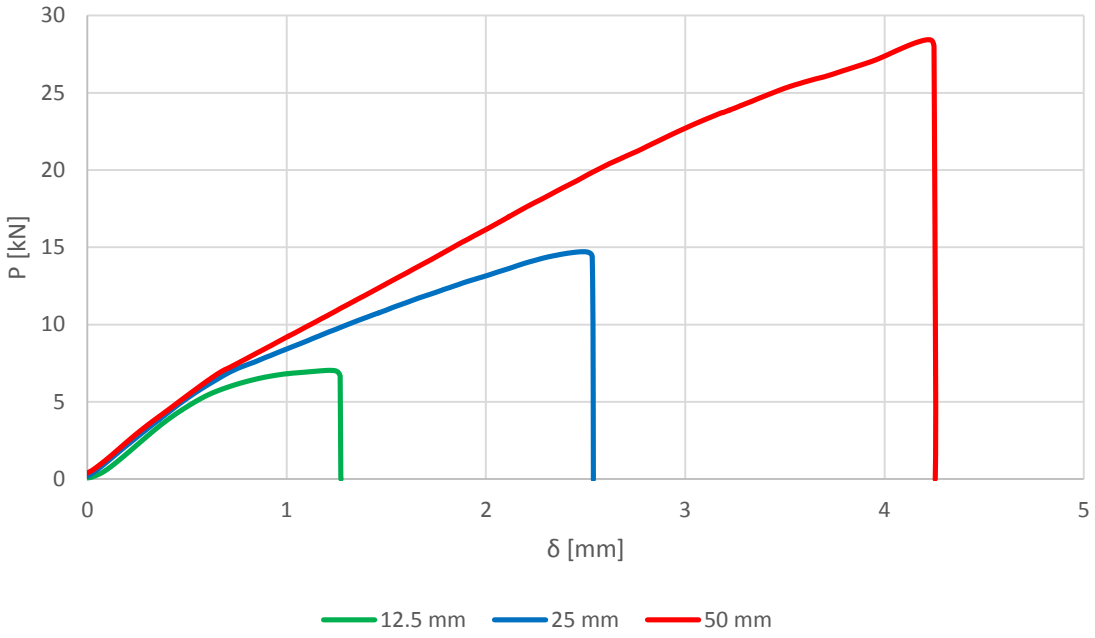

Figure 3.26 CFRP (2.1 mm)/HSS (2 mm) representative curves

3.5.1.3 CFRP (1.2 mm)/HSS (1 mm) SLJs

Since no delamination or adherend failure occurred for the 2.1 mm thick CFRP, the thickness of the composite adherend was reduced to 1.2 mm. In Figure 3.27 the load-displacement curves obtained from testing of the SLJs with 12.5 mm overlap are showed.

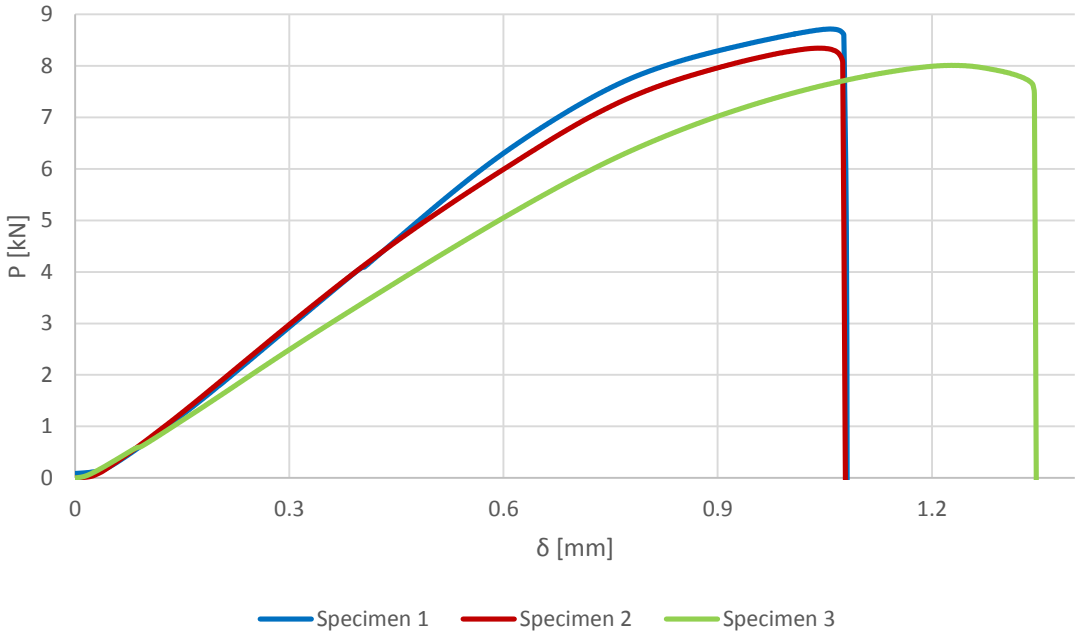

Figure 3.27 CFRP (1.2 mm)/HSS (1 mm) $P - \delta$ curves for 12.5 mm overlap

Failure mode obtained after testing the 12.5 mm overlap length joints is illustrated in Figure 3.28. A cohesive failure was observed.

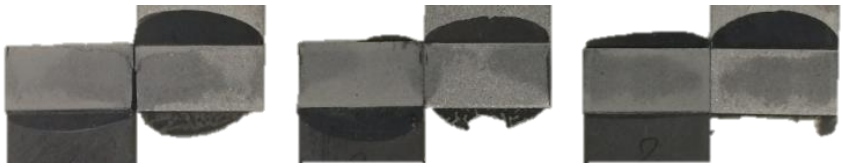

Figure 3.28 Failure modes of CFRP (1.2 mm)/HSS (1 mm) 12.5 mm overlap SLJs tested specimens

The results obtained after testing the specimens are summarized in Table 13.

Table 13 Experimental results of CFRP (1.2 mm)/HSS (1 mm) 12.5 mm overlap SLJs

Sample no.	Failure load (kN)	Average shear stress (MPa)	Displacement (mm)
1	8.72	27.90	1.21
2	8.35	26.71	1.08
3	8.01	25.64	1.36
Average	**8.36**	**26.75**	**1.22**
Standard deviation	**0.35**	**1.13**	**0.14**

`

For the 25 mm overlap, the average load of the specimens was 14.14 kN, with a 0.65 kN of standard deviation. The load-displacement curves obtained can be seen in Figure 3.29.

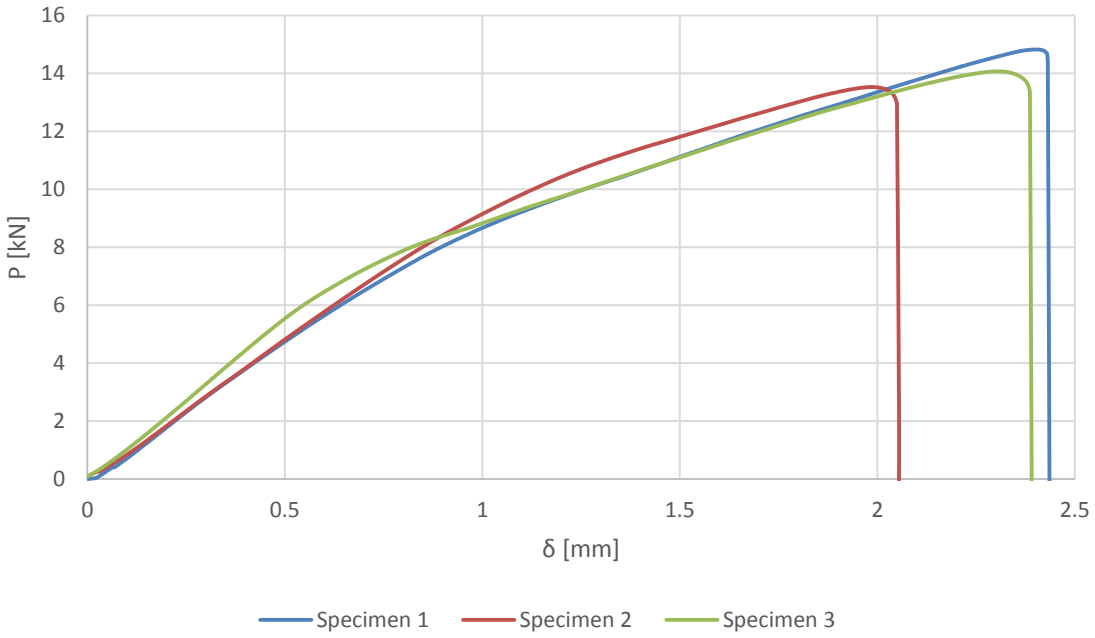

Figure 3.29 CFRP (1.2 mm)/HSS (1 mm) $P - \delta$ curves for 25 mm overlap

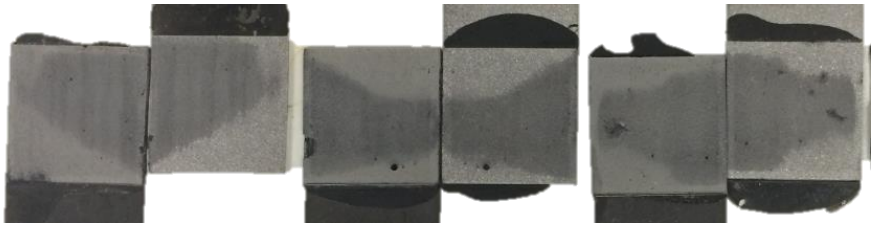

Figure 3.30 Failure modes of CFRP (2.1 mm)/HSS (2 mm) 25 mm overlap SLJs tested specimens

Failure mode obtained after testing the 25 mm overlap length joints is illustrated in Figure 3.30. By visual analyzing the fracture surface, a cohesive failure close to HSS adherend was observed.

`

Table 14 Experimental results of CFRP (1.2 mm)/HSS (1 mm) 25 mm overlap SLJs

Sample no.	Failure load (kN)	Average shear stress (MPa)	Displacement (mm)
1	14.83	23.72	2.45
2	13.53	21.65	2.12
3	14.07	22.51	2.42
Average	**14.14**	**22.63**	**2.33**
Standard deviation	**0.65**	**1.04**	**0.19**

For the 50 mm overlap joint the average load obtained was 28.66 kN, and a 1.11 kN of standard deviation. Load displacement curves are illustrated in Figure 3.21, while the failure mode of the tested specimens can be seen in Figure 3.32. The tests results were summarized in Table 15.

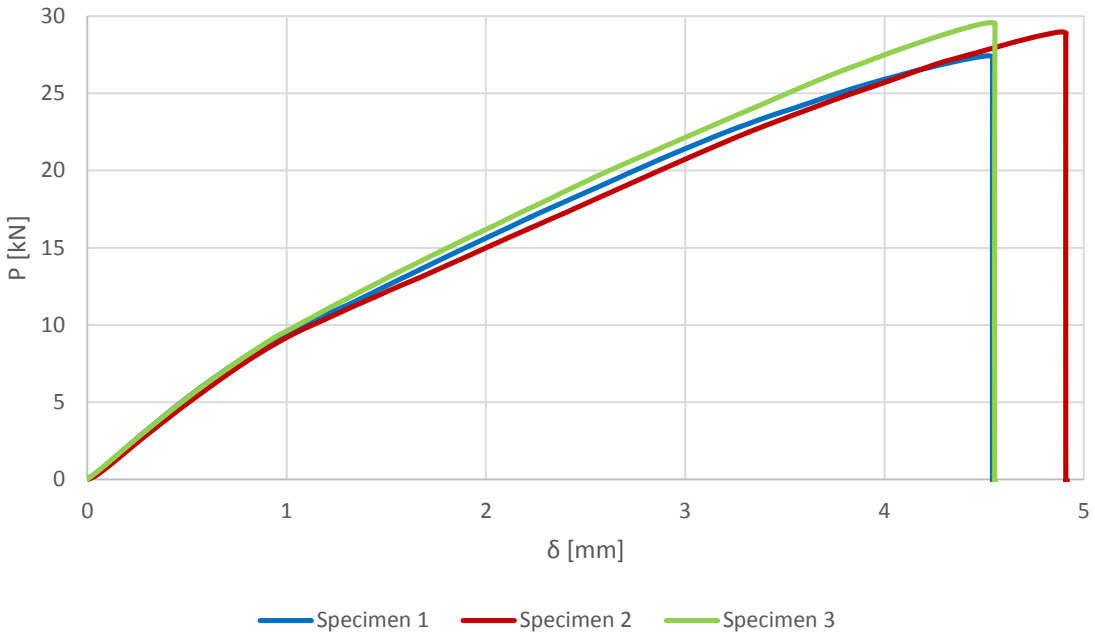

Figure 3.31 CFRP (1.2 mm)/HSS (1 mm) $P - \delta$ curves for 50 mm overlap

`

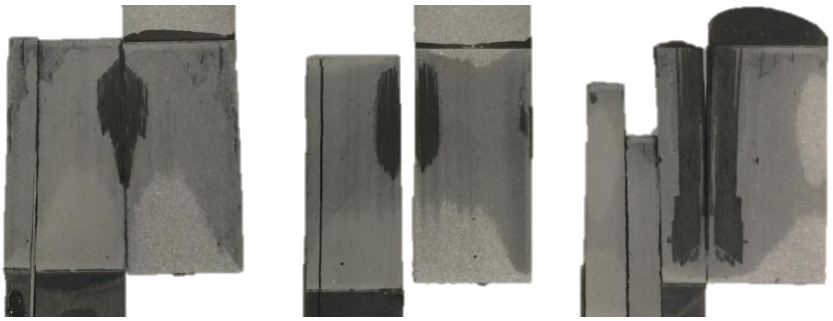

Figure 3.32 Failure modes of CFRP (1.2 mm)/HSS (1 mm) 50 mm overlap SLJs tested specimens

Table 15 Experimental results of CFRP (1.2 mm)/HSS (1 mm) 50 mm overlap SLJs

Sample no.	Failure load (kN)	Average shear stress (MPa)	Displacement (mm)
2	27.43	21.95	4.52
3	28.98	23.18	4.89
4	29.58	23.66	4.53
Average	**28.66**	**22.93**	**4.64**
Standard deviation	**1.11**	**0.88**	**0.21**

For 50 mm overlap the behavior of the present configuration was different. Analyzing the failure mode for this case, a mixed mode failure can be observed. However, in this case adherend failure also occurred, as shown in Figure 3.33. The present failure mode can be attributed to anticlastic bending of the adherend (da Silva, et al., 2009) and (Oterkus, et al., 2004).

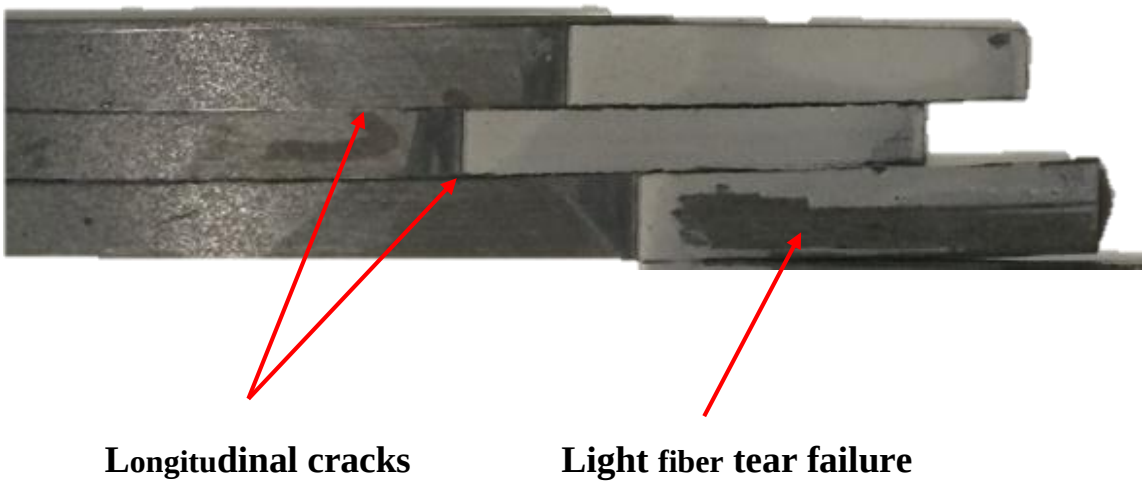

Figure 3.33 CFRP adherend failure mode

`

Representative load displacement curves as a function of the overlap length are plotted in Figure 3.34.

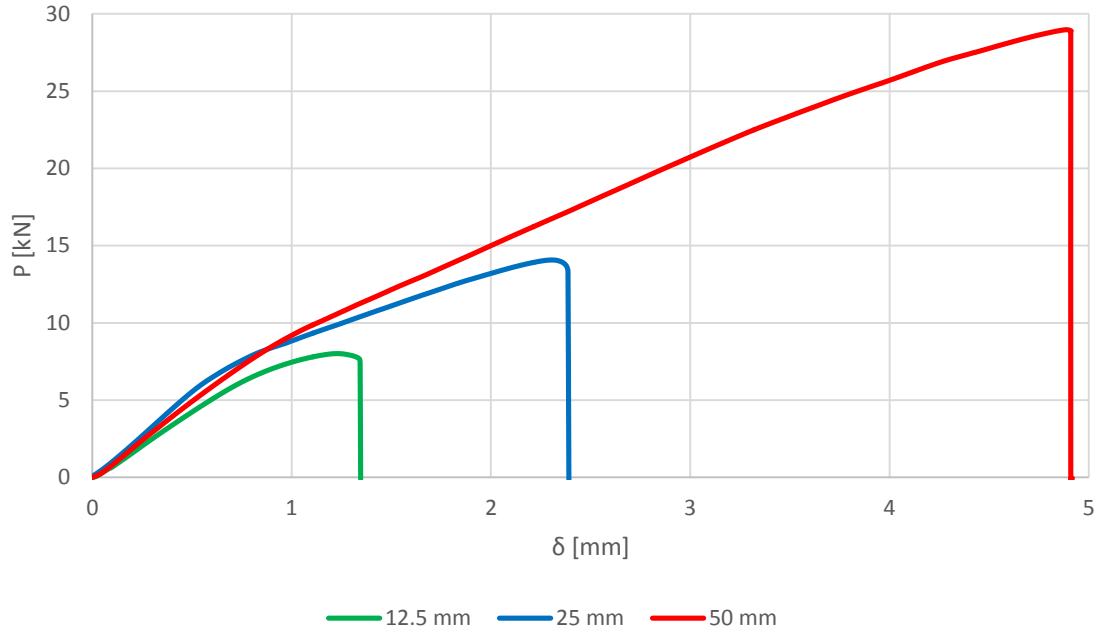

Figure 3.34 Unbalanced SLJs CFRP (1.2 mm) – HSS (1 mm) representative curves

3.5.2 CFRP/Al SLJs

3.5.2.1 CFRP (2.1 mm)/Al (3 mm) SLJs

Load-displacement curves for CFRP (2.1 mm)/Al (3 mm) SLJ configuration are showed in Figure 3.35. The average load was 11.16 kN, with a 0.81 kN of standard deviation, and a shear stress of 18.6 MPa in the adhesive layer. From the Figure 3.36, it can be seen that cohesive failure mode close to the interface occurred on this case.

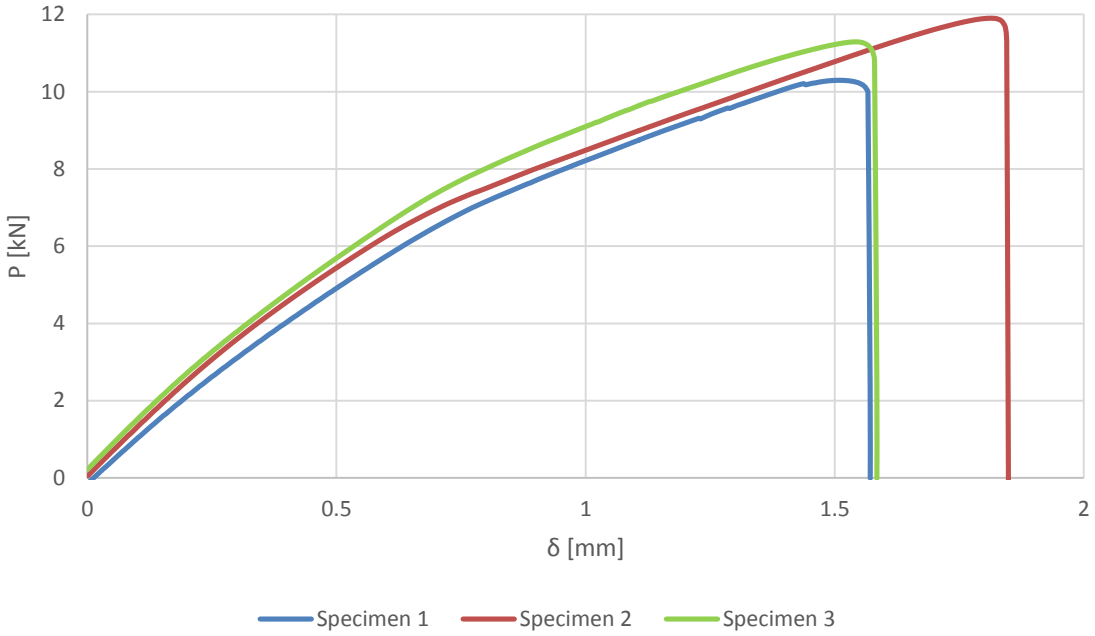

Figure 3.35 CFRP (2.1 mm)/Al (3 mm) $P - \delta$ curves

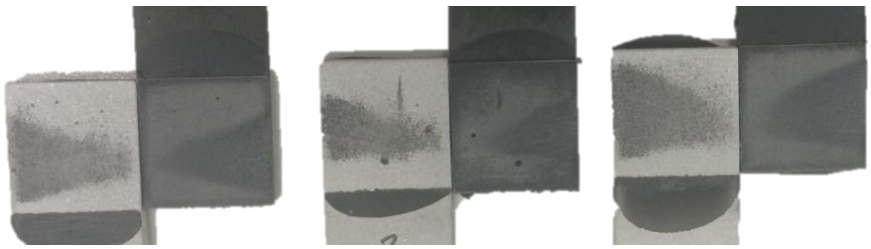

Figure 3.36 Failure modes of CFRP (2.1 mm)/Al (3 mm) SLJs tested specimens

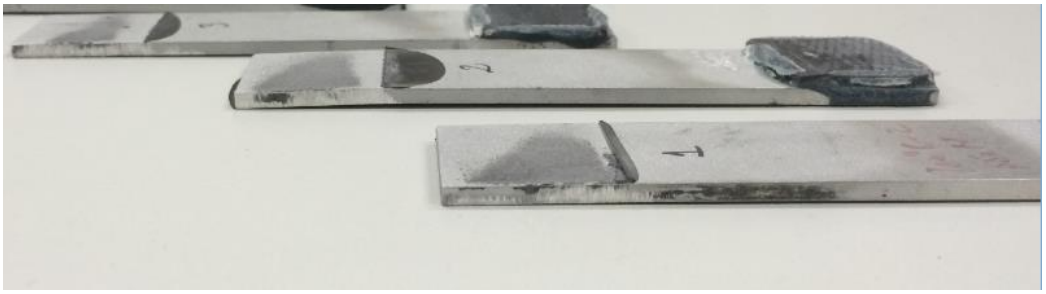

Figure 3.37 Plastic deformation of the 3 mm thick aluminum adherends

For the CFRP/Al joint, the strength of the adhesive joint exceeded the proportional limit of the adherend. In this case the aluminum substrate suffered a plastic deformation as can be observed in Figure 3.37.

`

The results obtained after testing the specimens are summarized in Table 16.

Table 16 Experimental results of balanced joint CFRP (2.1 mm)/Al (3 mm)

Sample no.	Failure load (kN)	Average shear stress (MPa)	Displacement (mm)
1	10.30	19.89	1.60
2	11.90	18.77	1.86
3	11.29	17.13	1.61
Average	**11.16**	**18.60**	**1.69**
Standard deviation	**0.81**	**1.39**	**0.15**

3.5.2.2 CFRP (2.1 mm)/Al (2 mm) SLJs

For the case of the SLJs using 2 mm thick aluminum, the load-displacement curves obtained after testing the specimens are illustrated in Figure 3.38. The results obtained after testing the specimens are summarized in Table 17.

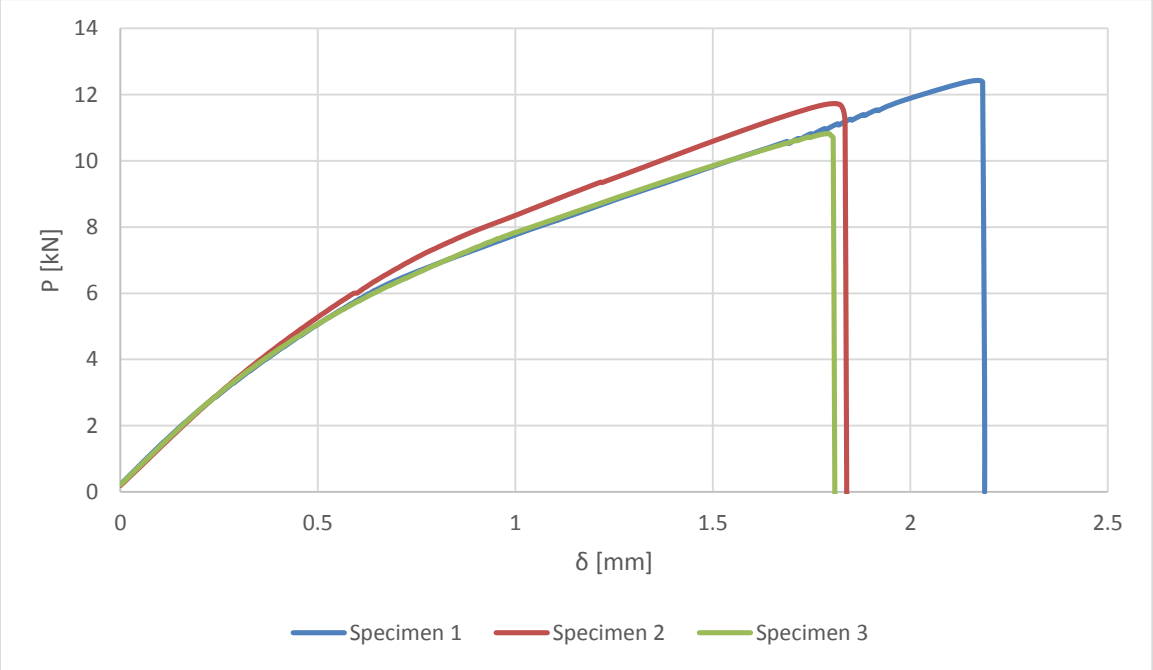

Figure 3.38 CFRP (2.1 mm) – Al (2 mm) *P-δ* curves with 25 mm overlap

Failure modes of the specimens can be observed in Figure 3.39. A cohesive failure mode close to the interface can be observed.

`

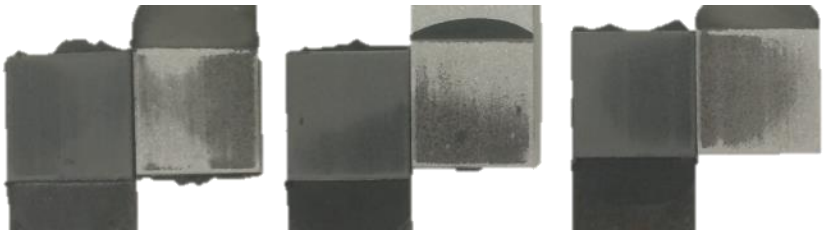

Figure 3.39 Failure modes of CFRP (2.1 mm)/Al (2 mm) SLJs tested specimens

Figure 3.40 Plastic deformation occurred by the 2 mm thick aluminum substrate

In comparison with the case studied before, for CFRP (2.1mm)/Al (3mm), due to the decrease of the aluminum thickness, the axial rigidity of the aluminum substrate lowered, so in consequence, the yielding of the aluminum substrate was more pronounced, as can be seen from Figure 3.40.

Table 17 Experimental results of unbalanced joint CFRP (2.1 mm)/Al (2 mm)

Sample no.	Failure load (kN)	Average shear stress (MPa)	Displacement (mm)
1	12.43	19.89	2.25
2	11.73	18.77	1.94
3	10.82	17.31	1.88
Average	**11.66**	**18.66**	**2.03**
Standard deviation	**0.81**	**1.29**	**0.20**

3.6 Experimental results discussion

3.6.1 Effect of the overlap length

The effect of overlap length for aluminum adherends was not studied because for overlaps lengths higher than 12.5 mm, global yielding of the adherend is dominant, as demonstrated in 3.2.2 section.

`

The overlap length of an adhesive joint defines the length by which the adherends transfer the load from one adherend to another. The overlap length is an important design parameter which influences joint rotation, the adhesive stress distribution and ultimately the strength of the joint. Increasing the overlap length will serve to reduce the rotation of the joint. The effect of the overlap length on the stress state in an adhesive joint has been studied by Hart-Smith (Hart-Smith, 1973) and Grant (Grant, 1976) within research programs aimed at developing design philosophies for aircraft construction.

In order to observe the effect of the overlap length on the failure load of the adhesive joint, representative load-displacement curves of the tested CFRP/HSS specimens were plotted in Figure 3.41.

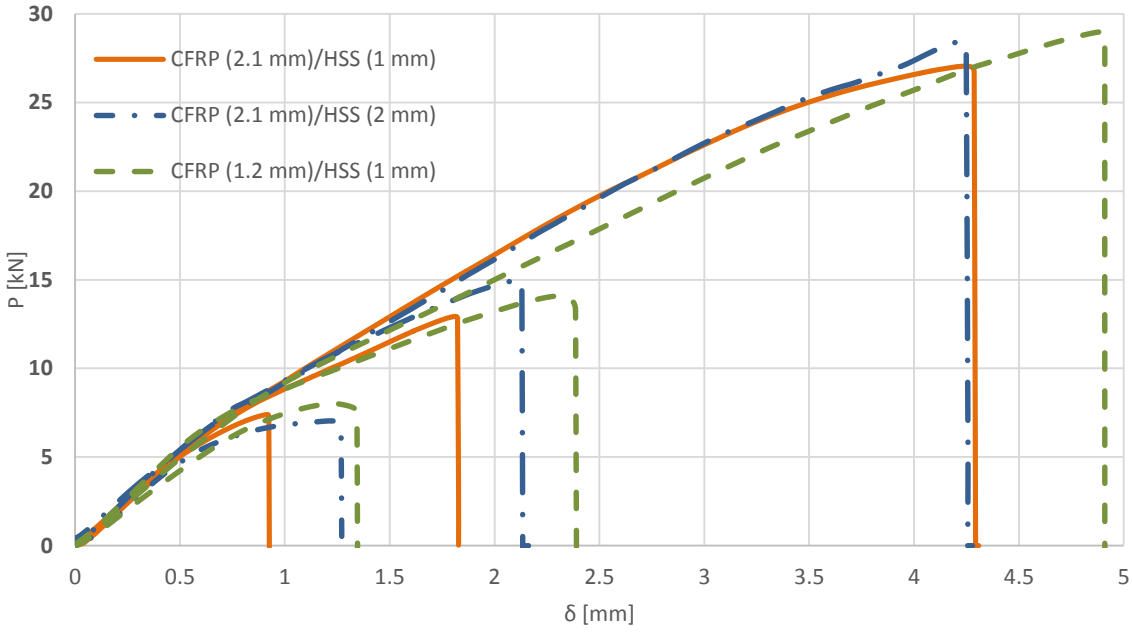

Figure 3.41 Representative $P - \delta$ curves as a function of overlap length of CFRP/HSS SLJs

As it can be seen in Figure 3.14, for all the CFRP/HSS configuration the failure loads had no significant variation. Although, increasing the overlap length will lead to an increase of the load-bearing capacity of the joints.

The average experimental failure loads values were plotted in the Figure 3.42.

`

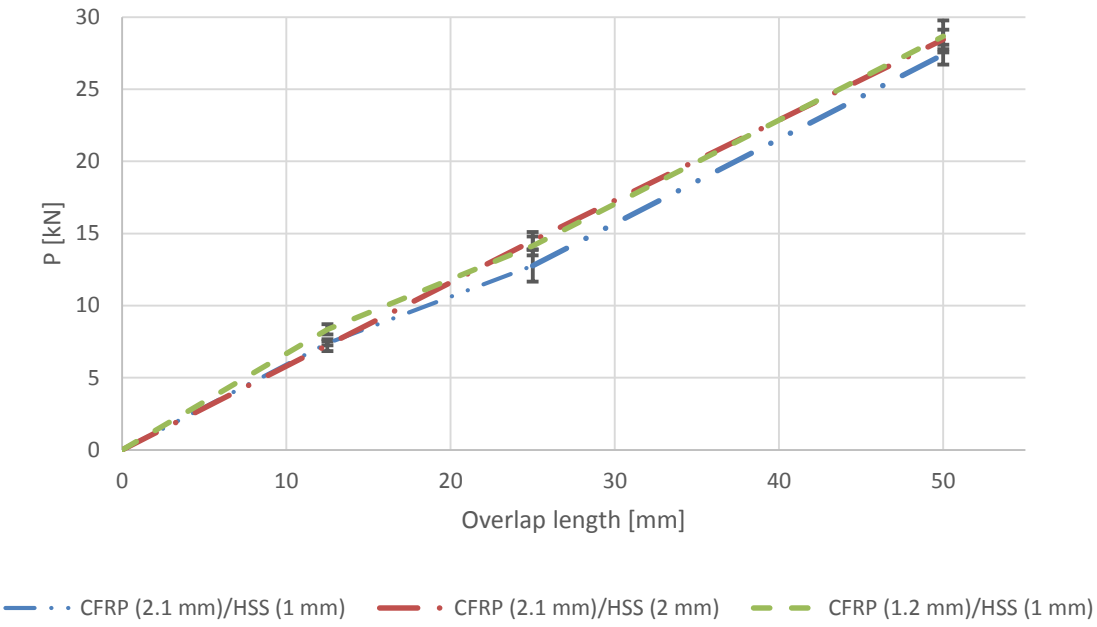

Figure 3.42 Effect of overlap length for CFRP/HSS SLJs

In the cases studied here, represented by the usage of elastic adherends and ductile adhesive (with more than 20% shear strain to failure), the joint strength is approximately proportional to the overlap, fact that can be seen in Figure 3.42. This can be attributed to the plastically deformation of the ductile adhesives, that is redistributing the stress as the load increases, and make use of the whole overlap.

It is known that ductile adhesives fail by tension, in the shear load direction due to high adhesive deformation. In order to concede the conclusion taken, a simple approach was used. A simple way to predict the failure load of single lap joints was proposed by Adams (Adams & Mallick, 1992), based on the yield shear stress of the adhesive. The load corresponding to failure is given by:

$$P = \tau_y \cdot b \cdot L \qquad \text{Equation 7}$$

Where

τ_y is the shear yield stress of the adhesive;

L is the overlap length;

b is the width of the joint.

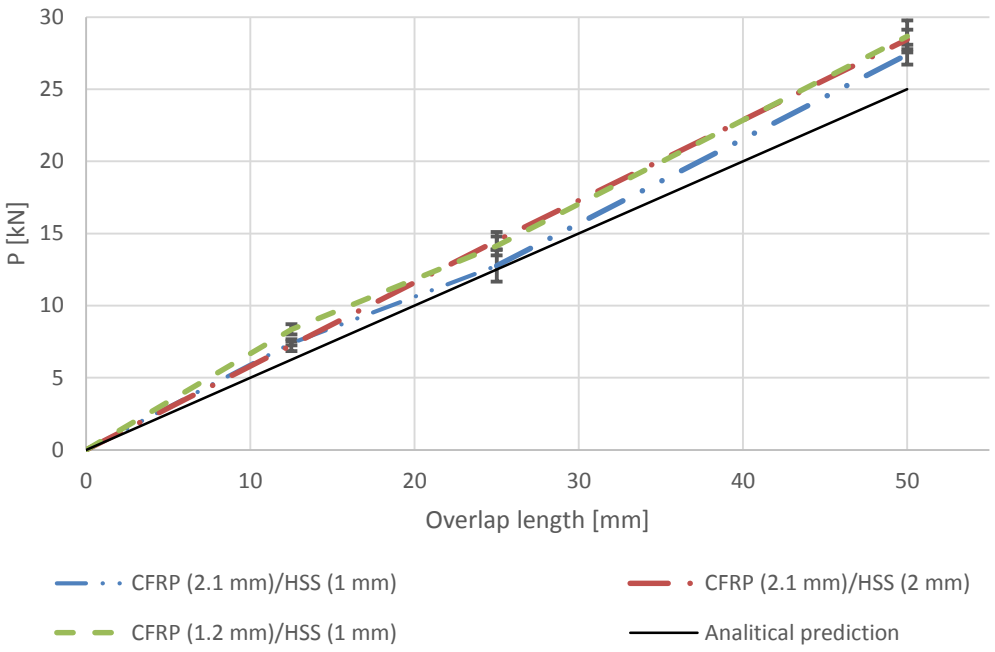

Figure 3.43 Global yielding predictions of the failure load

The analytical prediction is comparable with the experimental results, and in both cases the increase of the overlap length indicate a linear increase of the load-bearing capacity of the joint.

3.6.2 Effect of axial stiffness imbalance

3.6.2.1 CFRP/HSS SLJs

For evaluating the strength bonding of SLJs between CFRP and HSs, a comparison between the failure loads of the tested joints was made for each overlap length Figure 3.44.

For the all configurations of adherend thicknesses studied, the unbalanced CFRP/HSS joints strength had no significant variation.

In this case, two main joint geometry can be defined:

- Geometry balanced joints, in which adherends section are equal: $t_{s1} = t_{s2}$. The
- Stiffness balanced joints, in which adherends axial stiffness are equal $E_1 t_{s1} = E_2 t_{s2}$.

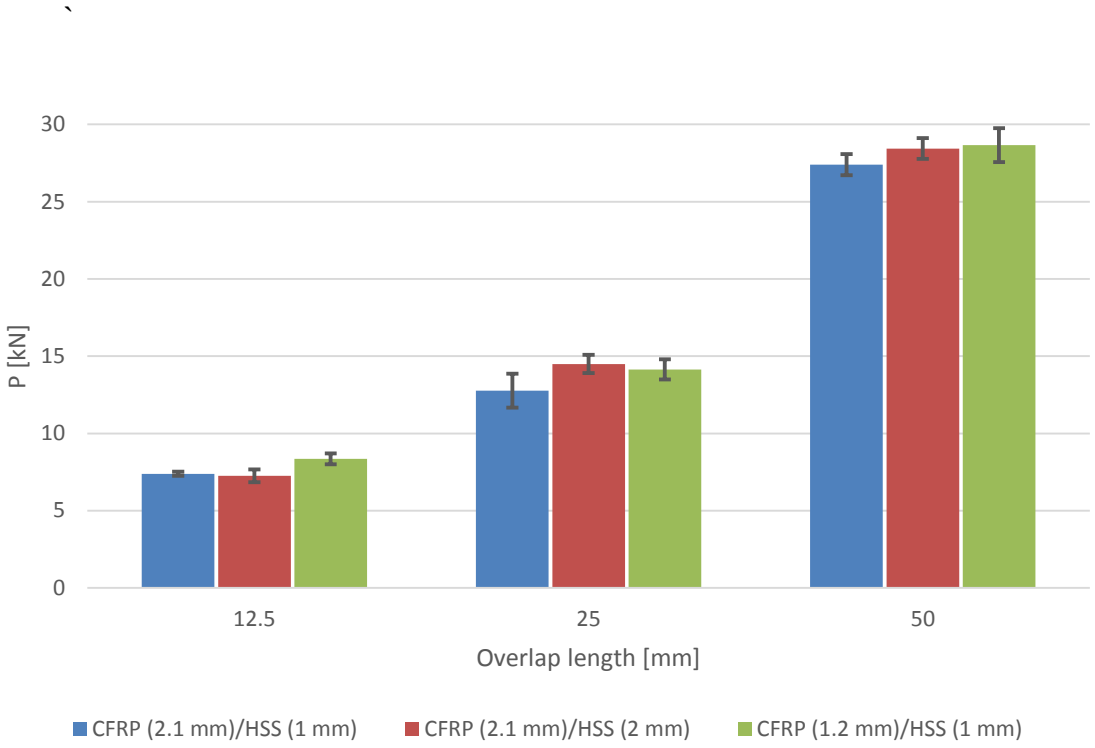

Figure 3.44 CFRP/HSS SLJs failure load.

Analyzing Figure 3.44, it can be noted that for all configurations of adherend thicknesses studied in this thesis, the unbalanced CFRP/HSS joints strength had no significant variation. However, for 25 and 50 mm overlaps, the geometry balanced joints promoted a higher strength than the stiffness balanced joints, in this case the axial balanced stiffness joint. The CFRP (2.1 mm)/HSS (1 mm) showed the lowest strength.

Another notable accomplishment is the fact that the decrease of the adherend thickness did not promoted a significative decrease in joint`s strength, thus a reduction of the mass may be achieved without losing the joint efficiency.

3.6.2.2 CFRP/Al SLJs

As showed before in the CFRP/HSS case, a similar behavior was observed for CFRP/Al joints, CFRP/Al 2 mm, behaved slightly better than the balanced stiffness joint CFRP/Al 3 mm. The CFRP/Al 2 mm configuration had a failure load average of 11.66 kN and a 0.81 kN standard deviation, while the CFRP/Al 3 mm configuration had a failure load average of 11.16 kN and 0.81 kN standard deviation.

`

3.6.3 Effect of dissimilar adherends on the failure load of multi-material SLJs

The unbalanced SLJs studied here were compared to balanced SLJs between HSS/HSS or CFRP/CFRP, which were investigated in a previous study by Banea et al (Banea et al, 2015b). As can be seen from the figure 3.45 a decrease of the strength of multi-material joints was observed, in the case of longer overlaps. This may be due to the fact that the use of dissimilar adherends decreases the joint strength due to a non-uniform stress distribution.

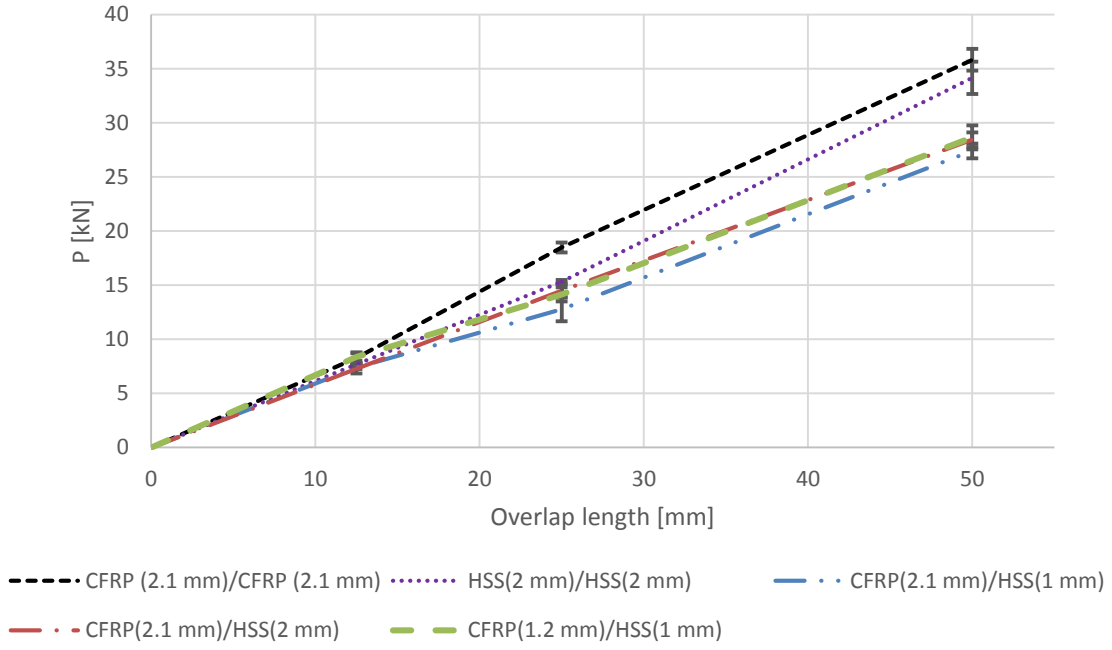

Figure 3.45 Comparison of unbalanced SLJs to balanced SLJs as a function of overlap length.

In order to compare the effect of dissimilar adherends on the failure load of the specimens, the experimental results obtained were plotted separately in column charts for 25 mm overlap (Figure 3.46) and for 50 mm overlap (Figure 3.47).

We can observe from Figure 3.47 and Figure 3.46 that the efficiency of the balanced joints is higher than in the cases of unbalanced joints. The highest values of failure loads were found for CFRP/CFRP balanced joints for both overlaps. Also, for the case of balanced HSS/HSS, the failure loads obtained was higher than the unbalanced joints between dissimilar materials.

`

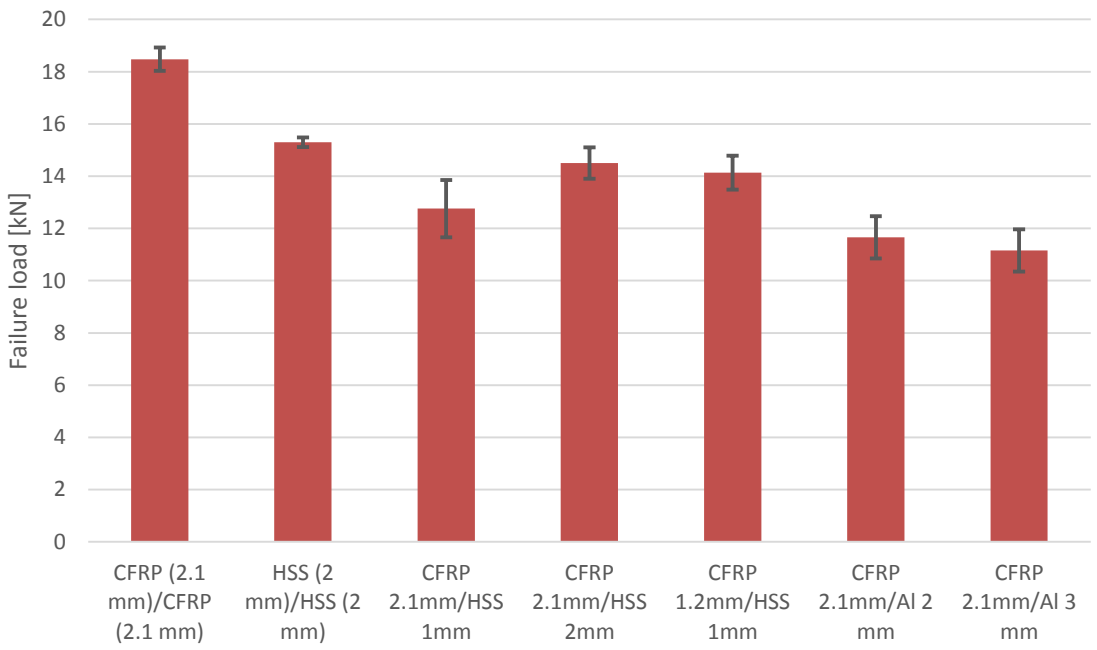

Figure 3.46 Effect of dissimilar adherends on the failure load for 25 mm overlap joints.

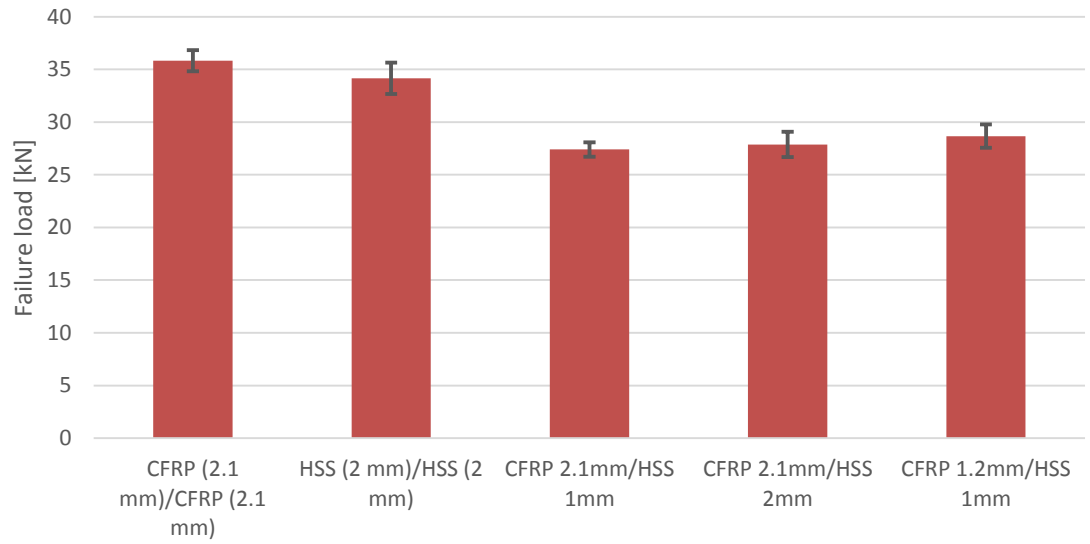

Figure 3.47 Effect of dissimilar adherends on the failure load for 50 mm overlap joints

Furthermore, in order to observe the effect of dissimilar adherends on the adhesive bonding strength, the experimental values are normalized to the value obtained with CFFR/CFRP configuration and the values are presented in Table 18. A decrease of failure load by approximately 30% for the unbalanced joints can be observed compared to CFRP/CFRP.

`

Table 18 Effect of dissimilar adherends on the failure load.

	25 mm overlap		50 mm overlap	
	Failure load [kN]	Percentage [%]	Failure load [kN]	Percentage [%]
CFRP 2.1mm/CFRP 2.1mm	18.48	100	35.82	100
HSS 2mm/HSS 2mm	15.3	82.79	34.16	95.37
CFRP 2.1mm/HSS 1mm	12.76	69.05	27.40	76.49
CFRP 2.1mm/HSS 2mm	14.5	78.46	27.87	77.81
CFRP 1.2mm/HSS 1mm	14.14	76.52	28.66	80.01
CFRP 2.1mm/Al 2 mm	11.66	63.10	-	-
CFRP 2.1mm/Al 3 mm	11.16	60.39	-	-

To summarize, for the adherend thicknesses studied here, the unbalanced CFRP/HSS joints strength had no significant variation. However, when they are compared to balanced joints a decrease in strength can be observed (approx. 24%), mainly for longer overlaps, due to the different flexural rigidities of the adherends which give a non-uniform stress distribution. Nevertheless, geometry balanced joints ($t_{s1}=t_{s2}$) promote a higher strength than the stiffness balanced joints ($E_1t_{s1}=E_2t_{s2}$). A similar behavior was observed for CFRP/Al joints (i.e. CFRP/Al 2mm performed better than stiffness balanced CFRP/Al 3 mm joints).

`

4 Numerical analysis

The experimental work carried out is accompanied by a detailed numerical analysis by Finite Elements, starting with the plot of elastic stress distributions, and strength prediction based on CZM.

4.1 Numerical model

In order to study the behavior of the adhesive joints a numerical simulation have been done using the finite element program ABAQUS®/standard (Dessault Systemes Providence, USA) in order to assess the viability of its CZM embedded form.

The geometry of the specimens were modelled with plane-strain 4-node quadrilateral solid elements (CPE4R: A 4-node bilinear plane strain quadrilateral, reduced integration, hourglass control). COH2D4 4-node CZM elements were used to model the adhesive layer.

4.1.1 Geometry and material properties

The geometry for the single lap joint is presented in Figure 4.1.

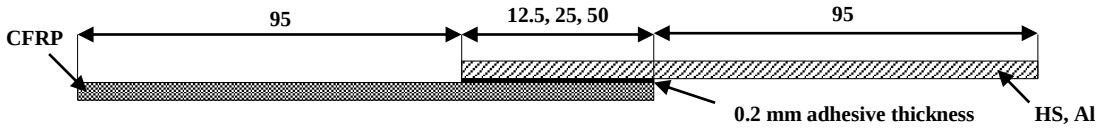

Figure 4.1 SLJs geometry

The adhesive properties, as well as the HSS and aluminum properties introduced to the numerical analysis were previous presented in the 3.1 chapter section. The material properties used for CFRP are the ones determined by Campilho (Campilho, 2009) and are presented in table 19.

Table 19 CFRP components elastic orthotropic properties for a unidirectional ply (Campilho, 2009)

E_1 [MPa]	E_2 [MPa]	E_3 [MPa]	ν_{12}	ν_{23}	ν_{13}	G_{12} [MPa]	G_{23} [MPa]	G_{13} [MPa]
109000	8819	8819	0.342	0.342	0.380	4315	4315	3200

`

4.1.2 Boundary conditions

Since one of the objectives of this simulation is to compare its results with the experimental values, the boundary conditions applied must be as similar as possible to the real experimental conditions. The joints were clamped at one of the edges and the other edge was subjected to a tensile displacement concurrently with transverse restraining.

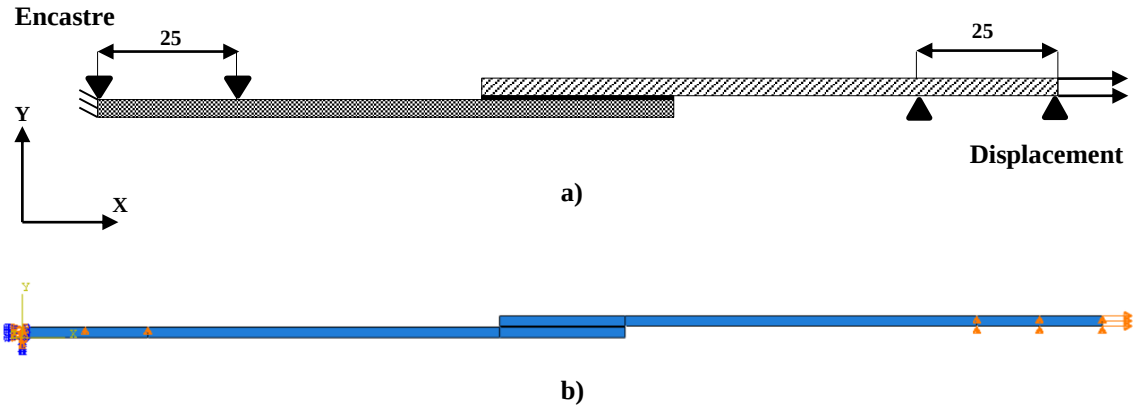

Figure 4.2 Boundary conditions a) specimen test, b) Abaqus

4.1.3 Mesh

Meshes for the FEM analysis were done considering the standard refinement and no symmetry conditions were considered. The mesh established was formed by CPE4R elements which are 4-node bilinear plane strain quadrilateral elements.

Figure 4.3 SLJs configuration

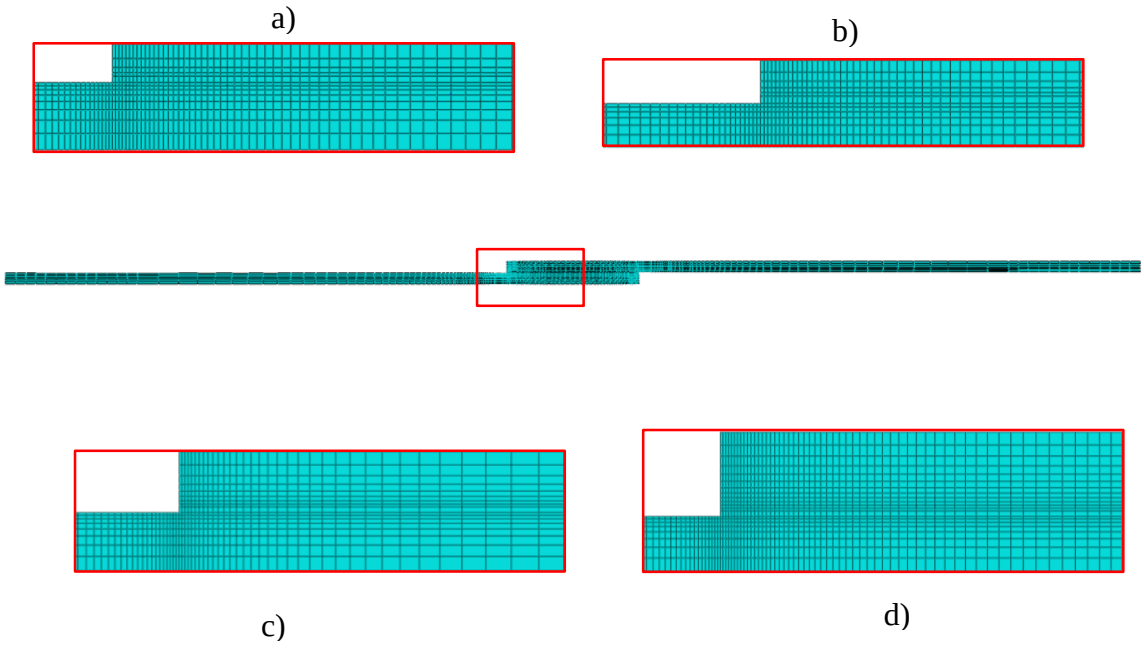

Figure 4.4 Detailed mesh view: a) CFRP (2.1 mm)/HSS (1 mm); b) CFRP (1.2 mm)/HSS (1 mm); c) CFRP (2.1 mm)/Al (2 mm); d) CFRP (2.1 mm)/Al (3 mm)

Cohesive elements were defined between the two substrates Figure 4.3, distributed in one layer of 4-node bilinear plane strain quadrilateral elements Figure 4.4. The element size was refined to a 0.1 mm length on the edge of the bonding, and gradually increased to 0.5 mm in the middle of the adhesive overlap.

4.2 Cohesive zone model

Cohesive zone models (CZMs) are now widely used to simulate fracture processes of different material systems and numerous CZM models have been presented in the literature. The key concept of CZM is that the fracture process zone (FPZ) can be described by a traction–separation law relating stresses and relative displacements between the crack faces, thus simulating the gradual degradation of the material properties. As a result, a second fracture parameter, the cohesive strength, is introduced in addition to the fracture toughness. The shape of the softening law can also be adjusted to conform to the behaviour of the material it is simulating. The only CZM implemented in ABAQUS uses a bilinear curve like the one presented in Figure 4.5 and was used in this thesis.

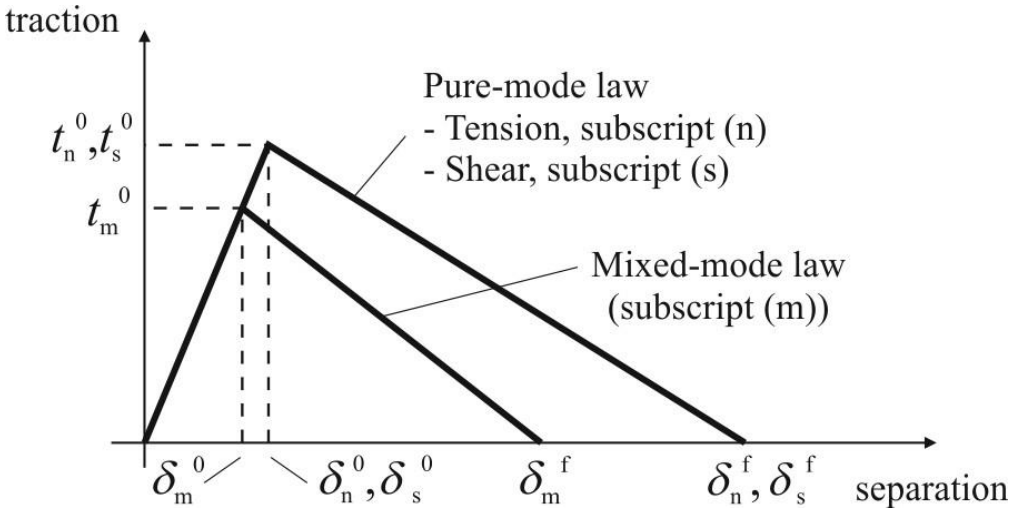

Figure 4.5 Traction-separation law with linear softening law available in ABAQUS®

4.3 Stress analysis

A shear (σ_y) and peel (τ_{xy}) stress analysis is carried out at the adhesive midthickness that enables further discussions on the obtained strength results.

In order to perform stress analysis of the bonded joints, new boundary conditions needed to be applied, than the ones defined before in 4.1.2 subchapter. Instead of applying a defined displacement one of the adherends edge, a 5000 N force was applied to all the studied SLJs. The value of the force was establish in order to remain in the elastic domain in all the cases studied.

For plotting the shear and peel stresses, the same configuration of the overlap was used as the one showed in Figure 4.6. A normalization procedure was carried out for the bonding length, L by plotting obtained stresses vs. x/L $(0 \leq x \leq L)$.]

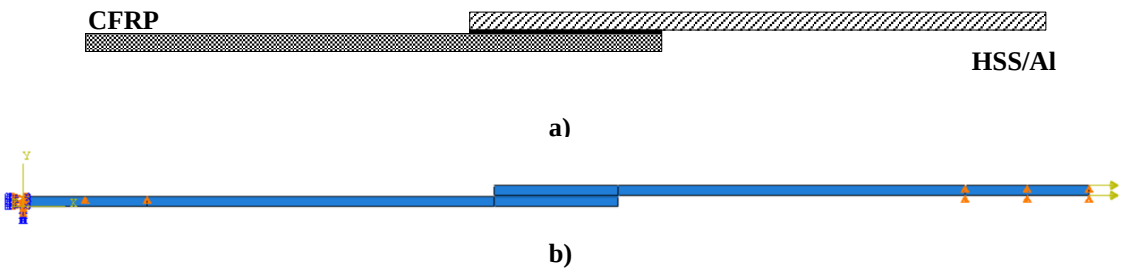

Figure 4.6 Boundary conditions for the stress analysis a) Adherends configuration, b) Boundary conditions defined in Abaqus

`

4.3.1 Shear stresses

Shear σ_y stresses are typically much lower in magnitude than τ_{xy} stresses, except at the bond edges. The shape of σ_y stresses is mainly due to the loading asymmetry, giving separation at the overlap edges and compression in-between (Fernandes, et al., 2015).

4.3.1.1 Shear stresses for CFRP/HSS SLJs

In Figure 4.7 and Figure 4.8, the shear stress distribution is represented for SLJs with 25 mm and 50 mm overlap. Also the stress distribution for balanced joints using HSS/HSS and CFRP/CFRP adherends was used as a comparison.

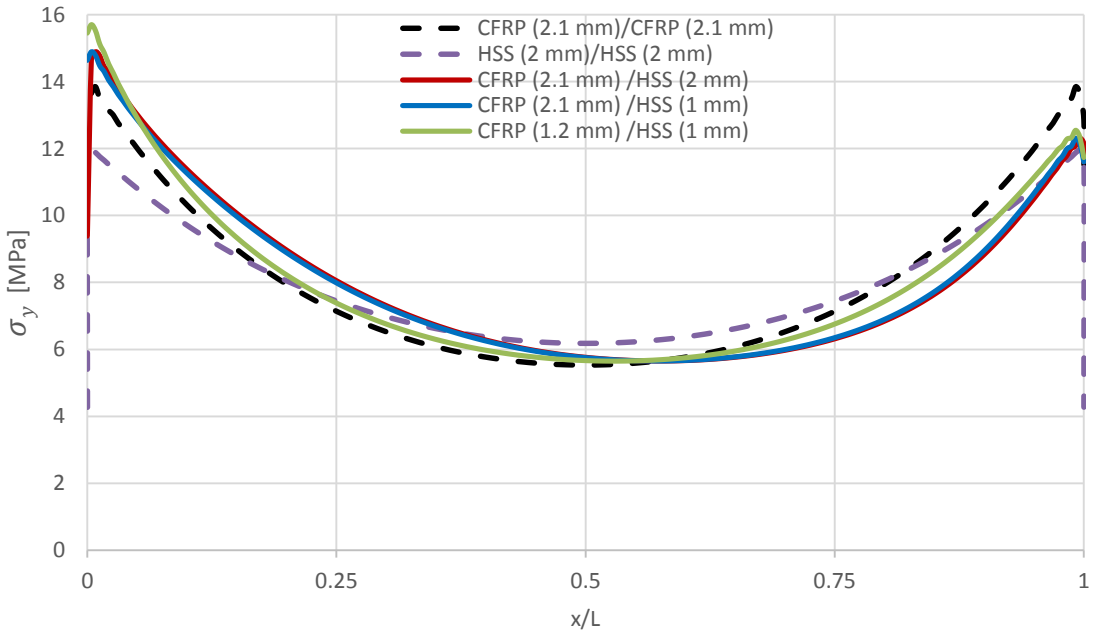

Figure 4.7 Shear stress distribution for 25 overlap adhesive joints

From analyzing the stress distribution for both overlaps, a symmetrical shear stress along the overlap length can be seen for the balanced joints. For the unbalanced joints, the adhesive shear stress distribution is uneven, having a highest value on the edge of the HSS adherend (Figure 4.6 a).

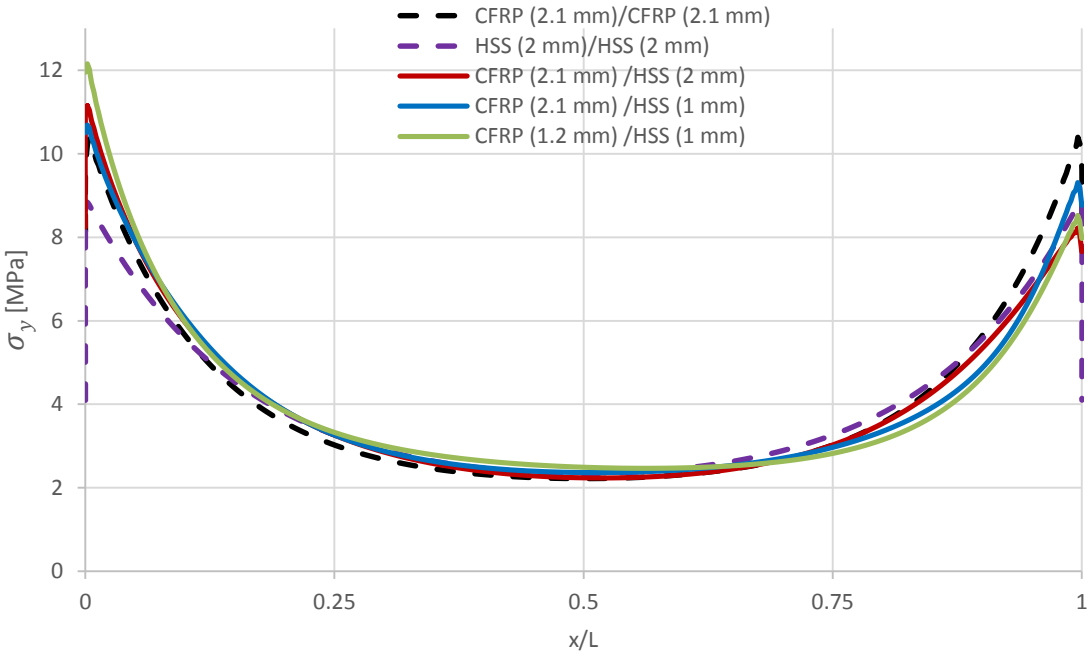

Figure 4.8 Shear stress distribution for 50 overlap adhesive joints

4.3.1.2 Shear stresses for CFRP/Al SLJs

In Figure 4.9, the shear stress distribution is represented for SLJs with 25 mm overlap. Also the stress distribution for balanced joints using HS/HSS and CFRP/CFRP adherends were used as a comparison with the unbalanced joints realized in this work.

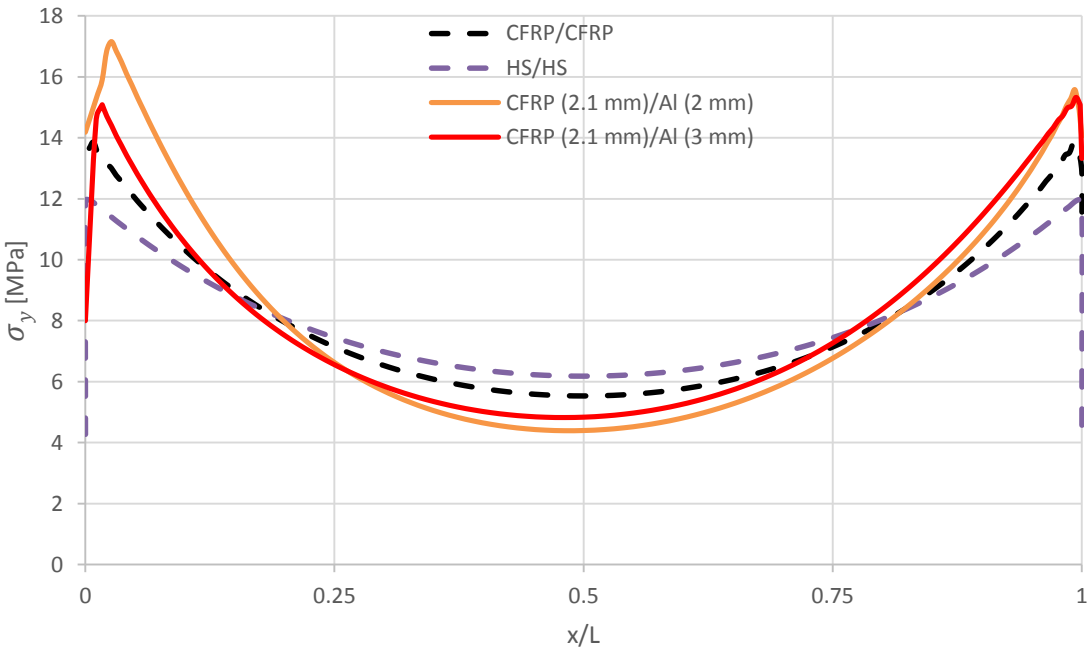

Figure 4.9 Shear stress distribution for 25 overlap adhesive joints

`

For the CFRP/Al unbalanced joints, the adhesive shear stress distribution is uneven, having a highest value on the edge of the Al adherend (Figure 4.6 a), the highest values of shear stress are traced for the CFRP (2.1 mm)/Al (2 mm) SLJ configuration.

4.3.2 Peel stresses

Peak peel stresses are responsible for a significant strength reduction of bonded joints (Campilho, et al., 2005). The peel stress distributions are also consistent with the available literature results, with a smaller load bearing potential at the overlap inner region and peaking toward the overlap edges. This behavior is due to the differential deformation of each one of the adherends along the overlap, from their free overlap edge towards the other overlap edge (Fernandes, et al., 2015). At the central region of the overlap these effects are cancelled, with peel stresses developing solely by the tensile pulling of the specimen. By using a ductile adhesive, this enables the redistribution of stresses at these regions while the inner region of the overlap is gradually put under loads, giving a bigger increase of the joint strength.

4.3.2.1 Peel stresses for CFRP/HSS SLJs

In Figure 4.10 and Figure 4.11, the peel stress distribution is represented for SLJs with 25 mm and 50 mm overlap. Also the peel stress distribution for balanced joints using HSS/HSS and CFRP/CFRP adherends was used as a comparison with the unbalanced joints realized in this work.

From analysing the stress distribution for both overlaps, a symmetrical peel stress distribution can be seen the overlap length for the balanced joints. For the unbalanced joints, the adhesive peel stress distribution is uneven, having a highest value on the edge of the CFRP adherend (Figure 4.6 a).

As it can be seen from both overlap lengths, in the case CFRP (2.1 mm)/HSS (1 mm) joints the maximum value of the peel stress was found. This is in accordance with the lowest joint strength found for this type of joint.

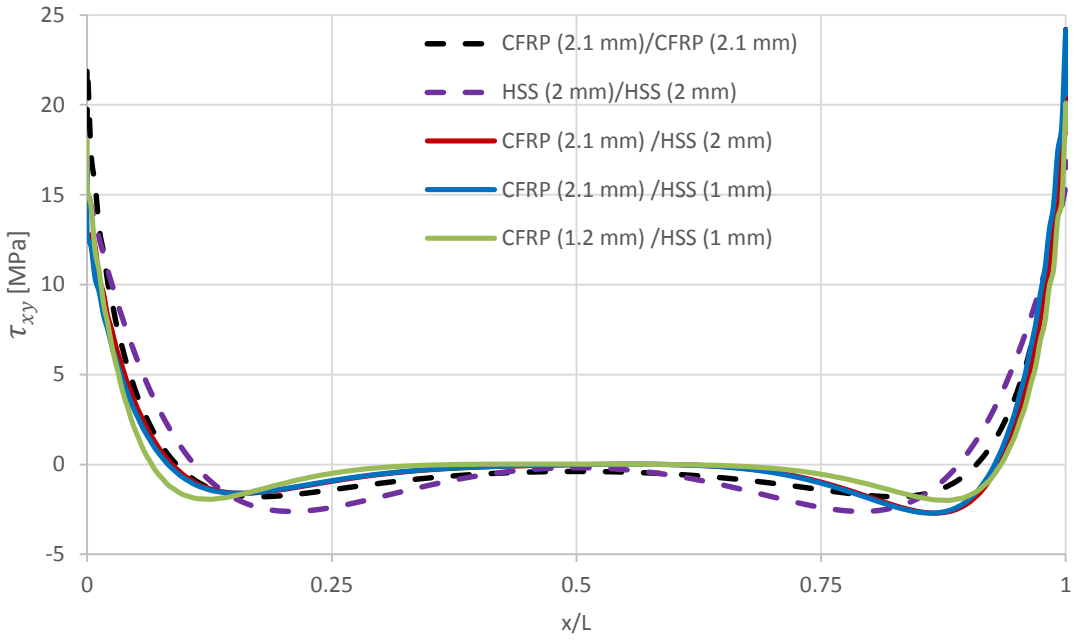

Figure 4.10 Peel stress distribution for 25 overlap adhesive joints

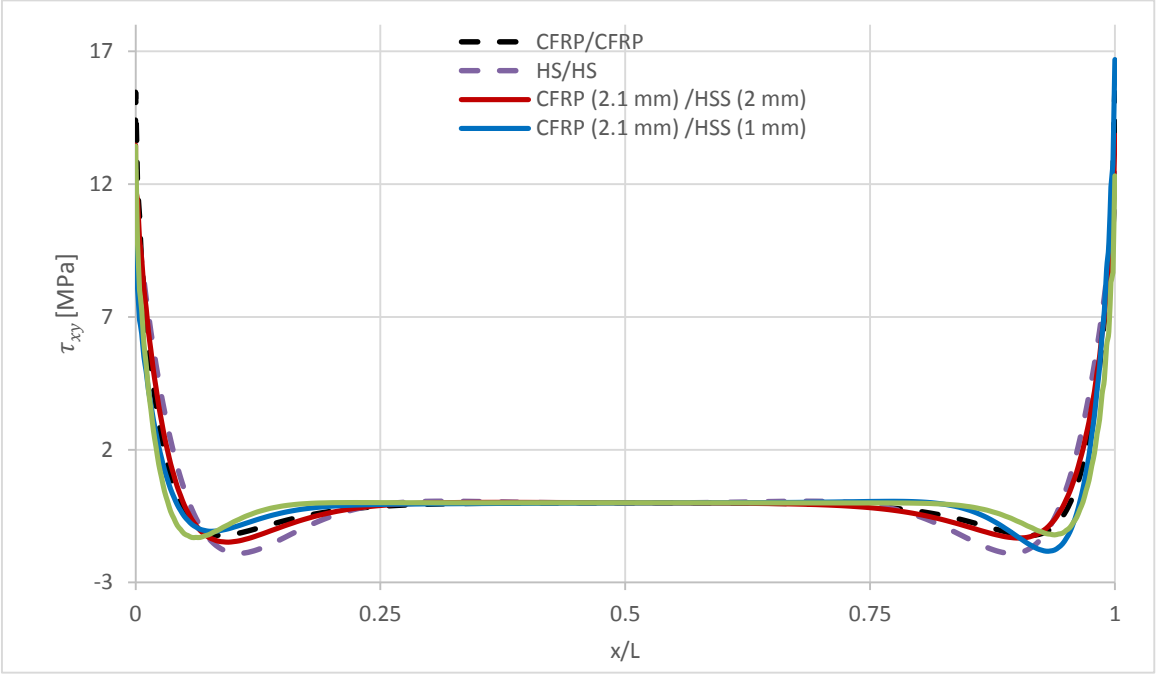

Figure 4.11 Peel stress distribution for 50 overlap adhesive joints

4.3.2.2 Peel stresses for CFRP/Al SLJs

In Figure 4.12, the peel stress distribution is represented for SLJs with 25 mm overlap. The peel stress distribution for balanced joints using HSS/HSS and CFRP/CFRP adherends was used as a comparison with the unbalanced joints realized in this work.

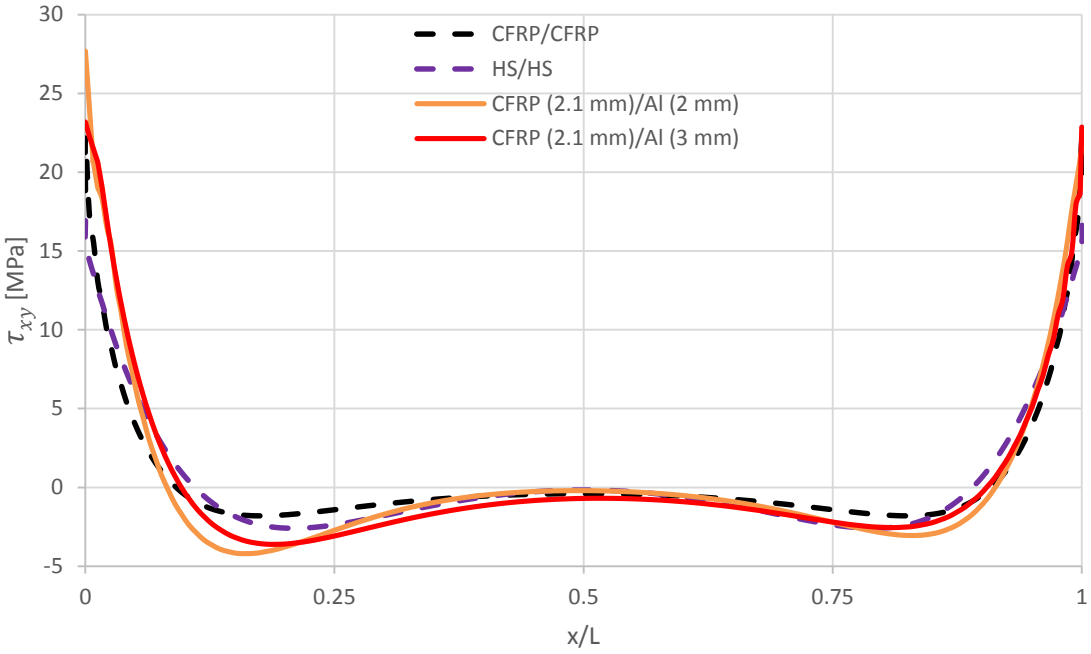

Figure 4.12 Peel stress distribution for 25 overlap adhesive joints.

As it can be seen from Figure 4.12, the peel stress in the adhesive layer reported a maximum value in the case of CFRP (2.1 mm)/Al (2 mm), located at the CFRP adherend edge. It was showed in the experimental results, Figure 3.37 and Figure 3.40, and further in numerical simulations, Figure 4.19, that the specified edge of the overlap, plastic deformation of the aluminum adherend occurred.

4.4 Strength prediction

In this section the results obtained from the experimental tests and from the finite element analysis are compared in terms of failure loads. Because of the simple geometry of the joint, 2D models were developed. All models used the same parameters:

- 4-node bilinear plane stress quadrilateral element, CPS4R, was used to mesh solid bodies;
- 4-node two-dimensional cohesive element, COH2D4; was used to mesh cohesive layer

The cohesive law used is the triangular law available in ABAQUS (see Figure 4.5).

`

The boundary conditions were the same as described in Figure 4.6. A 5 mm displacement in order to achieve joint failure was applied.

4.4.1 CFRP/HSS SLJs

4.4.1.1 CFRP (2.1 mm)/HSS (1 mm)

For the first case studied, ((CFRP (2.1 mm)/HSS (1 mm)), the adherends have the same stiffness. The cohesive elements placed between the layers of CFRP and HSS were damaged similar to the experimental tests where the failure started on the edge of the adherend with the lowest stiffness. The plot of element degradation is presented in Figure 4.13 a).

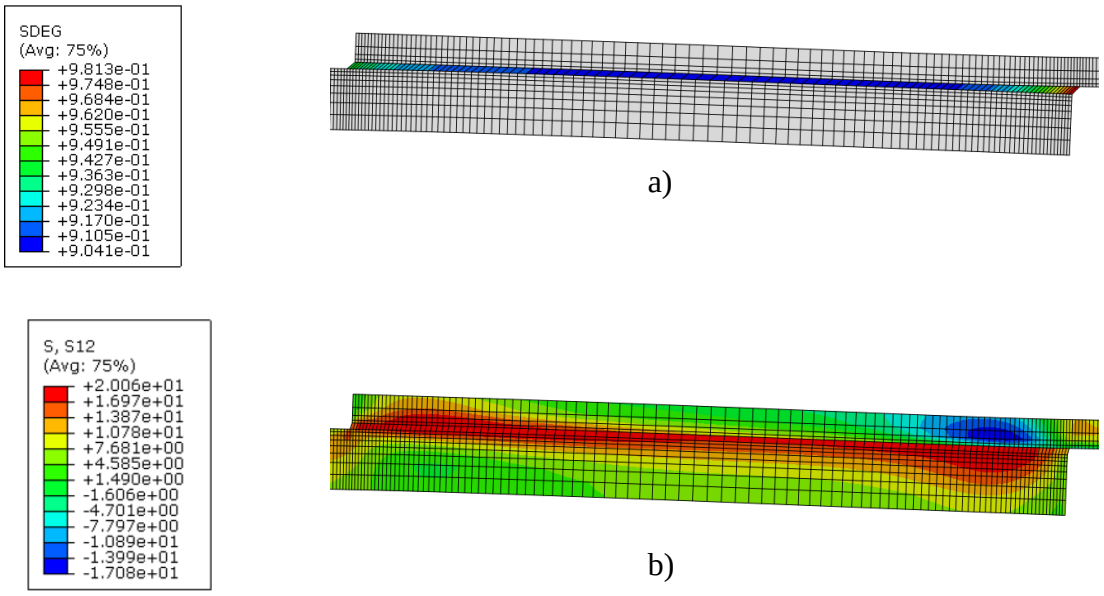

Figure 4.13 Adhesive joint detailed view: a) Adhesive layer degradation, b) Shear stress distribution for adhesive global yielding.

In Figure 4.13 b, global yielding of the adhesive occurred at 6.39 kN for the 12.5 mm overlap, 12.61 kN for 25 mm overlap and 25.18 kN for 50 mm overlap, respectively.

The adhesive layer degradation can be seen at the overlap edge with the maximum peel stress concentration, having a high impact on the adhesive bonding strength. The peel stress accumulation is actually the main reason why this configuration promoted the lowest strength compared to the other CFRP/HSS SLJs configurations.

`

The FEA results are showed in Table 20. It can be observed a very accurate numerical simulation, with a maximum error of 9.07%.

Table 20 Comparison of the experimental and numerical failure loads of CFRP (2.1 mm)/HSS (1 mm)

Overlap [mm]	Experimental failure load [kN]	Numerical failure load [kN]	Error [%]
12.50	7.39	6.72	9.07
25.00	12.93	12.05	6.81
50.00	27.05	25.75	4.81

In addition, Figure 4.14 provides a better view of the results obtained. The failure load as a function of overlap length are plotted, in which is shown that the numerical simulation can provide an accurate replica of the experimental results obtained.

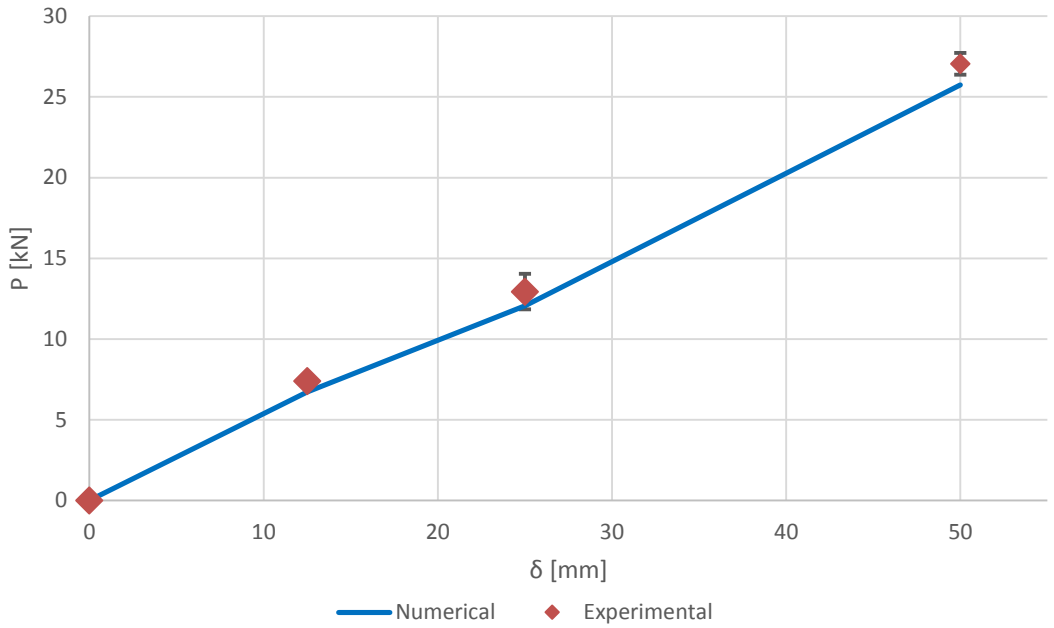

Figure 4.14 CFRP (2.1 mm)/HSS (1 mm) numerical/experimental results

4.4.1.2 CFRP (2.1 mm)/HSS (2 mm)

In order to verify if the bonding strength is influenced by the increase of the adherend thickness and by the increase in longitudinal stiffness, the present configuration (i.e. CFRP (2.1 mm)/HSS (2 mm)) was modelled.

`

The cohesive elements placed between the layers of CFRP and HSS were damaged similar to the experimental case, and the plot of element degradation is presented in Figure 4.15 a), while the shear stress distribution is represented in Figure 4.15 b).

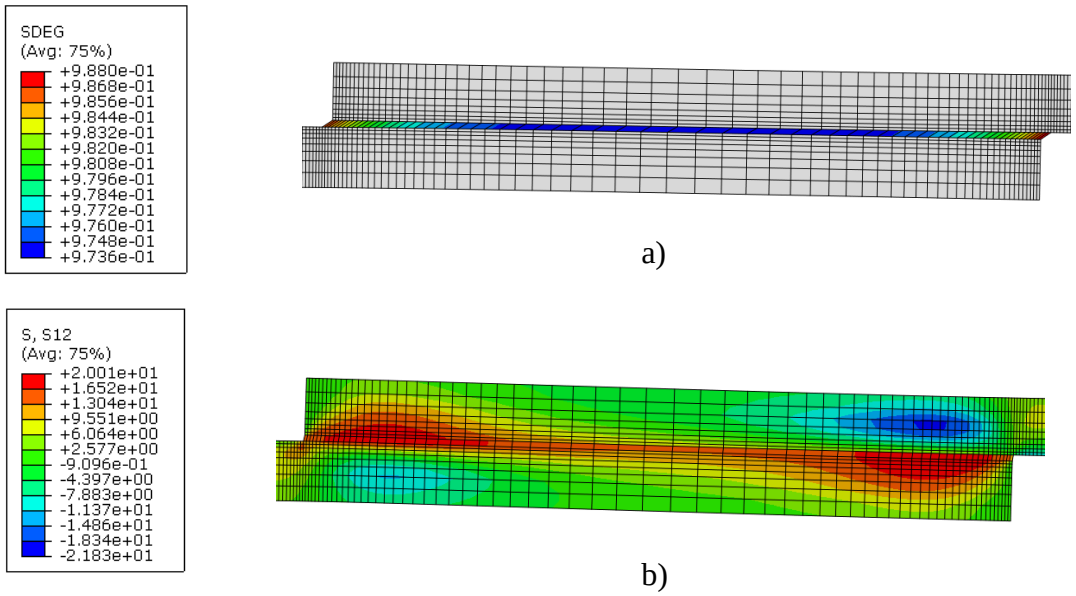

Figure 4.15 Numerical simulation: a) Adhesive layer degradation, b) Shear stress distribution for adhesive global yielding

An equal distribution of both shear stress and adhesive layer degradation, in comparison with the case studied before, can be seen. In Figure 4.15 b, global yielding of the adhesive occurred at 6.29 kN for 12.5 mm overlap, 11.54 kN for 25 mm overlap and 26.25 kN for 50 mm overlap, respectively.

The comparison of the experimental and numerical failure loads of CFRP (2.1 mm)/HSS (2 mm) are showed in Table 21. The obtained results revealed a very accurate numerical simulation, with a maximum error of 7.06 %.

Table 21 CFRP (2.1 mm)/HSS (2 mm) numerical/experimental results

Overlap [mm]	**Experimental failure load [kN]**	**Numerical failure load [kN]**	**Error [%]**
12.5	7.05	6.71	4.83
25	14.24	13.24	7.06
50	27.87	26.50	4.93

`

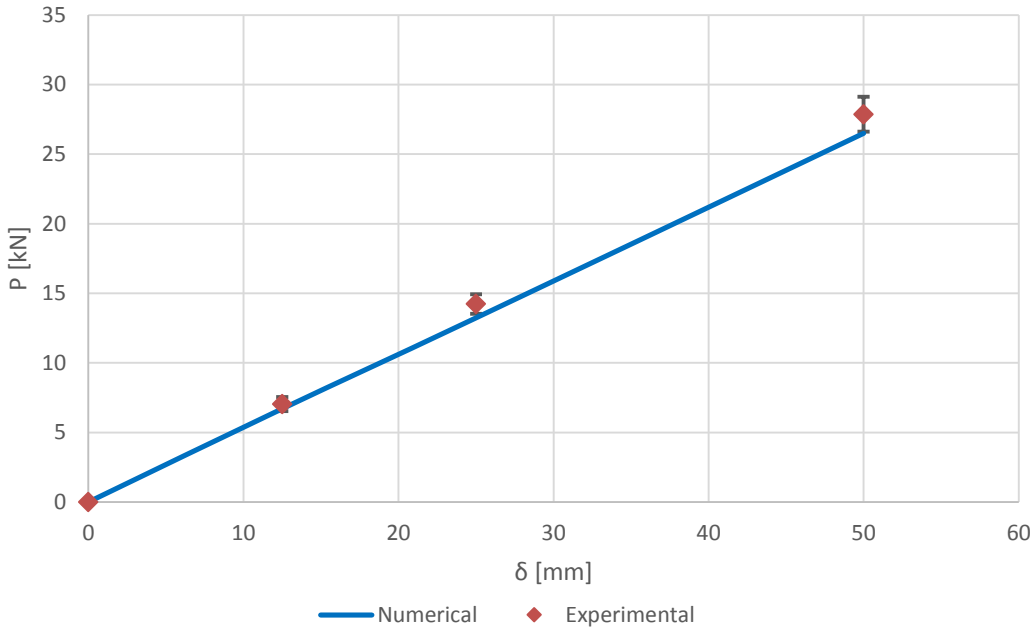

Figure 4.16 CFRP (2.1 mm)/HSS (2 mm) numerical/experimental results

4.4.1.3 CFRP (1.2 mm)/HSS (1 mm)

The comparison of the experimental and numerical failure loads are centralized in Table 22. It can be seen that the numerical results agree well with the experimental results. The error percent for different overlap length is calculated as 7.07% and 14.03% for 25 mm overlap, respectively.

In Figure 4.17b, global yielding of the adhesive can be seen. It occurred at 6.29 kN for 12.5 mm overlap, 11.72 kN for 25 mm overlap and 26.20 kN for 50 mm overlap, respectively.

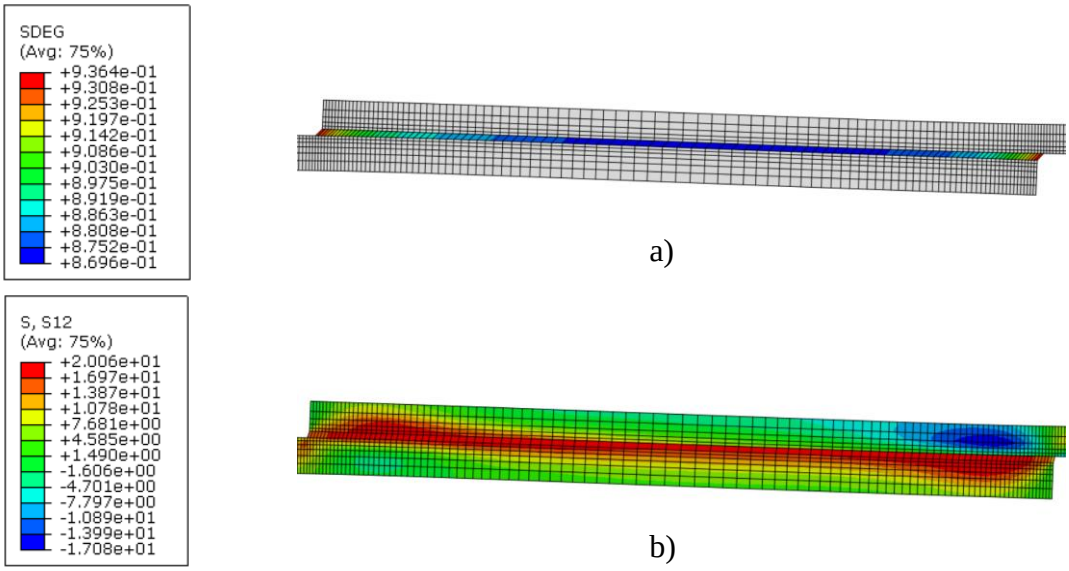

Figure 4.17 Numerical simulation of CFRP/HSS SLJs: a) Adhesive layer degradation, b) Shear stress distribution for adhesive global yielding

Table 22 CFRP (1.2 mm)/HSS (1 mm) numerical/experimental results

Overlap [mm]	Experimental failure load [mm]	Numerical failure load [mm]	Error [%]
12.5	8.36	7.78	7.07
25	12.15	13.16	14.03
50	28.66	26.54	7.41

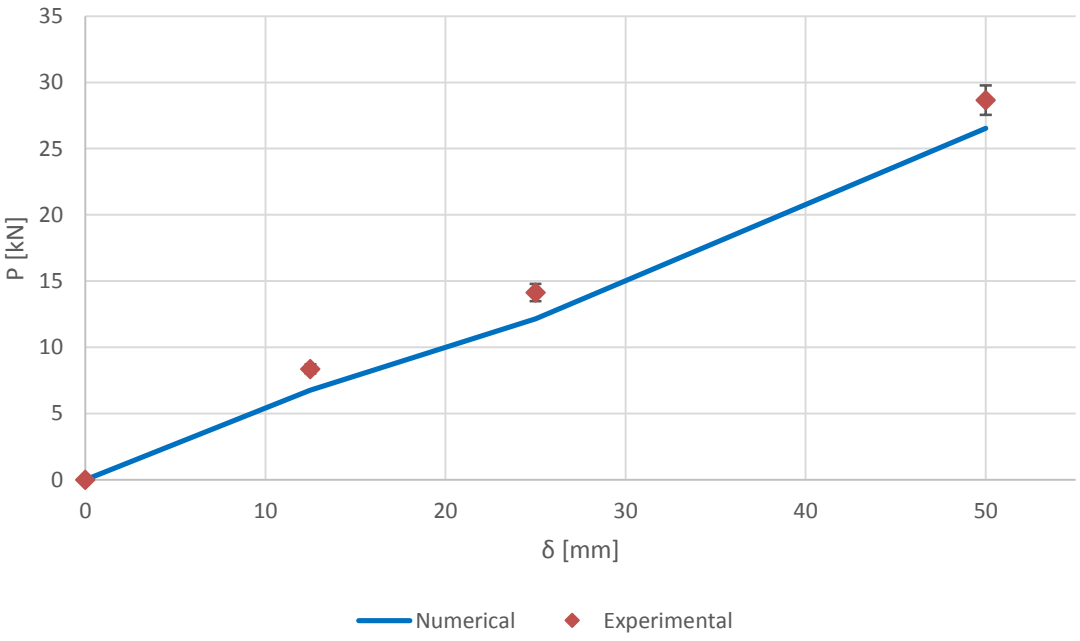

Figure 4.18 CFRP (1.2 mm)/HSS (1 mm) numerical/experimental results

`

4.4.2 CFRP/Al

The 2 mm thick aluminum substrate was chosen to obtain a geometrical balance joint and 3 mm thick substrate to obtain the balanced axial stiffness joint. The only overlap studied was the 25 mm overlap due to the high plastic deformation that might occur with bigger overlaps.

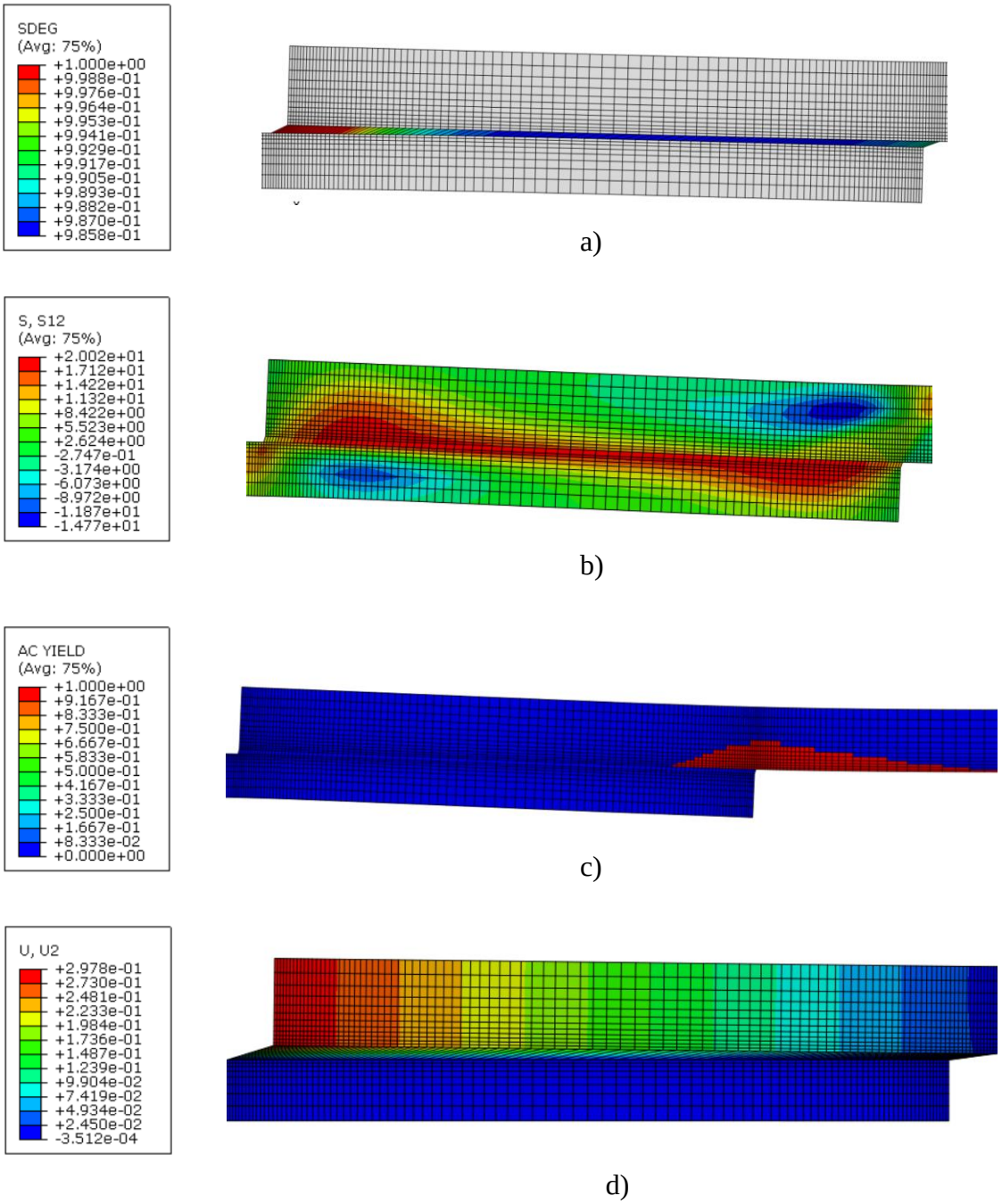

Figure 4.19 Numerical simulation of CFRP/Al SLJs: a) Adhesive degradation; b) Shear stress distribution for adhesive global yielding; c) AC yielding; d) Displacement occurred due to substrate yielding

`

In Figure 4.19a, an asymmetric degradation of the adhesive layer, which started from the edge of the aluminum substrate can be seen. The plastic deformation for the aluminum substrate is represented in Figure 4.19c, with a displacement of 0.2 mm for 3 mm substrate and 1.2 mm in the case of 2 mm substrate. Also, in Figure 4.19 b, global yielding of the adhesive can be seen, it occurred at 11.46 kN load for 2 mm thick aluminum and at 11.42 kN load for 3 mm thick aluminum adherend.

Values resulted after both numerical and experimental work were introduced in Table 23 and confirmed that the results obtained numerically are accurate. Failure load comparing the numerical simulation to the experimental single lap joint are presented in Figure 4.20.

Table 23 CFRP/Al numerical/experimental results

Thickness [mm]	Experimental load [kN]	Numerical load [kN]	Error [%]
2	11.61	11.77	1.46
3	11.16	11.66	4.45

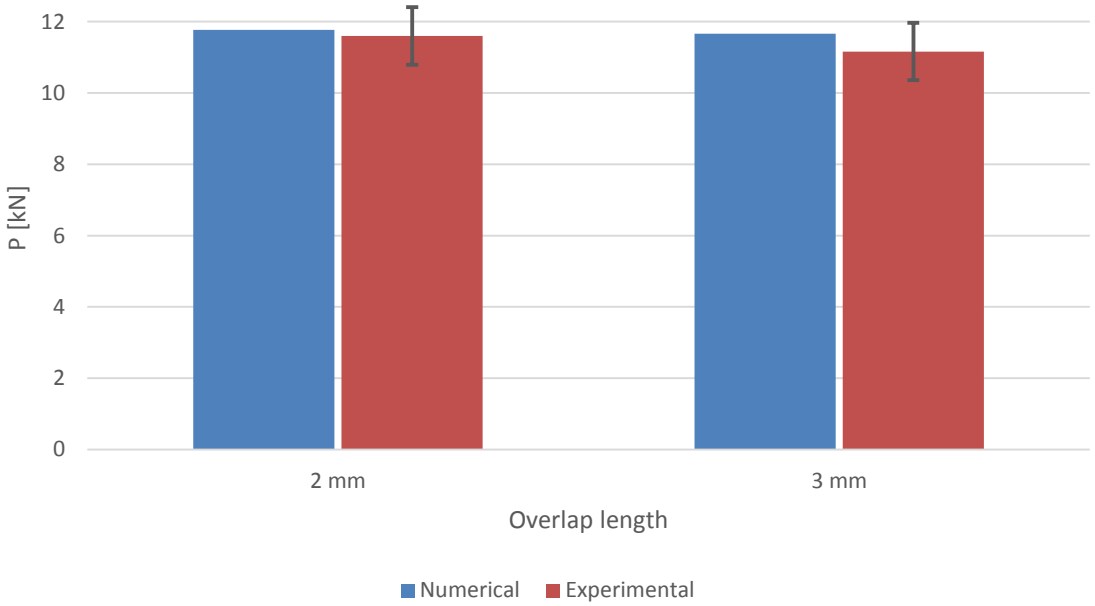

Figure 4.20 CFRP/Al numerical/experimental results chart

`

4.5 Conclusions of numerical analysis

The effect of the adherends material mismatch on the stress distributions was investigated by FEA, which explained the experimental results of the joints.

An assessment of the efficiency of bonded single lap joints with the structural polyurethane studied here must conclude that they are 100% efficient for similar CFRP adherends, becoming less so for dissimilar adherends, particularly for the case of unbalanced geometry joints (i.e. CFRP (2.1 mm)/HSS (1 mm)).

No significant difference in the multi-material joints' strength between CFRP/HSS was observed. However, when they are compared to joints with similar adherends a decrease in strength can be observed, mainly for longer overlaps, due to the non-uniform stress distribution. Nevertheless, geometry balanced joints ($t_{s1}=t_{s2}$) promote a higher strength than the stiffness balanced joints ($E_1t_{s1}=E_2t_{s2}$).

For the material combinations and adherend thickness studied here, the joint strength for unbalanced geometry joints (CFRP (2.1 mm)/HSS (1 mm)) is less than that for an unbalanced stiffness joint (CFRP (2.1 mm)/HSS (2 mm)) (Figure 4.21 and Figure 4.22).

It is important to be able to predict the general trends of the adhesive capability with different materials.

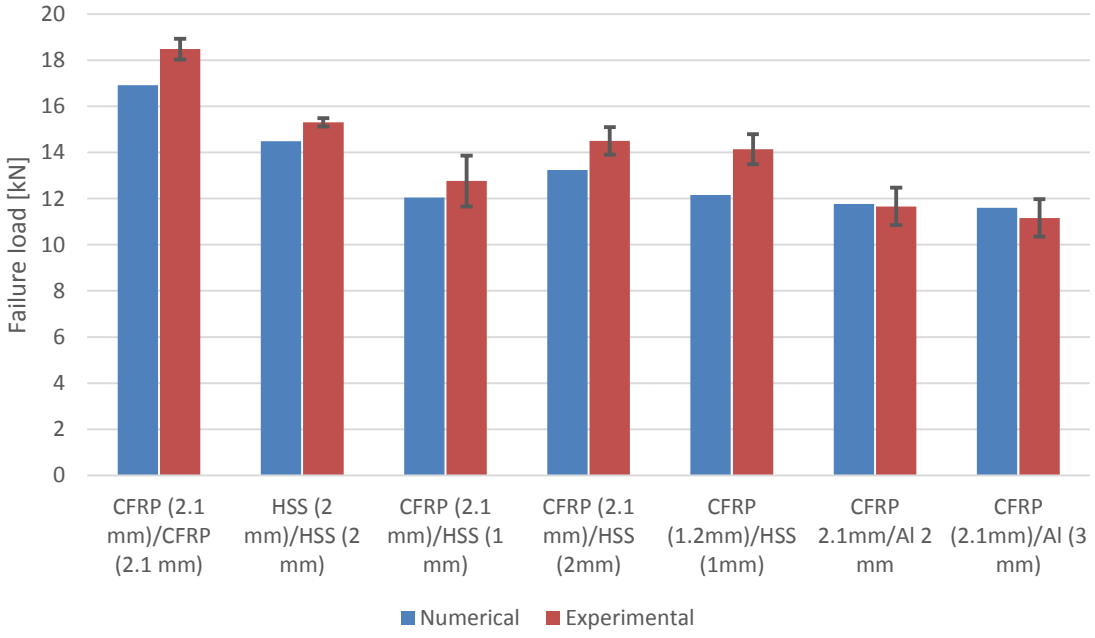

Figure 4.21 Effect of dissimilar adherends on the failure load of multi-material SLJs 25 mm overlap

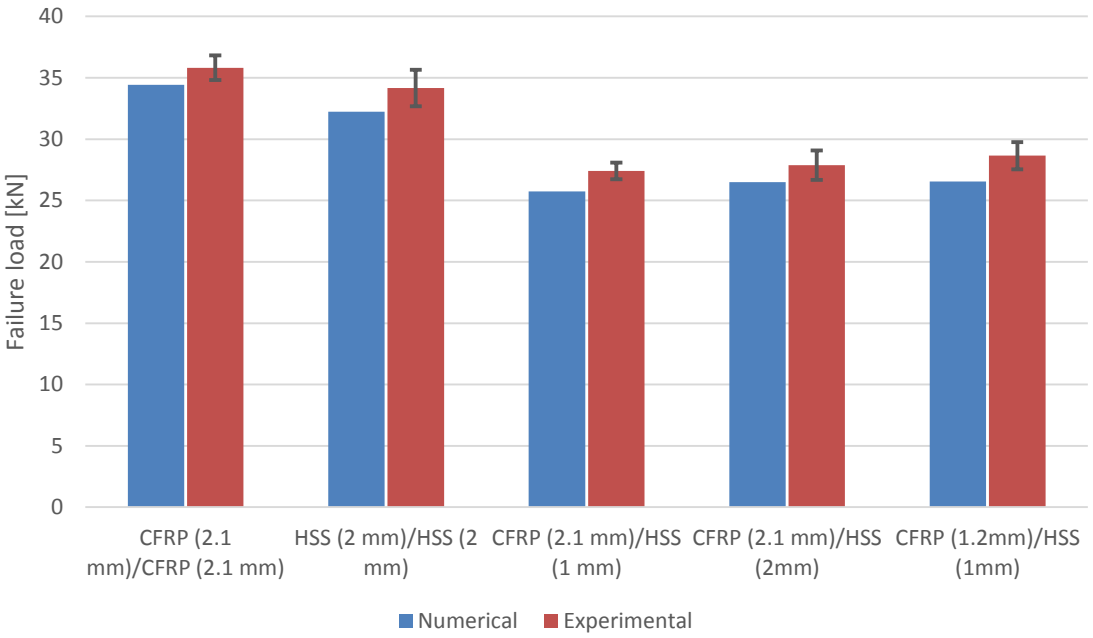

Figure 4.22 Effect of dissimilar adherends on the failure load of multi-material SLJs 50 mm overlap

`

5 Conclusions and future work

In this thesis, multi-material single lap joints for which the two adherends could have different geometries and/or mechanical properties (joints referred to as "unbalanced") were investigated and compared to "balanced" joints (similar adherend geometry and mechanical properties). The following conclusions can be drawn:

- For relatively short overlaps in SLJs bonded with structural modern tough adhesives, failure is dominated by adhesive global yielding and the influence of geometry and/or material on joint strength is not significant. Increasing the overlap length increases the load-bearing capacity of the joints;
- For the adherend thicknesses studied in the thesis, the unbalanced CFRP/HSS joints strength had no significant variation. However, when compared to balanced joints between HSS/HSS or CFRP/CFRP, a decrease of the strength was observed, in the case of longer overlaps, due to the different flexure rigidities of the adherends which give a non-uniform stress distribution;
- Geometrical balanced joints promote higher strength than the stiffness balanced joints, behavior that was observed also for the aluminum adherends;
- The bonded joints realized with SikaForce®7888 L10 were more efficient to similar CFRP adherends, becoming less efficient for dissimilar adherends, in particularly for the case of CFRP (2.1 mm)/HSS(1 mm);
- Increasing the adherend thickness for CFRP, from 1.2 mm to 2.1 mm, did not promote a significative increase in the joint`s strength, thus a reduction of mass may be achieved without losing the joint efficiency;
- Overall numerical values of the maximum load were very close to experimental results, validating the numerical methodology to predict the lap shear strength and providing the necessary data to explain the obtained behavior.

Future work

1. Tests with different combinations of material will be performed (i.e Al/HSS or CFRP/Mg);
2. CFRP/Al tests with different material thicknesses of aluminum adherends (i.e. 0.8 and 1 mm) will be performed.

`

References

(Adams & Harris, 1987)	Adams, R.D., and J.A. Harris. The Influence Of Local Geometry On The Strength Of Adhesive Joints, International Journal of Adhesion and Adhesives 7(2) (1987), pp. 69-80;
(Adams & Mallick, 1992)	Adams, R. D., and V. Mallick. A Method For The Stress Analysis Of Lap Joints. The Journal of Adhesion 38 (3-4) (1992), pp. 199-217;
(Adams, 2005)	Adams, Robert D. Adhesive Bonding. Boca Raton, FL: CRC Press, 2005;
(Ahmed, et al., 2012)	Ahmed, A. Study of Thermal Expansion in Carbon Fiber Reinforced Polymer Composites (Conference procedings): SAMPE International Symposium, 2012;
(Banea & da Silva, 2009)	Banea M.D., da Silva L.F.M., Adhesively bonded joints in composite materials – An Overview, Proc. IMechE, Part L: Journal of Materials: Design and Applications, 223(1), (2009), pp. 1-18.
(Banea et al, 2015a)	Banea M.D., da Silva L.F.M., Campilho R.D.S.G., The Effect of Adhesive Thickness on the Mechanical Behaviour of a Structural Polyurethane Adhesive, Journal of Adhesion, 91(5), (2015) pp. 331-346.
(Banea et al, 2015b)	Banea M.D., da Silva L.F.M., Carbas R.J.C., Campilho R.D.S.G., Effect of adherend material on the fracture behaviour of adhesive joints for automotive industry, Composite Part B, 2015, to be submitted
(Barenblatt, 1959)	Barenblatt, G.I. Concerning Equilibrium Cracks Forming During Brittle Fracture. The Stability Of Isolated Cracks. Relationships With Energetic Theories. Journal of Applied Mathematics and Mechanics 23.5 (1959), pp. 1273-1282;
(Campilho, 2009)	Campilho, R. D. S. G. Repair of Composite and Wood Structures. Oporto PhD thesis: s.n., 2009;

`

(Campilho, et al., 2009) Campilho, R.D.S.G., de Moura, M., and Dominigues J.. Modelling The Tensile Fracture Behaviour of CFRP Scarf Repairs. Composites Part B: Engineering 40(2) (2009), pp. 149-157;

(Campilho, et al., 2005) Campilho, R.D.S.G., M.F.S.F. de Moura, and J.J.M.S. Domingues. Modelling Single And Double-Lap Repairs On Composite Materials. Composites Science and Technology 65(13) (2005), pp. 1948-1958.

(Campilho, et al., 2011) Campilho, R.D.S.G., Banea, M.D., Pinto A. da Silva, L.F.M., de Jesus, A. Strength Prediction Of Single- And Double-Lap Joints By Standard And Extended Finite Element Modelling. International Journal of Adhesion and Adhesives 31(5) (2011), pp. 363-372;

(Car-Engineer, n.d.) Usage of Aluminum and structural adhesives in new Cadillac CTS and ATS, http://www.car-engineer.com/usage-of-aluminum-and-structural-adhesives-in-new-cadillac-cts-and-ats/#prettyPhoto, (last accessed 20.05.2015);

(Chaves, 2013) Chaves, F. J. P. Fracture Mechanics Applied To The Design Of Adhesively Bonded Joints. Ph.D Thesis. Universidade do Porto, 2013;

(Chiaberge, 2011) Chiaberge, Marcello. New Trends And Developments In Automotive Industry. Rijeka, Croatia: InTech, 2011;

(Cole & Sherman, 1995) Cole, G.S., and A.M. Sherman. Light Weight Materials For Automotive Applications. Materials Characterization 35(1) (1995), pp.3-9;

(Crocombe & Adams, 1981) Crocombe, A. D., and R. D. Adams. Influence Of The Spew Fillet And Other Parameters On The Stress Distribution In The Single Lap Joint. The Journal of Adhesion 13(2) (1981), pp. 141-155;

(da Silva & Campilho, 2012) da Silva, L.F.M. and Raul D. S. G Campilho. Advances in Numerical Modelling Of Adhesive Joints. Berlin: Springer, 2012;

`

(da Silva & Magalhaes, 2007)	da Silva, L.F.M. and Magalhaes, A.G. Juntas Adesivas Estruturais. s.l. : Publindústria, 2007;
(da Silva, et al., 2009)	da Silva, L.F.M., Das Neves, P.J., Adams R. and Spelt, J. Analytical Models Of Adhesively Bonded Joints—Part I: Literature Survey. International Journal of Adhesion and Adhesives 29(3) (2009), pp. 319-330;
(da Silva, et al., 2011)	da Silva, Lucas Filipe Martins, Andreas Öchsner, and Robert D Adams. Handbook Of Adhesion Technology. Berlin: Springer, 2011;
(Davis & Bond, n.d.)	Davis, M.J. and Bond, D.A., The importance of failure mode identification in adhesive bonded aircraft structures and repairs, Directorate General of Technical Airworthiness - Royal Australian Air Force;
(DeCicco, 2005)	DeCicco, J.M. Steel and Iron Technologies for Automotive Lightweighting, Environmental Defense. 2005;
(Dugdale, 1960)	Dugdale, D. S. Yielding of steel sheets containing slits, Journal of the Mechanics and Physics of Solids, *8*(2), (1960), pp. 100-104;
(Fernandes, et al., 2015)	Fernandes, T. A. B., Campilho, R.D.S.G, Banea, M.D., da Silva, L.F.M. Adhesive Selection For Single Lap Bonded Joints: Experimentation And Advanced Techniques For Strength Prediction. The Journal of Adhesion 91(10-11) (2015), pp. 841-862;
(Grant, 1976)	Grant, P. Stress and strength analysis of bonded joint. s.l. : British Aircraft Corparation, 1976;
(Hart-Smith, 1973a)	Hart-Smith, L. J. Adhesive-Bonded Double-Lap Joints. [Washington, DC]: National Aeronautics and Space Administration, 1973;
(Hart-Smith, 1973b)	Hart-Smith, L.J. Adhesive bonded single lap joints. s.l. : NASA, Langley Research Center, 1973;

`

(Hollaway, 2005) Hollaway, L.C, Advances in adhesive joining of dissimilar materials with special references to steels and CFRP composites: Proceedings of the International Symposium on Bond Behaviour of FRP in Structures, 2005;

(Kinloch, 1987) Kinloch, A. J. Adhesion And Adhesives. London: Chapman and Hall, 1987.

(lexus.co.uk, n.d.) Engineering innovations: advanced body adhesives – Lexus, http://blog.lexus.co.uk/engineering-innovations-advanced-body-adhesives/, (last accessed 20.05.2015);

(McGrath, 2011) McGrath, Gareth. Application and Joint Design, Materials Information Services. 2001;

(Mi, et al., 1998) Mi, Y. et al. 'Progressive Delamination Using Interface Elements'. *Journal of Composite Materials* 32.14 (1998): 1246-1272. Web.

(Neto, 2011) Neto, J.A. 'Estudo Paramétrico De Juntas Adesivas Em Material Compósito. Eg. Universidade do Porto, 2011;

(NIST, n.d.) New NIST Research Center Helps the Auto Industry 'Lighten Up', http://www.nist.gov/lightweighting/ncalfeature.cfm, (last accesed 14.05.2015);

(Omar, 2011) Omar, Mohammad A. The Automotive Body Manufacturing Systems And Processes. Chichester, West Sussex: Wiley, 2011;

(Oterkus, et al., 2004) Oterkus E., Barut A., Madenci E., Smeltzer III SS, Ambur D.R., Collection of technical papers - 45th AIAA/ASME/ASCE/AHS/ASC Struct Dyn and Mater Conf; 12th AIAA/ASME/AHS Adapt Struct Conf; 6th AIAA non-deterministic approaches forum; 5th AIAA Grossamer Sp, Palm Springs, CA, USA, 2004, pp. 555;

(Williams, 2008) Williams, Andrew. Adhesives Technology Handbook. 2 end edition. 2008;

(Wu, 1982) Wu, S. Polymer Interface and Adhesion. New York: Dekker, 1982;

`

(Zhao, et al., 2011) Zhao, X., Adams, R.D. and da Silva, L.F.M., Single lap joints with rounded adherend corners, J. Adhes. Sci. Tehnol, 25 (2011, pp. 837-856.